Ash behavior and de-fluidization in low temperature circulating fluidized bed biomass gasifier

Narayan, Vikas

Publication date:
2016

Document Version
Publisher's PDF, also known as Version of record

Ash behavior and de-fluidization in low temperature circulating fluidized bed biomass gasifier

Vikas Narayan

PhD Thesis

March 2016

DTU Chemical Engineering
Department of Chemical and Biochemical Engineering

TECHNICAL UNIVERSITY OF DENMARK

Ash behavior and de-fluidization in low temperature circulating fluidized bed biomass gasifier

Ph.D. Thesis

Vikas Narayan

March, 2016

Supervisors:

Peter Glarborg

Peter Arendt Jensen

Ulrik Birk Henriksen

Combustion and Harmful Emission Control Research Centre

Department of Chemical and Biochemical Engineering

Preface

This thesis is the outcome of a PhD study carried out at the Combustion and Harmful Emission Control (CHEC) research center at the Department of Chemical and Biochemical Engineering of the Technical University of Denmark (DTU) in the period from July 2011 to November 2014. The project work was supervised by Peter Glarborg, Peter Arendt Jensen and Ulrik Henriksen. The project was financially supported by DONG Energy and Energinet.dk.

I would first like to thank my supervisors Peter Glarborg, Peter Arendt Jensen and Ulrik Henriksen for their support and guidance throughout my PhD project. I am grateful to my supervisors for inspiring me and training me as a researcher to come up with simplified solutions to complex problems. I also owe my thanks to Anders Tiedje, Rasmus Lundgaard Christensen, Mette Larsen and Emine Yüksel Coskun for their support and assistance they have provided me during my experiments. I also wish to thank Rasmus Glar Nielsen and Benny Gøbel from DONG ENERGY and Jesper Ahrenfeldt, Kristian Estrup and Freddy Christensen from Risø for providing me their unconditional support and a pleasant work environment during my measurements at Risø and Kalundborg. I also wish to thank Weigang Lin for sharing his experience and guidance for my de-fluidization studies. I owe my thanks to Zsuzsa Sárossy and Helge Egsgaard from Risø for providing the analysis results of methyl chloride measurements. I would also like to thank Rolf Jensen from Mechanical Engineering (DTU) for his help with SEM analysis and Edith Thomsen from, Force Technology, Enstedværket for providing the chemical analysis of my samples.

Finally, I would like to thank my friends, Sunil, Chandresh, Ambareesh, Vikas, Dayanand, Amar, Sharat, Maulik and Kaushal for giving me such a wonderful social life during my stay in Denmark. Last but not the least; I dedicate my thesis to my mother Valsala Narayan, sister Sandhya Narayan and aunt Jayashree Narayanan who are always there for me, being my source of strength and motivation in every moment of my life.

Vikas Narayan,

Kgs Lyngby, November 2015.

Summary

Biomass is increasingly used as a fuel for power generation. Herbaceous fuels however, contain high amounts of alkali metals which get volatilized at high temperatures and forms salts with low melting points and thus condense on pipelines, reactor surfaces and may cause de-fluidization. A Low-Temperature Circulating Fluidized Bed System (LTCFB) gasifier allows pyrolysis and gasification of biomass to occur at low temperatures thereby improving the retention of alkali and other ash species within the system and minimizing the amount of ash species in the product gas. In addition, the low reactor temperature ensures that high-alkali biomass fuels can be used without risks of bed de-fluidization. This thesis aims to understand the behavior of alkali metals and ash in the LTCFB system. The thesis work involved measurements made on bed material and product gas dust samples on a 100kW LTCFB gasifier placed at Risø and a 6 MW LTCFB gasifier owned by DONG ENERGY and placed in Kalundborg. In addition to the analysis of the inorganic elemental composition of the collected samples, SEM and TGA analysis of the samples were made to improve understanding on the behavior of the ash forming species within the system. It was observed that of the total fuel ash entering the system, a large fraction (40-50%) of the ash was retained in the secondary cyclone bottoms and a lower amount (8-10%) was released as dust in the exit gas; the residual ash was accumulated within the fluidized bed system. A dominant fraction of alkali and alkaline earth metals were retained in condensed state along with Si and some Cl, while a large fraction of Cl and S appeared in gaseous form and was released with the product gas. Measurements on the product gas from the 100 kW LTCFB gasifier showed the presence of Cl in the form of gaseous methyl chlorides (90-100 ppm). Release of K and other inorganic species with the tar in the product gas from the LTCFB gasifier were found to be low. The major forms in which K and Si could exist in the LTCFB gasifier are K-salts (KCl and K_2CO_3), organically bound K (K bound to ion exchange sites of the char matrix and intercalated K), and K-silicates. At the temperature in the pyrolysis chamber (650^0C) of the LTCFB gasifier, the above K species are expected to be mostly present in the solid state. In the char reactor (where the char from the pyrolysis chamber is gasified and combusted at temperatures around 730^0C), KCl(s) will partially vaporize and the released K could react with silica to form silicates. When the flue gas enters the pyrolysis reactor, the temperature is reduced and KCl aerosols are formed. The release and retention of the

condensed ash species from the system was seen to be controlled by the ash particle size and the cut size of the primary and secondary cyclones. A model accounting for the ash collection by the plant cyclones was developed which predicted the product gas ash particle release reasonably well.

The present work also aims to understand the effect of biomass fuel ash composition and fluid bed operation conditions especially temperature on agglomeration and de-fluidization of alkali-rich bed material under gasification conditions. The de-fluidization studies involved measurements with mixtures of sand and pure potassium salts (KCl and K_2CO_3) as well as bed material samples obtained from a 6 MW Low Temperature Circulating Fluidized bed (LTCFB) gasifier on a bench-scale fluidized bed reactor set up. The mechanism of agglomeration in the bed particles was seen to vary with the speciation of K. It was seen that in sand and KCl agglomerates, the sand particles were bound by KCl melts. There was very limited chemical reaction observed between KCl and the sand particles with no presence of silicate melts in the agglomerates. In sand and K_2CO_3 mixtures and the LT-CFB bed material samples the agglomeration was seen to occur due to a coating of viscous silicate melts formed from reaction of alkaline and alkali earth species with silica from the bed particles (coating induced agglomeration). It was also seen that the composition of the bed particles affected the de-fluidization temperatures. The de-fluidization took place at higher temperatures in the case of LTCFB bed material particles (780-785^{0}C) as compared to the sand and K_2CO_3 mixtures (730^{0}C) with similar K contents (4.2-4.5%), though both showed that the de-fluidization occurred by the mechanism of coating induced agglomeration. This is attributed to the presence of Ca and Mg in the bed particles; these elements shift the formation of the eutectic melts to higher temperatures increasing the viscosity levels of the coatings. A mathematical model for de-fluidization of alkali rich bed material was developed to predict the de-fluidization temperatures as a function of parameters such as initial alkali concentrations within the bed particle diameters and the fraction of K entrained from the system. The model was also applied to study the de-fluidization behavior of alkali-rich samples in a large scale LTCFB gasifier. The model was used to predict the variations in de-fluidization time on a full scale LTCFB plant with respect to parameters such as temperature, fuel alkali concentrations and bed particle diameter.

Dansk resume

Biomasse bliver i stigende grad anvendt som brændsel til el produktion. Etårige biomasser som halm indeholder imidlertid relativt store mængder alkali metaller, som i form af salte overgår til gas fase ved høje temperature. Saltene kan så kondensere på rør og reaktor oveflader, samt kan forårsage de-fluidisering i Fluid beds. I en lav temperatur fluid bed forgasser (LTCFB) sker biomasse pyrolyse og forgasning ved lave temperaturer, hvorved alkali metaller og øvrige aske specier fastholdes i fluidbed reaktorerne og indholdet af aske specier i produktgassen minimeres. Herudover sikre de lave reaktor temperaturer, at biomasse med et højt alkali indhold kan anvendes, uden at dette føre til de-fluidisering af fluidbed forgasseren. Det udførte Ph.d. projekt sigter mod at opnå en forbedret forståelse af transformationen af alkali metaller og aske i LTCFB anlæg. Projektet har omfattet målinger på bed prøver og produkt gassen på dels et 100 KW LTCFB anlæg (placeret på Risø) og dels et 6 MW anlæg (Eget af DONG Energy og placeret i Kalundborg). Foruden en analyse af den uorganiske sammensætning af de indsamlede prøver, er der udført SEM (Scanning Elektron Mikroskopi) og TGA (Thermal Gravimetric Analysis) analyser på prøverne for at opnå en forståelse af askens opførsel i LTCFB systemerne. Undersøgelserne viste at ud af den totale mængde aske som indføres med brændslet udskilles den største mængde (40 – 50 %) i bunden af sekundær cyklonen og en mindre mængde (8-10 %) findes i partiklerne som forlader forgasseren med produkt gasserne. Resten af den tilførte brændselsaske akkumuleres i anlægget. En dominerende fraktion af alkali metallerne samt Ca, Mg og Si forbliver i den kondenserede fase og tilbageholdes i forgasser systemet. En væsentlig fraktion af den tilførte svovl og klor forefindes som gasfase specier og frigives fra forgasserne med produkt gassen. Målinger på produktgassen på 100 KW forgasseren viste et indhold af gasformig klor i form af methylklorid (90 – 100 ppm). Frigivelse af K og andre uorganiske grundstoffer med tjære produkter fandtes ved målinger at være meget lav. K forefandtes i LTCFB forgasser systemerne hovedsagelig som kalium salte (KCl og K_2CO_3) bundet til den organiske brændselsfraktion (K bundet til ion udvekslings positioner på koksmatricen eller som intercalated K) og som kalium silikater. Ved typiske pyrolyse kammer temperaturer (650 °C) vil de omtalte K specier stort set vare at finde i den kondenserede fase. I koks reaktoren (hvor koks fra pyrolyse kammeret forgasses ved temperaturer på cirka 730 °C) vil KCl i nogen grad forefindes på gasfase og vil i nogen grad kunne reagere med Si og danne

silikater. Når røggassen videreføres til pyrolysereaktoren reduceres temperaturen og der dannes KCl aerosoler. Fraktionen af fast fase aske specier der frigives, henholdsvis tilbageholdes i reaktor systemet, blev observeret til at være kontrolleret af askepartiklernes størrelse og afskærings-partikel-størrelsen af primær og sekundær cyklonerne. En model der beskriver aske partikel udskillelsen i anlæggets cykloner blev udviklet, og modellen blev med succes anvendt til at forudsige aske partikel afgivelsen med produkt gassen.

Ph.d. projektets formål omfattede også at undersøge indflydelsen af biomasse aske sammensætning og LTCFB driftsparametre, (specielt bed temperaturens) indflydelse på de-fluidisering af alkali right bed materiale ved forgasnings betingelser. De-fluidiserings studierne omfattede målinger på blandinger af sand og kalium salte (KCl og K_2CO_3) og undersøgelse af bed prøver modtaget fra 6 MW LTCFB anlægget i Kalundborg. De-fluidiserings undersøgelsen blev udført på CHECS laboratorie fluid bed. Agglomereringsmekanismen var afhængig af den anvendte type a K stoffer. Agglomerater af sand og KCl var sammenholdt af smeltet KCl. Kun en ganske begrænset reaktion mellem KCl og sandpartiklerne blev observeret, og der sås ikke smeltede silikater i agglomeraterne. I tilfældene med sand og K_2CO_3 og Kalundborg LTCFB bed prøver sås agglomereringen at være forårsaget via en viskos silikat smelte, dannet via reaktioner mellem alkali, kalcium og silicium (coating forårsaget agglomerering). Bed partiklernes kemi influerede de-fluidiseringstemperaturen. De-fluidiseringstemperaturen for LTCFB prøverne (780-785 °C) var højere end for prøver lavet af blandinger af sand og K_2CO_3 (730 °C) selv med ens K indhold (4.2-4.5 wt%). Dette skyldes indholdet af Ca og Mg i prøverne fra LTCFB forgasseren. Ca og Mg indholdet forøger smelte temperaturen, og øger viskositeten af de dannede smelter. En matematisk model af de-fluidisering af alkali rigt bed materiale er udviklet til at forudsige de-fluidiserings temperaturen som funktion a parametre som initiel alkali koncentration og fraktionen af alkali afgivet fra LTCFB systemet. Modellen er blevet anvendt til at forudsige variationer i de-fluidiseringstiden på et fuld skala LTCFB anlæg med hensyn til parametre som temperatur, bed alkali koncentration og bed materiale partikel diameter.

Table of Contents

List of Figures

List of Tables

1 Introduction

1.1 Biomass – Nature and characteristics in gasification

To decrease the net emission of CO_2 from electricity production biomass is increasingly used as fuel on power plants. Biomass is considered to be carbon neutral because the carbon dioxide released from the gasification process is recaptured through photosynthesis [1]. Annual biomass such as straw however contains high amounts of alkali metal and chlorine that may lead to increased corrosion and ash deposit formation problems in boilers. A low temperature gasification process, the LTCFB gasifier, has been developed to gasify high alkali biomass that will cause operational problems in other gasifiers. It is the objective of the LTCFB process to retain most of the biomass ash in the LTCFB system and then deliver the product gas containing the heating value of the fuel to a power plant boiler. The biomass heating value thereby can be utilized without introducing large amounts of alkali and chlorine into a power plant boiler. The objective of the present PhD project was to attain an improved understanding of transformation of inorganic elements such as K and Cl within the LTCFB process.

The term biomass generally refers to renewable organic matter generated from plants. Biomass can be classified based on many characteristics, ash content, moisture content, woody and non-woody biomass etc. It is in this context that the composition of inorganic elements is of interest.

As can be seen from Table 1-1, composition of biomass varies a lot, with wood having an ash content of typically 1 wt.% whereas herbaceous biomass such as straw have much higher ash contents. Woody fuels are characterized by low silica (0.1% by wt.), alkali content (0.1 % K by wt.) and chlorine content (0.02% by wt.). The biomass type available in large quantities but on the other hand proving to be the most problematic to handle are the herbaceous fuels and animal manure. Herbaceous fuels include, rice husk, wheat straw, bagasse, corn straw and others. The herbaceous fuels are found to contain high amount of alkali metals especially K, alkali earth metals like Ca, Cl, and sometimes Si. As shown in Table 1-1, the fuel Danish wheat straw is characterized by high ash content (4.5% by wt.) with high amounts of silica (0.8% by wt.), alkali (1 % of K by wt.) and chlorine (0.4% by wt.). During gasification at high temperatures, K, Cl and S present in these fuels may get volatilized and carried off with the product gas. If used in a boiler, the metal species

together with Cl form sticky deposits on boiler surfaces. Moreover K and Cl rich deposits cause increased corrosion compared to coal ash deposits. Furthermore, the cooling of the exhaust gas leads to saturation of the gaseous potassium species, resulting in the formation of aerosols and subsequent particle growth by condensation. These particles, rich in KCl and K_2SO_4, contribute to increased particle pollution from biomass fired thermal plants [4].

Table 1-1 Analysis of Biomass [2, 3]

	Unit	Wood Chips		Danish Wheat Straw	
		Typical	Variation	Typical	Variation
Moisture	% wt.	45	20-60	14	8-23
LHV (MJ/kg)	MJ/kg	19.5	18.5-20.5	18.6	18-19
% Ash	% wt. (dry)	1	0.3-6	4.5	2-7
Volatile Matter	% wt. (dry)	81	70-85	78	75-81
Composition					
C	% wt. (dry)	50	49-52	47.5	47-48
H	% wt. (dry)	5.8	5.2-6.1	5.9	5.4-6.4
N	% wt. (dry)	0.8	0.1-0.7	0.7	0.3-1.5
Si	% wt. (dry)	0.1	<1	0.8	0.1-1.5
Al	% wt. (dry)	0.015	<0.1	0.005	<0.03
Ca	% wt. (dry)	0.2	0.1-0.9	0.4	0.2-0.5
Mg	% wt. (dry)	0.04	<0.1	0.07	0.04-0.13
Na	% wt. (dry)	0.015	<0.1	0.05	<0.3
K	% wt. (dry)	0.1	0.05-0.4	1	0.2-1.9
P		0.02	<0.1	0.08	0.03-0.2
Fe		0.015	<0.1	0.01	<0.03
Cl		0.02	<0.1	0.4	0.1-1.1
S		0.05	<0.1	0.15	0.1-0.2

.

The above issues brought out a need for an improvement and innovation in the technology for gasification of herbaceous fuels. The Low Temperature Circulating Fluidized Bed Reactor is a solution found in this context. As claimed in [5, 6], the gasifier functions without in-situ ash sintering and corrosion problems and most potassium and chlorine is simply retained in a separate biomass ash stream. In this way a fuel-gas with low alkali content and a relatively high calorific value is produced.

1.2 Low Temperature Circulating Fluid Bed (LTCFB) Process.

The Low Temperature Circulating Fluid Bed (Figure 1-1) is designed for the gasification of cumbersome biomass fuels with high levels of low-melting ash substances and is based on separate stages of pyrolysis and gasification. As shown in Figure1-1, the LT-CFB process consists of two reactors. The biomass fuel is reduced to a particle size of no more than 3 mm and is fed through a screw conveyor to the first reactor which is the pyrolysis chamber. The fuel is then pyrolysed at around 650°C due to good thermal contact with mainly re-circulated sand and ash particles from the other (char) reactor.

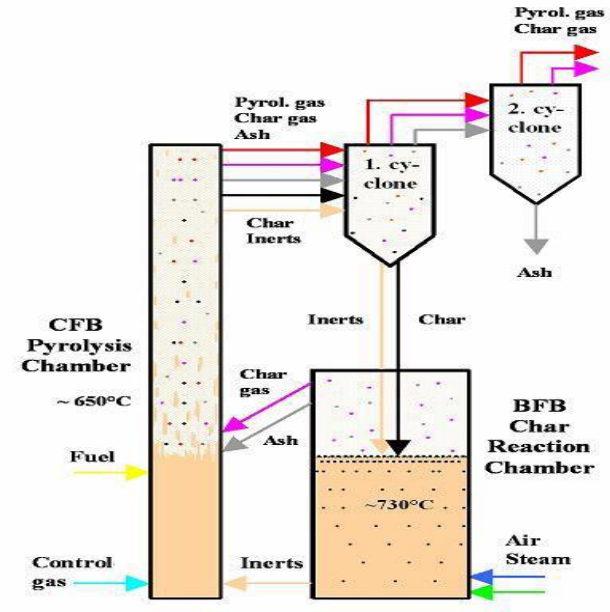

Figure 1-1 LT-CFB flow diagram [5, 6]

Due to the high gas velocity in the pyrolysis chamber, the residual char, pyrolysis gases and inert particles are blown upwards to the primary cyclone, which separates char and inert particles to a bubbling bed char reactor. Here, char is mixed with air to undergo gasification at typically around 730°C [5, 6]. Some steam or water may also be added in order to improve the conversion of char and limit the reactor temperature. The produced gas and fine ash particles leave the top of the char reactor and enter the pyrolysis chamber, where the volatiles contribute to a high gas velocity in the upper part of the chamber. Heavier inert particles re-

circulate to the pyrolysis chamber from the bottom of the char reaction chamber while serving as a heat carrier. The char particles in the upper part of the char reaction chamber thus experience a high retention time in the process, improving the overall conversion efficiency. The smaller ash particles not separated by the primary cyclone, are further collected by the secondary cyclone, separating the ash particles from the exit product gas. The energy for heating, drying and pyrolysis of the fuel in the pyrolysis chamber where the reactions are predominantly exothermic is supplied via the circulating sand from the char reactor. This thus avoids the necessity for additional heat exchange surfaces for the pyrolysis. The temperature in the char reactor is controlled by appropriate supply of air (to burn char) and some steam to limit the reaction temperature through endothermic reactions. The temperature in the pyrolysis chamber is controlled by the circulation of sand from the char reactor to the pyrolysis chamber. Due to the recirculation of the char and bed materials and long retention time of the char and fuel particles in the pyrolysis chamber, the pyrolysis takes place at a lower temperature. Consequently, the low temperatures restrict the release of alkali species with the product gas retaining them in the solid state which is separated and collected by the cyclones. Moreover, the relatively low temperatures in the process also limit the tendencies of de-fluidization in the system.

The LTCFB gasifier thus works on the principle of gas cleaning with using hot cyclones without flue gas cooling, as the hot gas is directly applied to a power plant boiler. The cooling of the exit gas is avoided as the gas contains predominant amounts of tar which on cooling would form sticky coatings and produce problems of fouling increasing the cost of the process. The tar being combustible hydrocarbons, on the contrary, improves the heating value of the gas and when fed directly to the boiler for power generation provide higher electrical efficiencies (40-45%) as compared to conventional burning of straw in grate-fired boilers (30%) [7].

LTCFB gas can also be used in gas turbines and fuel cells, if a more efficient dust separation and tar cracking is implemented. The high amounts of tar in the exit gas can also be collected and used as liquid biofuels or as a basis for the production of more valuable chemicals or fuels. Figure 1-2 summarizes the possible applications of the LTCFB process.

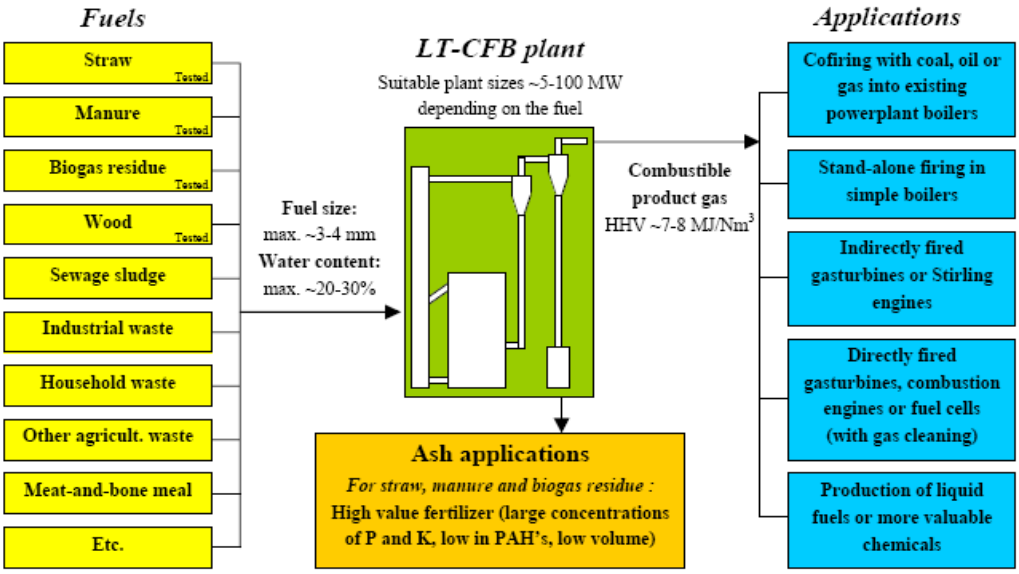

Figure 1-2 LTCFB process and its various applications [7]

Figure 1-3 100kW LTCFB Gasifier at Risø.

Figure 1-3 shows the picture of a 100 kW LTCFB gasifier located at Risø, Denmark. The gasifier is the part in alumunium-folio, while the blue barrels are the(elevated) fuel bin and the bin for ash separated by the

secondary cyclones. The pilot plant set has been used for tests and demonstrations and the exit gas was flared out.

Figure 1-4 6 MW LTCFB Gasifier at Kalundborg, Denmark

Figure 1-4 shows a picture of a 6 MW LTCFB Gasifier at Kalundborg, Denmark. Unlike the 100 K gasifier, the exit gas from the 6MW LTCFB gasifier was sent to a boiler. The plant has also been run for various tests and measurements.

1.3 Objectives of PhD work

The objective of the present work is to understand the ash chemistry and transformation of the ash species in the LTCFB system. Measurements were performed on a 100 kW LTCFB gasifier at DTU Risø and a 6 MW LTCFB (Pyroneer) gasifier at Kalundborg. In addition to particle sampling in the product gas, also bed material and cyclone ash samples were collected and analyzed for the composition. A model accounting for the ash collection by the plant cyclones in the LTCFB gasifier was developed. Through analysis of the measurements, together with the simplified model for the cyclone separation, the release and retention of alkali and other ash forming species in the LTCFB system was investigated.

It is of interest to increase the temperatures in the LTCFB gasifier to improve the overall conversion and efficiency, but still keeping the temperature at a level where gas phase alkali release is prevented. Such an increase in temperature of the fluidized bed system containing alkali and silica rich ash particles could however pose risks of de-fluidization. It is therefore useful to understand the de-fluidization

behavior of the alkali-rich ash particles within the LTCFB gasifier. The present work involves studies on the de-fluidization behavior of the alkali-rich ash from the LTCFB gasifier, with respect to temperature and varying alkali concentrations. The de-fluidization studies involved measurements made on a lab scale fluidized bed set up with sand and pure potassium salts (KCl and K_2CO_3) as well as with bed material samples obtained from the 6 MW Low Temperature Circulating Fluidized Bed (LT-CFB) gasifier using straw as a fuel. A mathematical model that addresses the de-fluidization behavior of the alkali rich samples was developed based on the experiments performed in the bench-scale fluidized bed reactor as well as on results from literature. The model studies were then extended to predict the de-fluidization behavior of alkali rich bed material in a large-scale LTCFB gasifier.

The subsequent chapters in the thesis begin with the literature survey (Chapter 2) on the behavior of inorganic species under reducing conditions and on de-fluidization studies made in fluidized bed biomass gasifiers. Chapter 3 involves a summary of the article submitted for publication in the journal, Energy and Fuels, entitled 'The behavior of alkali metals and ash in a Low Temperature Circulating Fluidized Bed (LTCFB) Gasifier'. The full paper is provided in Appendix A.1. The paper discusses the measurements and results obtained from the studies made on the behavior of ash species in the LTCFB system. Chapter 4 involves a summary of the article submitted for publication in Biomass and Bioenergy Journal, entitled 'Defluidization in Fluidized Bed Gasifiers Using High-Alkali Content Fuels'. The full paper is provided in Appendix A.2. The paper discusses the measurements and results obtained from the de-fluidization studies made on the alkali rich bed particles from the LTCFB system. The overall conclusions obtained from the present study are discussed in Chapter 5. The Appendices (A.1 and A.2 as mentioned above) are described in Chapter 6.

1.4 References:

1. Berg J M, Tymoczko J L, Stryer L. Biochemistry. 5th edition., New York, Freeman W H, 2002; ISBN:0-7167-3051-0.
2. Frandsen FJ. Ash formation, deposition and corrosion when utilizing straw for heat and power production. Technical University of Denmark, Lyngby, Denmark, 2011; ISBN:978-87-92481-40-5.

3. Sander B. Properties of Danish biofuels and the requirements for power production. Biomass and Bioenergy 1997;12:177–83.
4. Christensen K A, Stenholm M, Livbjerg H. The formation of submicron aerosol particles, HCl and SO_2 in straw-fired boilers. J. Aerosol Sci. 1998; 29(4):421–444.
5. Stoholm P, Nielsen H RG, Sarbæk L, Tobiasen L, Fcok WM, Richardt K, Sander B, Wolff L, Henriksen U. The Low Temperature CFB Gasifier-Further Test Results and Possible Applications. Proceedings of the 12. European Biomass Conference (ISBN) ETA-Florence & WIP-Munich 2002:706-709
6. Stoholm P, Ahrenfeldt J, Henriksen U, Gomez A, Krogh J, Nielsen RG, Sander B. The Low Temperature CFB Gasifier-500 kW Test on Biogas Fiber Residue. 16th European Biomass Conference and Exhibition Valencia Spain 2008.
7. Nielsen, R G. Optimering af Lav Temperatur Cirkulerende Fluid Bed forgasningsprocessen til biomasse med højt askeindhold. Ph.D. Thesis, Technical University of Denmark, Dept. of Mech. Eng., Energy Eng. Section, 2007: ISBN No.: 978-87-90130-15-2.

2 Literature Survey

2.1 Behavior of inorganic elements in straw under reducing conditions

The transformation of the major inorganic species in straw during pyrolysis and gasification is reviewed in this section.

Table 2-1 Mass fraction of various inorganic elements in typical Danish Wheat Straw

Ash Content (% wt.)	4.52 %
Species in the fuel	**% (wt.)**
Al	0.037
Ca	0.36
Fe	0.025
K	0.71
Mg	0.073
Na	0.024
P	0.077
S	0.092
Si	1.6
Cl	0.21

Table 2-1 shows the inorganic elemental composition of Danish wheat straw. Straw is found to have high contents of K, Si and Ca with some Cl and S. In this chapter, the thermal behavior of the major inorganic constituents, K, Si, Cl and S during pyrolysis and gasification of wheat straw is reviewed. Concerning the fact that the present work involves a study of low temperature gasification systems, the thermal behavior of the elements are reviewed at maximum temperatures of around 800^0C. To begin with, the probable nature and state of the ash forming species within wheat straw is discussed.

2.1.1 Occurrence of the inorganic elements (K, Si, Cl and S) in Straw

Information on the occurrence of the inorganic elements in straw can be obtained from chemical fractionation analysis of straw. Chemical fractionation techniques involved leaching of the material (straw) with demonized water and then by 1M ammonium acetate solution followed by 1M HCl [1]. The solubility of the inorganic elements in the various solvents used in the CF procedure provides insight on the nature of the occurrence of the elements in the fuel. The easily leachable elements (such as alkali sulfates, carbonates, chlorides and earth alkali chlorides) are supposed to be leached from the fuel in the first step using demonized water [1]. The ion

exchange sites of carboxylic acids (organically associated elements in the fuel) are separated by ammonium acetate. The alkali earth carbonates and sulfates are removed by hydrochloric acid. The sample that remains behind after the fractionation, is supposed to contain silicates and insoluble minerals.

As seen in literature [1], about 80-90% of the K and Cl were removed by leaching with demonized water and ammonium acetate solution. Only a marginal fraction of the potassium (10%) was not extractable with mineral acid and this fraction could be bound by silicates. This implied that the elements occurred mainly as easily soluble salts or loosely bound to organic exchange sites. The above interpretations agrees with plant physiology studies [2] according to which, chlorine and potassium are in the form of free ions in solution within the plants. Following harvest, Cl and K in solution is likely to precipitate as salts or become attached to charged groups in the organic matrix as the drying process progresses.

Sulfur is present in straw as both inorganic sulfate (ionic form) and organically associated sulfur of aliphatic nature [3]. S is taken from the roots in the form of sulfates by the plants [4]. The sulfates are incorporated into the organic structure of the plant via transformation into the basic amino acids cysteine and methionine, from which plant protein is synthesized. Excess sulfate in the soil is absorbed by the plant roots and either stored as sulfate esters or emitted in a reduced form, such as H_2S.

Silicon is present in relatively high concentrations (1.6% by wt.) in straw (Table 2.1). Silicon is suggested to be present in the form of a silicate network structure of hydrated silicon oxide ($SiO_2 \cdot nH_2O$) in the cell walls [2]. It was seen that silica was not removed from the straw on leaching [5] which indicates that silicon is immobile.

The following section involves the discussion on the thermal behavior of the inorganic species in straw, under reducing conditions. To begin with, the behavior of K species under reducing conditions is discussed.

2.1.2 Behavior of K species under reducing conditions

As suggested in literature [6], during pyrolysis, upon heating and de-volatilization, K^+ ions in solution and bound to organic molecules of low thermal stability, precipitate as inorganic salts or become ion-exchanged to functional groups in the char matrix or are intercalated into the char matrix. The inorganic salts such as KCl,

K_2CO_3, and K_2SO_4 in the biomass migrate to form discrete grains in the pores and on the surface of the char particles, possibly through a liquid tar phase [6]. K could also be bound to tar which were found to be predominantly water soluble and probably in the form of derivatives of COOH and OH groups.

Figure 2-1 summarizes pathways for K release and transformation during gasification of biomass. Measurements in literature [6-8] have shown a low release of K (less than 10% of K in the fuel) at temperatures less than 700^0C. This release was suggested to be due to the decomposition of the K bonded to the organic matrix as shown in Figure 2-1. At these temperatures, the vapor pressures of K salts are too low to allow them to be released in significant quantities [7]. During the pyrolysis process, K as inorganic salt KCl is also suggested to interact with proton donating sites in the char matrix and form char-K as shown in Figure 2-1. At temperatures within 700-800^0C, under combustion conditions, some K was released due to initiation of KCl vaporization due to high saturation vapor pressures of KCl above 700^0C [7] (Figure 2-1).

The initial release pattern of K at low temperatures (<700^0C) was observed to be very limited and similar at both pyrolysis and combustion conditions as shown in Figure 2-2 [7]. A slower release and thereby a shift towards higher temperatures (by around 200^0C) for release of K as KCl was observed for pyrolysis as compared to combustion as can be seen from Figure 2-2 [7]. One of the possible reasons for the lower K release was suggested to be due to a higher diffusional resistance during pyrolysis caused by the still partially intact organic matrix which thus demands higher residence times for K release. Measurements by Knudsen et al. [7] supported the above observation which showed K volatilization to increase with increase in residence times during pyrolysis of straw.

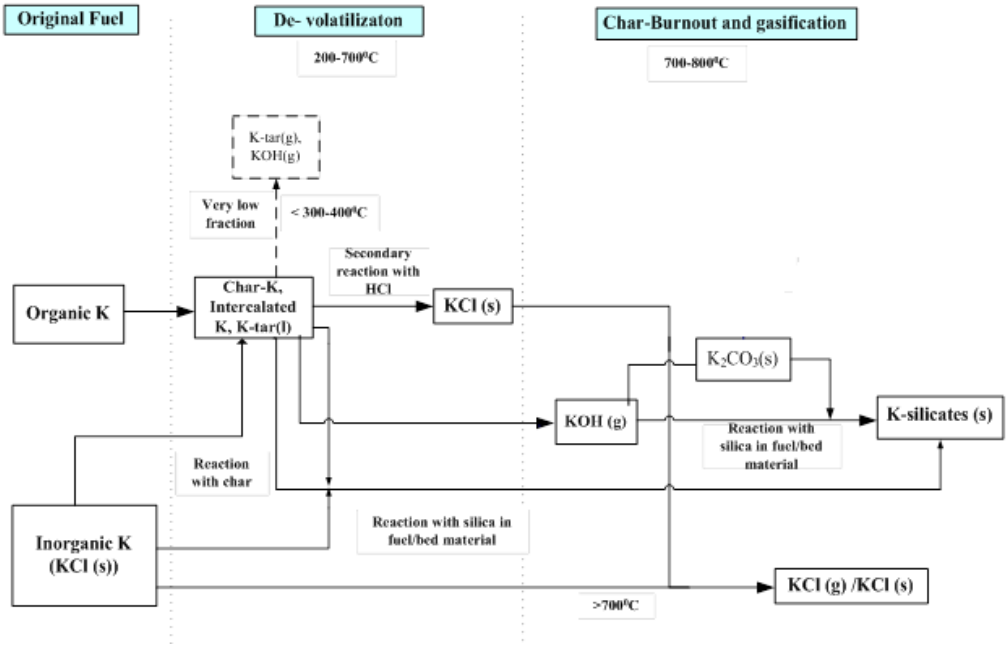

Figure 2-1 Possible reaction paths and release mechanisms of K during devolatilization and gasification

Above 700^{0}C, after biomass de-volatilization, in addition to release of K as KCl (g) (as mentioned earlier), K could also be released from the char matrix due to oxidation or gasification with steam [6-8] (Figure 2-1). Some released K may combine with silica from straw or present in the bed material to form K-silicates as shown in Figure 2-1. Such retention reactions of K are favored at higher temperatures during char burnout where the organic matrix collapses thereby bringing K and Si in closer contact. K released could also form K_2CO_3 though K is suggested to be thermodynamically favored to be retained as silicates rather than carbonates for silica rich fuels such as straw [7]. K organically bound to the char matrix could also react with silica in the fuel and in the bed material to form silicates as shown in Figure 2-1.

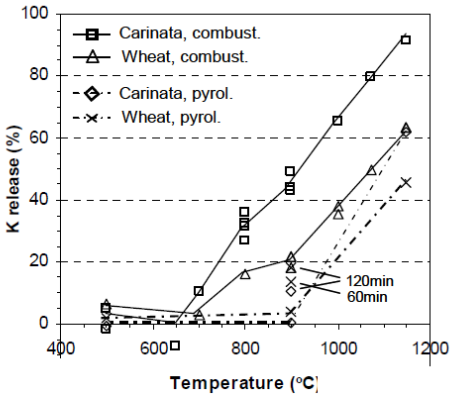

Figure 2-2 Comparison of K-release during pyrolysis and combustion. Except where noted, the pyrolysis time was 25 min [7]

2.1.3 Behavior of Cl species under reducing conditions

It was seen in literature [2] that 90% of Cl in the fuel was leached by demonized water. This thus shows that 90% of Cl in the biomass are water soluble and thus present in ionic form.

Figure 2-3 summarizes pathways for Cl release during biomass gasification. Saleh et al. [9] found 64% chlorine to be released from straw during pyrolysis at 350°C. The measurements by Saleh [9] showed the released chlorine to be dominated by methyl chlorides as shown in Figure 2-3. Measurements by Egsgaard et al. [10] have also shown release of methyl chloride beyond 200^0C. Some Cl may also be released above 400^0C as HCl probably by reaction of KCl with proton donating sites in char as shown in Figure 2-3 [11]. Cl as HCl may also be recaptured during pyrolysis by secondary reactions [6,7] and precipitate as KCl on char particles (Figure 2-3). As mentioned earlier, at temperatures >700 °C, the vapor pressure of KCl increases significantly and the evaporation of KCl becomes the main pathway for the release of Cl from biomass as shown in Figure 2-3. During char burnout, some methyl chloride could form HCl by oxidation.

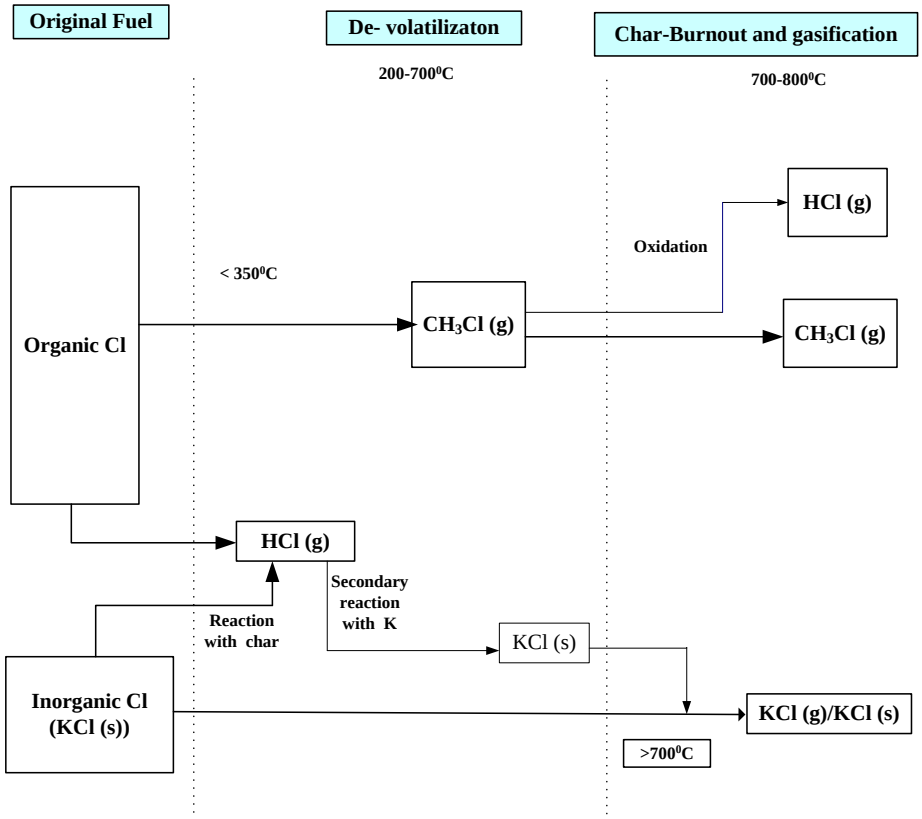

Figure 2-3 Possible reaction paths and release mechanisms of Cl during devolatilization and gasification.

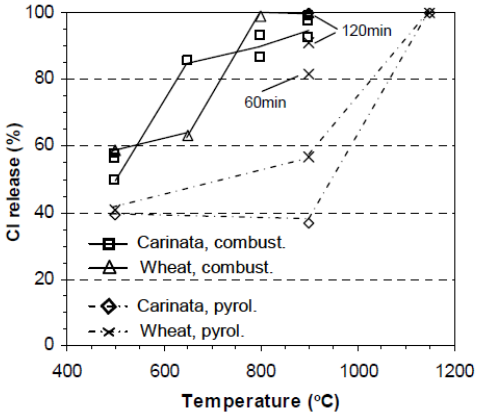

Figure 2-4 Comparison of Cl-release during pyrolysis and combustion. Except where noted, the pyrolysis time was 25 min [7].

The low temperature release behavior of Cl (< 500^0C) was found to be nearly similar at both pyrolysis and combustion of the biomass as shown in Figure 2-4 [7]. At higher temperatures (>700 °C), the release of Cl was found to be slower in case of pyrolysis as compared to the release in combustion. As mentioned earlier, the slow release rate in case of pyrolysis could be due to high diffusion resistance offered by the partially intact organic matrix [7]

2.1.4 Behavior of S species under reducing conditions

Figure 2-5 summarizes pathways for S release during biomass gasification. As mentioned earlier, sulfur was found to be partly associated as inorganic sulfate (40-50% of the total S) and partly as organic sulfur (50-40%) in Danish wheat straw [3]. S was found to be released in two steps. Saleh et al. [9] found that 60 % of sulfur was released at 500^0C. The low temperature release of sulfur was suggested to be due to decomposition of organically associated sulfur in the fuels [3]. The fraction of sulfur release at these temperatures was thus found to be strongly dependent on the fraction of organic sulfur present in the fuel. S could be released as H_2S or COS under pyrolysis conditions as shown in Figure 2-5. A part of the initially released sulfur may react with functional groups in the char under pyrolysis conditions and become retained in the char matrix [3] (Figure 2-5).

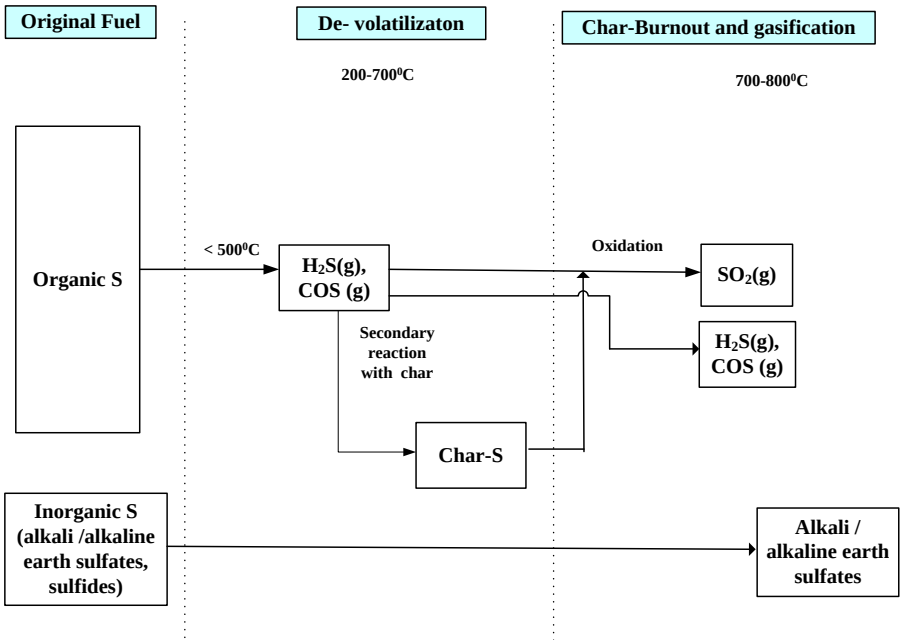

Figure 2-5 Possible reaction paths and release mechanisms of S during devolatilization and gasification

The initial release of sulfur (< 500^{0}C) has been observed to be similar for both pyrolysis and combustion of straw as shown in Figure 2-6. No further release was observed in pyrolysis of straw at high temperatures. During combustion, further release of S was observed above 850^{0}C, due to the conversion of alkali sulfates to silicates thereby releasing SO_2. During char burnout, some H_2S and COS could form SO_2 by oxidation as shown in Figure 2-5. It has been observed [3] that alkali and alkaline earth sulfates are not stable at reducing conditions (in contrast with oxidizing conditions wherein they are found stable as shown Figure 2-5).

The present thesis involves the study of ash transformation in LTCFB system. It is desirable to understand the mechanism of transformation of the major ash forming species, K, Si, Cl and S in the LTCFB system since the ash speciation influences bed sintering and release of inorganic species with the exit gas. The literature study on the behavior of K, Cl and S in reducing conditions below 800^{0}C (lower temperatures were considered for the study since the present work involves low temperature gasification) is helpful in analysis of the ash transformation in LTCFB system. The analysis results are explained later in the thesis.

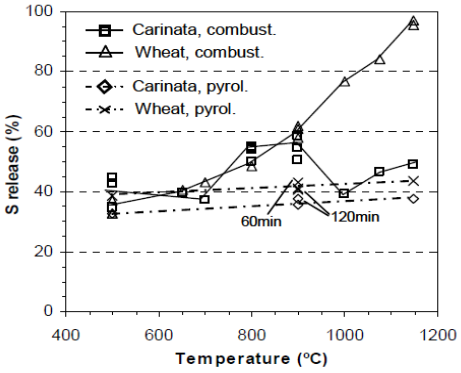

Figure 2-6 Comparison of S-release during pyrolysis and combustion. Except where noted, the pyrolysis time was 25 min [7]

2.2 Defluidization in fluidized bed biomass gasifiers

A major problem often encountered in fluidized beds is bed agglomeration, which may result in total de-fluidization, leading to unscheduled downtime and additional costs. This problem is found to be critical in fluidized bed combustion and gasification of biomass fuels which have high ash and alkali contents [12]. Biomass fuels, especially herbaceous plants, often contain significant amounts of silicon, potassium and calcium, together with chlorine and sulphur. These elements tend to form viscous melts which adhere on the surface of the colliding bed particles. When the sticky bed particles collide, the viscous material at the point of contact migrates forming a neck, thus binding the particles to form agglomerates. This phenomenon is called viscous flow sintering. The temperature at which the process of sintering initiates to form agglomerates is called the initial sintering temperature, T_s. As the process continues, the agglomerates increase in size and de-fluidization takes place. As per the Geldart's classification [13], the particles tend to change to Class C type that is difficult to fluidize. This difficulty arises due to inter-particle forces (adhesive forces) which are greater than those the fluid motion can exert on the particles. The phenomenon of agglomeration is believed to occur through two mechanisms [3, 4]:

- Melt-induced agglomeration: Inorganic salts present in the fuel ash melt and the melts then act as necks to bind the bed particles to form agglomerates. This mechanism does not involve any chemical reaction between the ash species and the bed material.
- Coating-induced agglomeration: Viscous melts are formed due to reaction of inorganic species, from the fuel ash, with the bed material. The melts form a coating layer around the bed particles, making them sticky and adhesive. On intermittent collisions, the sticky coated bed particles bind with each other leading to the formation of agglomerates

Measurements reported in literature on de-fluidization in fluidized bed biomass gasifiers elucidate the role of alkali and alkaline earth species in the agglomerates formed during the process. Fryda et al. [12] and Mac an Baird et al. [14] observed necks between coated agglomerated bed particles, rich in alkali and silicon, in fluidized bed gasifiers for herbaceous fuels (wheat straw). Ghaly et al. [15], Andersson et al. [16], Onderwater et al. [17,18], Steenari et al. [19, 20], and Liu et al. [21] found similar results in their studies using wheat straw. The reported measurements showed that the temperatures at which de-fluidization occurred differed among fuels with varying composition of inorganic species. Thus, the concentration and chemistry of inorganic elements strongly influence the formation of agglomerates and subsequent de-fluidization inside the fluidized bed biomass gasifier. For this reason it is imperative to conduct an explicit study on the behavior of the inorganic species and their sensitivity to process parameters on de-fluidization in fluidized bed systems.

There have been numerous approaches made in developing mathematical models to predict the bed agglomeration and de-fluidization in fluidized bed systems. A summary of some of the proposed models of bed agglomeration/de-fluidization is provided by in Table 2-2. The description of the symbols used in Table 2-2 is provided in Table 2-3.

Table 2-2 Model studies in literature on bed agglomeration and de-fluidization

Author	Model Equation
Moseley et al. [22]	$U_{mfs} = U_{mf} + C_3 \rho_p{}^{q_1} \rho_f{}^{q_2} \mu_f{}^{q_3} (T - T_s)^{q_4}$
Ennis et al. [25]	$St^*{}_D = 8\rho\alpha \left(\frac{(U_{mfs} - U_{mf0})a}{9\mu}\right)^{1/2} = \left(1 + \frac{1}{e}\right) (\ln(h) - \ln(h_a))$
Tardos et al. [27],[28]	$\frac{(U_s - U_{mf})}{U_{mf}} = k_3 [\frac{(1-\epsilon)}{\epsilon^2}] (\frac{d_{ag}^{\frac{7}{4}} d_b^{\frac{1}{2}}}{d_B^{\frac{1}{2}} D_p^{\frac{3}{2}}}) (\frac{\rho_g \sigma_s}{\emptyset \rho_s \mu_s g^{1/2}})^{1/2}$
Zhong et al.[29]	$F_d = \frac{C\pi b^2 t}{d_p \mu_s}$
Basu et al. [30]	$U_{mfs} = \frac{1}{1650} \frac{{d_p}^2 g}{\mu_g} \left(\rho_p - \rho_g + \frac{\psi(T, H_b, d_p)}{(1-\varepsilon)}\right)$ $\psi(T, H_b, d_p) = K(T - T_s) f_1(d_p) f_2(H_b)$ Where, $T_s = f_3(d_p, H_b)$ *and* $f_3(d_p, H_b)$ $\psi(T, H_b, d_p) = 0$ at $T \leq T_s$
Lin et al. [32]	$t_{def} = C \left(\frac{(U - U_{mf})}{(d_p)}\right)^{1/2} exp \frac{(E_\mu)}{(RT)}$
Lin et al. [33]	$t_{def} = C \left(\frac{1}{(f_N \psi_N)}\right) \left(\frac{M^k}{(d_p)}\right)^{1/4} exp \frac{(E_\mu)}{(RT)}$ $M = 0.67(1 - \varepsilon_{mf}) \rho_p \left(\frac{1}{\emptyset} - 1\right) (U - U_{mf})$ $\emptyset = \{1 - 0.3\exp[-8(U - U_{mf})]\} \exp(-\beta H_b)$ $\beta = 7.2\{(U - U_{mf})\} \exp(-4.1(U - U_{mf}))$

Table 2-3 Description of symbols used in Table 2.2

a	Particle or granule radius	µm
b	Neck radius of the coating layer around the two particles in an agglomerate	m
d_b	Bubble diameter	m
D_p, d_p	Particle diameter	m
d_{ag}	Diameter of the agglomerate	m
F_d	Adhesive force	N
H_b	Bed Height	m
h	Binder layer thickness covering colliding granules	µm
h_a	Characteristic length scales of surface asperities	µm
M	Mass flow per unit bed area	kg/m^{2}s
St_D^*	De-fluidization Stokes Number	Dimensionless
t	Time taken for the particles to agglomerate	M
t_{def}	De-fluidization time	s
T	Temperature within the fluidized bed	^{0}C
T_s	Initial Sintering Temperature	^{0}C
U	Superficial velocity of fluidizing gas	m/s
U_{mf} , U_{mf0}	Minimum fluidization velocity	m/s
U_{mfs}	Minimum fluidization velocity	m/s
U_s	Limiting velocity to break the largest agglomerate in the bed	m/s
α	Thickness of coating Layer	m
μ_f, μ_g	Viscosity of fluidizing gas	kg/ms
μ_s	Surface viscosity of solid iron	kg/ms
μ	Binder viscosity	kg/ms
e	Coefficient of restitution	Dimensionless
$f_1, f_2, f_3, \beta, \psi$	Different functions	
σ_s	Yield strength of the neck within the agglomerate	N/m^2
ϵ	Porosity in the fluidized Bed	Dimensionless
$q_1, C, C_3, q_2, q_3, q_4, K, k_3, k$	Constants	Dimensionless
f_N	Mass fraction of Na in bed material	Dimensionless
ρ_p, ρ_s, ρ	Density of the bed particles in the fluidized bed	kg/m^3
ρ_f, ρ_g	Density of the fluidizing gas	kg/m^3
$\emptyset$	Shape Factor	Dimensionless
ψ_N	Mass of Na fed per unit time	kg/s

The models shown in Table 2-2 in general predict the change in parameters such as minimum fluidization velocity of the gas in the fluidized beds, above the initial sintering temperature. Some models also predict the time of de-fluidization of the bed particles as a function of various parameters such as temperature and particle diameters. Moseley et al. [22] used a two particle collision model to estimate the minimum superficial velocity needed to avoid de-fluidization of coal ash particles due to agglomeration at temperatures above the initial sintering temperature T_s. The values of T_s for coal ash were obtained from the dilatometer tests made by Siegell et al. [23]. The model assumption is that when the energy dissipated by the binding (adhesive) force between two particles during recoil exceeds the initial kinetic energy of the colliding particles, the particles agglomerate. With the above criterion, using the two particle collision model and a model for the granular energy of the particles in the bed, a correlation for the de-fluidization velocity as a function of temperature was developed.

The binding force was assumed to be proportional to the contact surface area between the two particles and the constant of proportionality was introduced as K_A, the adhesiveness coefficient. An empirical correlation for K_A as a function of temperature was developed using the experimental data from Liss et al. [24]. The adhesive force in the model was thus not related to material properties but a function of temperature alone. Apart from the uncertainties in the model due to simplifications and assumptions made in the particle dynamics calculations, the model does not explain the effect of particle properties (composition and size) on de-fluidization.

Ennis et al. [25] followed a similar principle to estimate the modified minimum fluidization velocity of the agglomerated granular particles, bound by a viscous liquid binder. Similar to Moseley et al.[22], Ennis et al. [25] also proposed a two particle collision model wherein the particles agglomerate if the energy dissipated by the viscous adhesive force exerted by the binder during recoil exceeds the initial kinetic energy of the colliding particles. Ennis et al. [25] used a critical Stokes number (ratio of collisional kinetic energy of the particles to the viscous dissipation brought about by interstitial binder) and proposed the agglomeration to occur if the Stokes number is below the above critical value. The Stokes number was expressed as proportional

to the difference between the modified minimum fluidization velocity of the particles with the viscous binder and the initial minimum fluidization velocity without the viscous liquid. The proportionality terms were obtained by regression using experimental data from Gluckman et al. [26]. Apart from the uncertainties in the regressed correlation, the model did not consider the effect of temperature on the de-fluidization phenomenon.

Tardos et al. [27, 28] predicted the gas velocity, U_s, required to break the largest agglomerate in the fluidized bed and thus maintain the bed fluidized at temperatures exceeding the minimum sintering temperature, T_s. The values of T_s were obtained from the dilatometer test measurements from Siegell et al. [23]. The model was developed for two cases, one in which the particles are bound by a viscous liquid (wet agglomerates) and the other where the particles become sticky due to high temperature softening/sintering (sintered agglomerates). Tardos et al. compared the breaking forces and the adhesive forces acting on the agglomerate to develop the model. The breakage force for both cases was considered to be the shear force generated by the bubble motion on the agglomerate and was expressed as a function of the dimensions of the agglomerate and excess velocity above minimum fluidization ($U_s - U_{mf}$). The adhesive force for the wet agglomerates was developed as a function of the liquid surface tension, wetting angle and amount of liquid (degree of saturation). The adhesive force between particles with sintered surfaces at high temperatures was considered to be a function of the sinter neck yield strength which in turn was dependent on the viscosity of the granule's surface (measured by dilatometer) and the time of contact during which the sintering occurred. Apart from the uncertainties in the empirical equations developed for the forces acting on the agglomerate, the model does not explain the dependence of particle composition on de-fluidization. As claimed by Tardos et al. [27] the model may not apply for large fluidized beds where de-fluidization could occur before the agglomerate reaches the maximum size as considered in this model.

Zhong et al. [29] studied the fluidization of iron particles and proposed a model to estimate the total de-fluidization time by comparing the adhesive force and breakage force between the particles. The breakage force was assumed to be proportional to the drag exerted by the fluidizing gas on the particle. Basu et al. [30] modified Ergun's equation for a fluidized bed of coal ash by including an adhesive force in the force balance. The model predicted a higher minimum fluidization velocity beyond the initial sintering temperature,

T_s, by correlating the adhesive forces with excess temperature ($T - T_s$). The values of T_s for coal ash were obtained from the dilatometer tests made by Siegell et al. [23]. The adhesive force between the particles was considered to be a function of bed temperature, particle diameter and bed depth. The exact form of the function for the adhesive force however was not provided in the study. The model was thus a qualitative one which could predict that the bed de-fluidizes at velocities even above the minimum fluidization velocity determined from Ergun's equation. The model was also fundamentally flawed as pointed out by Seville et al. [31] as under conditions of fluidization, the pressure drop across the bed must equal the weight of the particles per unit area independent of the interparticle forces.

The above force balance approach and statistical analysis were employed for non-biomass feeds. The force balance approach was also extended to develop models to predict de-fluidization in fluidized bed biomass combustion/gasification systems. Lin et al. [32] proposed a model for de-fluidization in fluidized bed combustors for wheat straw. The model involved a correlation for de-fluidization time as a function of parameters such as temperature, fluidization velocity and particle size by comparing the adhesive force between the particles with the breakage force. The particles were considered to be bound due to the viscous coating layer of potassium silicates around the particles forming necks between them. The adhesive forces were assumed to be proportional to the tensile strength of the coating layer between the particles which in turn was assumed to be proportional to time and inversely proportional to the viscosity of the coating. The breakage force was considered to be due to shear force induced by bubbles and was assumed to be proportional to the difference between the operational velocity of the gas and the minimum fluidizing velocity of the gas. The viscosity of the silicate melts was assumed to follow an Arrhenius relationship with temperature. Later Lin et al. [33] modified the model so that the breakage force was represented by the average convective solid mass flow per unit bed area which was a function of the static bed height, the porosity of the bed, the bubble shape and the gas velocity. These models for de-fluidization however do not explicitly predict the influence of the inorganic species composition in the fluidized bed on de-fluidization. As mentioned earlier, the concentration and chemistry of inorganic elements strongly influence the formation of agglomerates and subsequent de-fluidization inside the fluidized bed reactor. The present work involves development of a model

that addresses the effect of concentration of the inorganic (alkali) species on thickness and viscosity of the coating layer around the particles and the influence of variation in concentration of these species on de-fluidization.

2.3 References:

1. Pettersson A, Zevenhoven M, Steenari M B, Amand L E, Application of chemical fractionation methods for characterization of biofuels, waste derived fuels and CFB co-combustion fly ashes, Fuel 2008; 87:3183-3193.
2. Marschner, H. Mineral nutrients in higher plants. 2nd edition, Academic Press, London 2002, 229-404.
3. Knudsen J N, Jensen P A, Lin W, Frandsen F J, Dam-Johansen K. Sulfur tranformations during thermal conversion of herbaceous biomass.Energy and Fuels 2004;18:810-819.
4. Rennenberg H, Brunold C H, De Kok L J, Stulen I. Sulfur nutrition and sulfur assimilation in higher plants. SBP Academic Publishing: The Hague, Netherlands, 1990;3-76.
5. Jenkins B M, Bakker R R, Wei J B. On the properties of washed straw. Biomass and Bioenergy 1996;10:177-200.
6. Jensen P, Frandsen F, Dam-Johansen K. Experimental investigation of the transformation and release to gas phase of potassium and chlorine during straw pyrolysis. Energy and Fuels 2000;14:1280–1285.
7. Knudsen J N, Jensen PA, Dam-Johansen K. Transformation and release to the gas phase of Cl, K, and S during combustion of annual biomass. Energy and Fuels 2004;18:1385–99.
8. Johansen J M, Jakobsen J G, Frandsen F J, Glarborg P. Release of K, Cl, and S during pyrolysis and combustion of high-chlorine biomass. Energy and Fuels 2011;25:4961–71.
9. Saleh S B, Flensborg J P, Shoulaifar T K, Sárossy Z, Hansen B B, Egsgaard H, Dermatini N, Jensen P A, Glarborg P, Johansen K D. Release of chlorine and sulfur during biomass torrefaction and pyrolysis. Energy and Fuels 2014;28:3738–46.
10. Egsgaard, H, Ahrenfeldt J, Henriksen U.B. On the Significance of Methyl Chloride in Gasification Processes.18th European Biomass Conference and Exhibition, Lyon, France 2010.

11. Björkman, E, Strömberg B. Release of Chlorine from Biomass at Pyrolysis and Gasification Conditions. Energy & Fuels 1997; 11:1026-1032
12. Fryda LE, Panopoulos KD, Kakaras E. Agglomeration in fluidised bed gasification of biomass. Powder Technol 2008;181:307–20.
13. Geldart D. Types of gas fluidization. Powder Technol 1973;7:285–92
14. Mac an Bhaird ST, Walsh E, Hemmingway P, Maglinao AL, Capareda SC, McDonnell KP. Analysis of bed agglomeration during gasification of wheat straw in a bubbling fluidised bed gasifier using mullite as bed material. Powder Technol 2014;254:448–59.
15. Ergudenler A, Ghaly AE. Agglomeration of silica sand in a fluidized bed gasifier operating on wheat straw. Biomass Bioenergy 1993;4:135–47.
16. Olofsson G, Ye Z, Bjerle I, Andersson A. Bed Agglomeration Problems in Fluidized-Bed Biomass Combustion. Ind Eng Chem Res 2002;41:2888–94
17. Zevenhoven-Onderwater M, Backman R, Skrifvars BJ, Hupa M, Liliendahl T, Rosén C, et al. The ash chemistry in fluidised bed gasification of biomass fuels. Part I: Predicting the chemistry of melting ashes and ash-bed material interaction. Fuel 2001;80:1489–502.
18. Zevenhoven-Onderwater M, Backman R, Skrifvars BJ, Hupa M. The ash chemistry in fluidised bed gasification of biomass fuels. Part II: Ash behaviour prediction versus bench scale agglomeration tests. Fuel 2001;80:1503–12.
19. Steenari B-M, Lundberg A, Pettersson H, Wilewska-Bien M, Andersson D. Investigation of Ash Sintering during Combustion of Agricultural Residues and the Effect of Additives. Energy Fuels 2009;23:5655–62
20. Olanders B, Steenari B-M. Characterization of ashes from wood and straw. Biomass Bioenergy 1995;8:105–15.
21. Liu H, Feng Y, Wu S, Liu D. The role of ash particles in the bed agglomeration during the fluidized bed combustion of rice straw. Bioresour Technol 2009;100:6505–13

22. Moseley JL, Obrien TJ. A Model for Agglomeration in a Fluidized-Bed. Chem Eng Sci 1993;48:3043–50.
23. Siegell JH. High-Temperature Defluidization. Powder Tech 1984;38:13–22.
24. Liss B, Blake TR, Squires AM, Bryson R. Incipient defluidization of sinterable solids. In: Kunii D, et al. (Eds). Fluidization IV 1984: 249–56.
25. Ennis BJ, Tardos G, Pfeffer R. A microlevel-based characterization of granulation phenomena.Powder Tech 1991;65:257-272.
26. Gluckman MJ, Yerushalmi J, Squires AM. Defluidization characteristics of sticky materials on agglomerating bed, Fluidization Technology**,** Vol. II (Keairns (ed.) DL.).1976; 395-422.
27. Tardos G, Mazzone D, Pfeffer R. Destabilization of Fluidized Beds Due to Agglomeration Part I : Theoretical Model. Can J Chem.Eng 1985;63:377-83.
28. Tardos G, Pfeffer R. Destabilization of Fluidized Beds Due to Aqqlomeration Part II: Experimental Verification. Can J Chem.Eng 1985;63:384-89.
29. Zhong Y, Wang Z, Guo Z, Tang Q. Defluidization behavior of iron powders at elevated temperature: Influence of fluidizing gas and particle adhesion. Powder Technol 2012;230:225–31.
30. Basu P. A study of agglomeration of coal-ash in fluidized beds. Can J Chem Eng 1982;60:791-795.
31. Seville JPK, Silomon-Pflug H, Knight PC. Modelling of sintering in high temperature gas fluidisation. Powder Technol 1998;97:160–9
32. Lin W, Dam-Johansen K, Frandsen F. Agglomeration in bio-fuel fired fluidized bed combustors. Chem Eng J 2003;96:171–85.
33. Lin C-L, Wey M-Y, Lu C-Y. Prediction of defluidization time of alkali composition at various operating conditions during incineration. Powder Technol 2006;161:150–7.

3 Behavior and transformation of inorganic species in a Low Temperature Circulating Fluidized Bed (LTCFB) Gasifier.

This chapter summarizes an article submitted for publication in Energy and Fuels Journal, entitled 'The behavior of alkali metals and ash in a Low Temperature Circulating Fluidized Bed (LTCFB) Gasifier'. The article is provided in Appendix A.1.

A Low-Temperature Circulating Fluidized Bed System (LTCFB) gasifier allows pyrolysis and gasification to occur at low temperatures, thereby improving the retention of alkali and other inorganic elements within the system and minimizing the amount of ash species in the product gas. In addition, the low reactor temperature ensures that high-alkali biomass fuels can be used without risk of bed de-fluidization. This paper presents the first investigation of the fate of alkali metals and ash in low-temperature gasifiers. Measurements on bed material and product gas dust samples were made on a 100 kW and a 6 MW LTCFB gasifier. Of the total fuel ash entering the system, the largest fraction (40-50%) was retained in the secondary cyclone bottoms while a lower amount (8-10%) was released as dust in the exit gas. Most of the alkali and alkaline earth metals were retained in the solid ash, along with Si and a minor fraction of the Cl. Most Cl and S were released in gaseous form, chlorine partly as methyl chloride. The tar in the product gas from the LTCFB gasifier contained only negligible amounts of potassium and other inorganic elements. The release of condensed ash species from the system was controlled by the particle size and the cut size of the primary and secondary cyclones. A model accounting for the ash collection by the plant cyclones was shown to predict the product gas ash particle release reasonably well.

4 Defluidization in Fluidized Bed Gasifiers Using High-Alkali Content Fuels

This chapter summarizes an article submitted for publication in Biomass and Bioenergy Journal, entitled 'Defluidization in Fluidized Bed Gasifiers Using High-Alkali Content Fuels'. The article is provided in Appendix A.2.

A major concern in thermal conversion of biomass encountered in fluidized beds is bed agglomeration, which may result in de-fluidization, leading to unscheduled downtime and additional costs. Biomass fuels, especially herbaceous plants, often contain dominant amounts of silicon, potassium and calcium, which may form viscous melts that adhere on the surface of the colliding bed particles and bind them to form agglomerates. This chapter deals with studies made to understand the behavior of inorganic elements (mainly K, Si and Ca) on agglomeration and de-fluidization of alkali rich bed-material samples under non-oxidizing conditions in a bench-scale fluidized bed reactor set up. The de-fluidization studies involved measurements with sand and pure potassium salts (KCl and K_2CO_3) as well as with bed material samples obtained from a 6 MW Low Temperature Circulating Fluidized Bed (LT-CFB) gasifier using straw as a fuel. It was seen that in sand + KCl agglomerates, the sand particles were bound by KCl melts. There was no chemical reaction observed between KCl and the sand particles. In sand + K_2CO_3 mixtures and the LT-CFB bed material samples, the agglomeration was seen to occur due to the viscous silicate melts formed from reaction of inorganic alkaline and alkali earth species with silica from the bed particles. A mathematical model that addresses the de-fluidization behavior of the alkali rich samples was developed based on the experiments performed in the bench-scale fluidized bed reactor as well as on results from literature. The model studies were then extended to predict the de-fluidization behavior of alkali rich bed material in a large-scale LTCFB gasifier.

5 Conclusions

A Low-Temperature Circulating Fluidized Bed System (LTCFB) gasifier allows pyrolysis and gasification to occur at low temperatures thereby improving the retention of alkali and other ash species within the system and minimizing the amount of ash species in the product gas. In addition, the low reactor temperature ensures that high-alkali biomass fuels can be used without risks of bed de-fluidization. The LTCFB gasifier has been tested in both bench scale and pilot scale with promising results. However, little is known about the partitioning of the inorganic elements in the system or the release of K, Cl, and S with the product gas. The objective of this study is to obtain an improved understanding of the transport and transformation of inorganic elements within a low temperature circulation fluid bed system. Furthermore, it is wanted to obtain an improved understanding of the conditions that would lead to de-fluidization in a LTCFB system.

To investigate the ash behavior, the ash release with the product gas was quantified through particle measurements on a 100kW and a 6 MW gasifier, respectively. In addition, secondary cyclone ash bottoms and bed material samples from the gasifiers were collected and analyzed with respect to their inorganic elemental composition. For the mass balance on the system, it was imperative to estimate the total volumetric flow rate of the product gas leaving the gasifier. A direct estimation of the flow rate was difficult as the composition of the product gas was unknown. For the 100 kW LTCFB gasifier, an inert gas (argon) was injected and from a balance on the argon in the system, the total output volumetric flow rate of the gas was calculated. At the 6 MW plant where this method would require prohibitively large amounts of argon, the total exit gas flow and mass of dust particles were estimated by a rough mass balance on the inert solids in the system. The mass balance studies in this work could be further enhanced in future by performing measurements for estimation of species circulating within the LTCB system and concentration of gaseous species leaving the gas stream.

It was seen that of the total ash that enters the system with the fuel, 45-50% was retained by the secondary cyclones and a lower amount (8-10%) was released as dust in the exit gas. The collected cyclone bottom particles and product gas dust particles showed the samples to be dominated by inorganic ash forming species

(45-50%) and char (35-40%), the rest being organic volatiles. Furthermore, it was seen that a large fraction of alkali and alkaline earth metals were retained in condensed state in the LTCFB system along with Si, while most Cl and S were released in gaseous form. The major forms in which K and Si could exist in the LTCFB gasifier are K-salts (KCl and K_2CO_3), organically bound K (K bound to ion exchange sites of the char matrix and intercalated K), and K-silicates. At the temperature in the pyrolysis chamber (650^0C), the above K species are expected to be mostly in the solid state. K-silicates could be formed in the pyrolysis reactor due to reaction of silica present in the fuel and in the bed material with organically bound K and K_2CO_3, though the reaction is limited by kinetic and mass transfer limitations. In the char reactor (at temperatures around 730^0C), KCl(s) would start vaporizing. When flue gas enters the pyrolysis reactor, the temperature is reduced and KCl aerosols are formed. Chlorine in the form of methyl chloride is released from the biomass when heated at temperatures > 200^0C; presence of this species is confirmed by the measurements on the LTCFB gasifier. Chlorine may also be released as HCl (g), which could be re-captured either by K-salts such as K_2CO_3 or K in the char matrix (Char-K).

The release and retention of solid particles from the system is controlled by the particle size and the cut size of the primary and secondary cyclones. A cyclone model was developed to study the role of the cyclones for ash release and retention in the LTCFB system. Modeling predictions for the fraction of ash retained in the cyclone bottoms and entrained with the exit gas, respectively, agreed favorably with measured values for the 100 kW and 6 MW gasifiers. .

In this work, the effect of biomass fuel ash composition and fluid bed operation conditions on agglomeration and de-fluidization under gasification conditions was investigated. It is of interest to increase the temperatures in the LTCFB gasifier to improve the capacity but still keeping the temperature a level where gas phase alkali release is prevented. Such an increase in temperature of the fluidized bed system containing alkali and silica rich ash particles could however pose risks of de-fluidization. It was therefore useful to understand the de-fluidization behavior of the LTCFB gasifier, with respect to temperature and varying alkali concentrations. De-fluidization laboratory studies involved measurements with sand and pure potassium salts (KCl and K_2CO_3) as well as bed material samples obtained from a 6 MW LTCFB unit.

The mechanism of agglomeration in the bed particles was seen to vary with the nature of K. It was seen that in sand and KCl experiments that, the sand particles were bound by KCl melts. There was very limited chemical reaction observed between KCl and the sand particles with no presence of silicate melts in the agglomerates. In experiments with sand + K_2CO_3 mixtures and the LT-CFB bed material samples the agglomeration was seen to occur due to coating of viscous silicate melts formed from reaction of alkaline and alkali earth species with silica from the bed particles (coating induced agglomeration). It was also seen that the composition of the bed particles affected the de-fluidization temperatures. The de-fluidization took place at higher temperatures in the case of LTCFB bed material particles (780-785^{0}C) as compared to the sand and K_2CO_3 mixtures (730^{0}C) with similar K contents (4.2-4.5%), though in both cases the de-fluidization occurred by the mechanism of coating induced agglomeration. This is attributed to the presence of Ca and Mg; these elements shift the formation of the eutectic melts to higher temperatures increasing the viscosity levels of the coatings. A mathematical model for de-fluidization of alkali rich bed material was developed to predict the de-fluidization temperatures as a function of parameters such as initial alkali concentration, particle diameter and fraction of K entrained from the system. The model was also applied to study the de-fluidization behavior of the large scale LTCFB gasifier. The model can be used to predict the variations in de-fluidization time with respect to changed fuels and LTCFB operation parameters. The results of the present work showed that both the speciation (chlorides or silicates) and the concentration of K have a significant impact on the agglomeration and de-fluidization characteristics in the LTCFB gasifier. The model also predicted that increase in particle diameters and temperatures inside the LTCFB gasifier decreased the de-fluidization time. The present model, contrary to models available in literature, is capable of predicting influence of the speciation as well as process parameters, for coating-induced de-fluidization of alkali rich bed materials.

6 APPENDICES

A.1. Paper 1 : The behavior of alkali metals and ash in a Low Temperature Circulating Fluidized Bed (LTCFB) Gasifier

Authors: Vikas Narayan, Peter Arendt Jensen, Ulrik Birk Henriksen, Helge Egsgaard, Rasmus Glar Nielsen, Peter Glarborg.

(The article is published in Energy and Fuels journal)

energy&fuels

Article

pubs.acs.org/EF

Behavior of Alkali Metals and Ash in a Low-Temperature Circulating Fluidized Bed (LTCFB) Gasifier

Vikas Narayan,[†] Peter Arendt Jensen,[†] Ulrik Birk Henriksen,[†] Helge Egsgaard,[†] Rasmus Glar Nielsen,[‡] and Peter Glarborg*[,†]

[†]Department of Chemical Engineering, Technical University of Denmark, Building 229, DK-2800 Lyngby, Denmark

[‡]Pyroneer A/S, Nesa Allé 1, DK-2820 Gentofte, Denmark

Supporting Information

ABSTRACT: A low-temperature circulating fluidized bed system (LTCFB) gasifier allows for pyrolysis and gasification to occur at low temperatures, thereby improving the retention of alkali and other inorganic elements within the system and minimizing the amount of ash species in the product gas. In addition, the low reactor temperature ensures that high-alkali biomass fuels can be used without risk of bed defluidization. This paper presents the first investigation of the fate of alkali metals and ash in low-temperature gasifiers. Measurements on bed material and product gas dust samples were made on a 100 kW and a 6 MW LTCFB gasifier. Of the total fuel ash entering the system, the largest fraction (40−50%) was retained in the secondary cyclone bottoms, while a lower amount (8−10%) was released as dust in the exit gas. Most of the alkali and alkaline earth metals were retained in the solid ash, along with Si and a minor fraction of Cl. Most Cl and S were released in gaseous form, with chlorine partly as methyl chloride. The tar in the product gas from the LTCFB gasifier contained only negligible amounts of potassium and other inorganic elements. The release of condensed ash species from the system was controlled by the particle size and the cut size of the primary and secondary cyclones. A model accounting for the ash collection by the plant cyclones was shown to predict the product gas ash particle release reasonably well.

1. INTRODUCTION

Gasification of herbaceous-based fuels shows a large potential for power generation. Herbaceous fuels, such as wheat straw, however, contain considerable amounts of alkali metals. Even at temperatures as low as 850−900 °C, typical of conventional circulating fluidized bed biomass gasifiers, the alkali is partly volatilized and forms salts with low melting points. These salts may condense on reactor surfaces, causing fouling and corrosion of downstream equipment. Another problem with the alkali content of the fuel is that it may facilitate defluidization of the bed, with the probability increasing with the temperature.

The problems caused by the high alkali content in agricultural biomass limit the use of this important resource for energy purposes. The low-temperature circulating fluidized bed (LTCFB) gasifier has been developed to overcome these problems.[1,2] It works on the principle of gasifying biomass at lower temperatures (650−700 °C) than conventional gasification systems to restrict the release of the alkali species to the product gas. As shown in Figure 1, the LTCFB system consists of two reactors. The biomass fuel enters the first reactor, the pyrolysis chamber, where it is pyrolyzed at around 650 °C. The heat for the pyrolysis is provided by recirculated sand and ash particles from the other reactor, a bubbling bed char reactor. The pyrolysis gas, residual char, and inert particles are transported upward to the primary cyclone, which separates and recycles char and inert particles to the bubbling bed char reactor. Here, char is mixed with air and steam to undergo gasification at typically around 730 °C.[1,2] Some steam or water may also be added to improve the conversion of char and limit the reactor temperature. The produced gas and fine ash particles leave the top of the char reactor and enter the pyrolysis chamber, where the volatiles contribute to a high gas velocity in the upper part of the chamber. Heavier inert particles are recirculated to the pyrolysis chamber from the

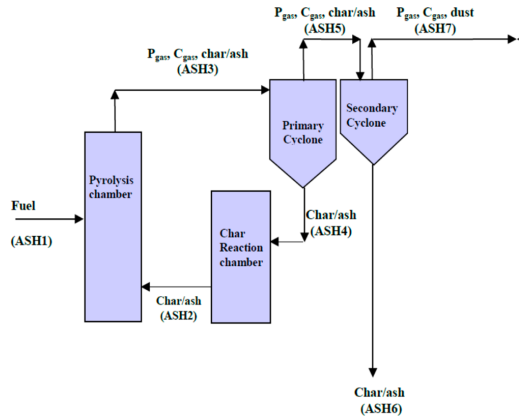

Figure 1. Schematic diagram of a LTCFB process. P_{gas} is the gas produced from the pyrolysis chamber (CO, H_2, tar, CO_2, and CH_4), while C_{gas} is the gas produced in the char reaction chamber (CO_2, CO, and H_2). ASHi (i = 1−7) denotes the streams containing inorganic elements.

Received: October 19, 2015
Revised: January 12, 2016
Published: January 13, 2016

DOI: 10.1021/acs.energyfuels.5b02464
Energy Fuels 2016, 30, 1050−1061

bottom of the char reactor while serving as a heat carrier. The char particles in the upper part of the char reaction chamber thus experience a high retention time in the process, improving the overall conversion efficiency. The heat released as a result of the generally exothermic reactions in the char reactor is consumed by the endothermic processes in the pyrolysis chamber.

The exit stream from the pyrolysis chamber has a lower temperature (600−650 °C) compared to that of the char reactor. Consequently, most of the alkali species are present in the solid state and can be separated from the gas by cyclones. Moreover, the relatively low temperatures in the process limit the tendencies of defluidization in the system that is often a problem for alkali-rich fuels in fluidized beds. As shown in Figure 1, the product gas is fed to two cyclones. Using the primary and secondary cyclones in series, fine ash particles with the problematic alkali materials are separated from the product gas, facilitating use of the gas for power generation in a boiler. It is desirable that as much potassium as possible is retained within the LTCFB system.

The LTCFB gasifier has been tested in both bench scale and pilot scale with promising results.[1,2] However, little is known about the partitioning of the inorganic elements in the system or the release of K, Cl, and S with the product gas. The objective of this study is to obtain an improved understanding of the transport and transformation of inorganic elements within a LTCFB system. Measurements were performed on a 100 kW LTCFB gasifier at DTU Risø and a 6 MW LTCFB gasifier at Kalundborg. Through analysis of the measurements, together with a simplified model for the cyclone separation, the release and retention of alkali and other ash-forming species in the LTCFB system are investigated.

2. TRANSFORMATION OF K, S, AND CL IN GASIFICATION

The transformation of the major inorganic elements (K, Cl, and S) in straw during pyrolysis and gasification has been studied extensively. Chemical fractionation studies of straw[3−6] show that about 80−90% of K is removed by leaching with water and ammonium acetate. This implies that K is present in straw mainly as easily soluble salts or loosely bound to organic exchange sites. Only a marginal fraction of K (10%) is not extractable with mineral acid, and this fraction could be bound in silicates. During pyrolysis, K^+ ions in solution or bound to organic molecules of low thermal stability precipitate as inorganic salts, become ion-exchanged to functional groups in the char matrix, or are intercalated into the char matrix.[3,4] Experiments[3−5,7] show a release of K from the fuel of less than 10% during pyrolysis below 700 °C. Above 700 °C, K is believed to be released as a result of vaporization of KCl.[3−5] In addition, K could be released from the organic matrix during char oxidation or through gasification with steam.[3−5,7] Some K may combine with silica from straw or from the bed material to form K silicates. Potassium may also be present as KCl, KOH, K_2SO_4, or K_2CO_3, even though K silicates are thermodynamically favored for silica-rich fuels, such as straw.[4] Experimental results[8] indicate a low probability of KCl reacting with bed material (sand).

About 90% of Cl in agricultural biomass is water-soluble and, thus, present in ionic form.[3−6] Saleh et al.[9] found 64% of chlorine in straw to be released during pyrolysis at 350 °C, mostly as methyl chlorides with minor amounts of HCl. Gaseous Cl can be partially recaptured by secondary reactions and precipitate as KCl on char particles.[3−5] At temperatures above 700 °C, the vapor pressure of KCl increases significantly and the evaporation of KCl becomes the main pathway for the release of Cl from biomass.

Sulfur is partly associated as inorganic sulfate and partly as organic sulfur in wheat straw.[3,4,7] About 50−60% of S is released during pyrolysis at 350 °C.[9] No additional sulfur release was observed below 800 °C. The low-temperature sulfur release is caused by decomposition of organically associated sulfur in the fuel.[3,4,7,9] The fraction of sulfur released at these temperatures is thus strongly dependent upon the ratio of inorganic and organic sulfur present in the fuel. A part of released sulfur may react with functional groups in the char under pyrolysis conditions and become retained in the char matrix.[3,4,7]

3. MATERIALS AND METHODS

3.1. Properties of Straw and Bed Material. The fuel used for the campaigns was Danish wheat straw. The proximate analysis of the straw is provided in Table 1, while Table 2 shows the composition of the inorganic fraction of the fuel. The straw was found to be rich in Si, K, Ca, and Cl, while elements like Fe and Al were present only in trace amounts. The fresh bed material used in the char reactors of the two gasifiers consisted mainly of Si (Table 2).

Table 1. Proximate Analysis of Danish Wheat Straw Used at the 6 MW Gasifier (Kalundborg)

volatiles (wt %)	fixed carbon (wt %)	moisture (wt %)	ash (wt %)	LHV (MJ/kg)
70.2	14	11.3	4.5	17.1

3.2. Experimental Setup and Operational Procedures. To perform the particle measurements on the output gas, an experimental setup was devised, as shown in Figure 2. The exit gas from the secondary cyclone of the LTCFB gasifier was sampled using the probe PR1, with a sampling rate of 0.1 m^3/min. Because the sampled gas contained large amounts of tar, the probe was kept electrically heated to 400 °C throughout the experiment to avoid tar condensation. The gas was then filtered by a metallic filter F1, also kept at 400 °C by the heater H1. The dust particles were later separated from the F1 filter for further analysis. The tar-laden dust-free gas was then washed with acetone in a Petersen Column PT1 to remove tar. The tar and dust-free gas was analyzed by the gas analyzer GA. The suction flow of the sampled gas through the setup was provided by the pump P1. The gas meter GM measured the volumetric flow of the gas sampled during the experiments.

Table 3 provides an overview of the measurement campaigns, types of samples collected, and analyses made. Samples of bed material, cyclone ash, and dust in the product gas were collected during the plant runs and analyzed for their inorganic elemental composition. In addition, scanning electron microscopy (SEM) and thermogravimetric analysis (TGA) of the collected samples were made to improve the understanding of the behavior of the ash-forming species within the system. During selected plant runs at the 100 kW gasifier (Risø runs 1b and 2), measurements were performed on a product gas, which was already pre-filtered by a high-capacity baghouse filter.

In TGA, the sample (about 5 mg) was thermally treated by a predetermined temperature program.[10] It was initially heated in an inert atmosphere (N_2) to 600 °C and then cooled to 100 °C at a rate of 10 °C/min. It was then heated in the presence of oxygen (10%) to a temperature of 1200 °C, maintaining a heating rate of 10 °C/min. The change in mass of the sample was continuously recorded as a function of the time and temperature.

Some properties of the samples were then interpreted from the TGA curve (see Figure SM1 of the Supporting Information). The change in mass observed at temperatures below 200 °C was attributed

DOI: 10.1021/acs.energyfuels.5b02464
Energy Fuels 2016, 30, 1050−1061

Table 2. Mass Fraction (wt %) of Inorganic Elements in the Fuel (Danish Wheat Straw), the Bed Material, the Secondary Cyclone Ash, and the Product Gas Dust and Tar for the 100 kW (Risø) and the 6 MW (Kalundborg) Gasifier Tests

	fuel ash (100 kW)	fuel ash (6 MW)	bed material	secondary cyclone ash Risø 1a/Kalundborg	exit gas dust Risø 1a/Kalundborg	exit gas tar
Al	0.037	0.01	2.9			
Ca	0.36	0.35	0.03	2.5/2.3	2.9/2.5	<0.0005
Fe	0.025	0.008	0.45			
K	0.71	0.83	1.6	7.3/6.4	6.7/4.8	<0.004
Mg	0.073	0.077				
Na	0.024	0.014	0.28			
P	0.077	0.077				
Si	1.6	1.1	93.8	16/13	10.5/6.68	<0.01
Ti			0.64			
Cl	0.21	0.18		0.96/1.12	1.5/1.4	<0.0046
S	0.092	0.11		0.15/0.28	0.19/0.32	0.006

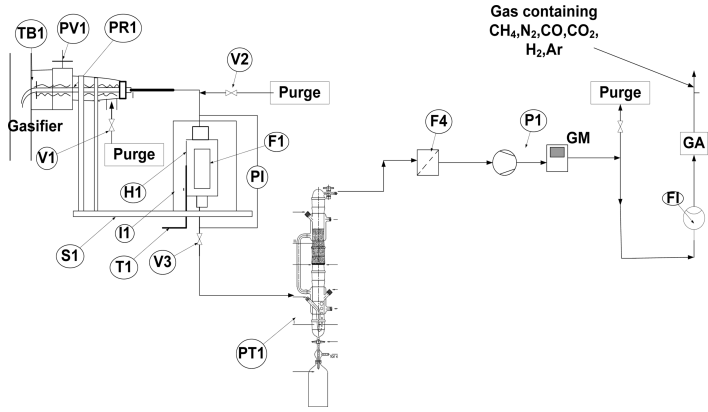

Figure 2. Experimental setup for exit gas measurements and particle sampling in the LTCFB gasifier: PR-1, sample probe with electric heating; TB-1, outer probe; PV-1, valve for the sample probe; F1, filter housing; H1, heater for the filter; I1, insulation; T1, thermocouple; PT, Peterson column; F4, cold filter; V1 and V2, purge valves; P1, gas pump; GM, gas meter; FI, flow indicator; GA, gas analyzer for O_2, CO, and CO_2; PI, pressure indicator; V3, valve downstream of the filter; and S1, support for the insulation.

to evaporation of moisture, while the mass loss above 200 °C in the inert atmosphere was caused by release of volatiles during pyrolysis. With the supply of oxygen to the sample, the residual char was oxidized; the mass remaining at 600 °C was taken as a measure of the total ash present in the sample. The observed mass loss when the sample was heated further from 600 to 1200 °C indicated the percentage of volatile inorganic elements in the ash. The loss in weight of the ash could be due to the presence of alkali salts, such as KCl, which becomes volatile at these temperatures.

For a mass balance on the system, it is required to estimate the total volumetric flow rate of the product gas leaving the gasifier. A direct estimation of the flow rate was difficult because the composition of the product gas was unknown. Instead, an inert gas (argon) was injected into the system at the 100 kW plant in a known concentration, and its concentration in the product gas leaving the system was measured using a micro gas chromatograph (GC). From a balance on argon in the system, the total output volumetric flow rate of the gas could be calculated. At the 6 MW plant, where this method would require prohibitively large amounts of argon, the total exit gas flow and mass of dust particles were estimated by a rough mass balance on the inert solids in the system.

The present study also involved the development of a model for ash particle retention in the LTCFB system.

4. RESULTS AND ANALYSES

4.1. Particle Concentrations and Size Distributions. The particle concentrations (dust load) in the product gas were measured in the 100 kW and 6 MW gasifiers to be 8−11 and 20−30 g/Nm^3, respectively. The particle loading in the gas samples pre-filtered by the high-capacity filter (Risø runs 1b and 2) was generally as low as 0.5−1.5 g/Nm^3.

The particle size distribution (PSD) of the collected samples (bed material, secondary cyclone bottoms, and product gas dust) was measured by a Malvern Mastersizer. Figure 3 shows the size distribution of particles collected during tests at the 6 MW gasifier. The d_{50} value for the secondary cyclone ash was 50 μm, while it was 30 μm for the particles in the product gas. The bed material consisted of larger particles, with a d_{50} value of around 213 μm. These observations show that the larger particles in the gasifier were mostly retained by the primary cyclone and recirculated back into the system, while the secondary cyclone retained particles of smaller sizes, at around 50 μm. The primary and secondary cyclones thus seem to play an important role in controlling the retention and release of the ash particles within the LTCFB system.

4.2. TGA and SEM. The collected samples were analyzed by TGA and SEM. Table 4 shows TGA results for the cyclone ash and dust particles in the product gas collected during measurements in the 100 kW gasifier (Risø runs 1a and 2). TGA shows that the cyclone ash and dust samples were reasonably similar. Both samples were found to contain major fractions of char (30−40%) and ash (45−50%). The cyclone ash and dust particles were mostly non-volatile, with volatile

DOI: 10.1021/acs.energyfuels.5b02464
Energy Fuels 2016, 30, 1050−1061

Table 3. Measurement Campaigns and Analyses Made during Plant Runs at the 100 kW (Risø) and 6 MW (Kalundborg) Gasifiers[a]

campaign	samples collected	sample analyses	other analyses
Risø runs 1a (without high-capacity filter) and 1b (with high-capacity filter)	secondary cyclone ash, bed material, and particles in the product gas (from metallic filters and from high-capacity filters)	inorganic elemental composition of samples, TGA, and SEM	argon measurements to determine the flow of product gas
Risø run 2 (with high-capacity filter)	particles in the product gas (from metallic filters and from high-capacity filters)	TGA, SEM, and exit gas concentration of methyl chloride	argon measurements to determine the flow of product gas
Kalundborg	secondary cyclone ash, bed material, and particles in the product gas (from metallic filters and from high-capacity filters)	inorganic elemental composition of samples and particle size distribution	

[a]The fuel was Danish wheat straw in all tests.

contents of 6−10%. The volatile fraction of the inorganic ash, presumably mostly KCl, was 3−4%. For dust samples collected after the high-capacity filter, the ash content was as low as 5%. The dust consisted mostly of char (65%) and unreleased organic volatiles (27%). The low ash content in the dust samples was expected because the larger inorganic ash particles would have been separated in the high-capacity filter.

About 99% of the bed material samples was composed of inorganic material (Table 4). Because the fresh bed material and char are recirculated between the char reactor and the pyrolysis reactor, there is a continuous buildup of ash as a result of gasification within the char reactor; for this reason, the bed material will contain an increasing amount of fuel ash over time. There was no volatile material in the sampled bed material, indicating negligible amounts of salts, such as KCl. TGA also showed a minimal char content in the bed material samples. This could be because the bed material samples were taken from the bottom of the char reactor, where the low-density char particles are depleted.

To further elucidate the composition and morphology of the samples, SEM of the cyclone ash, dust particles, and bed material samples was performed. SEM of the secondary cyclone ash particles from the 100 kW gasifier (Figure 4) showed irregular-sized particles dominated by ash, in agreement with the TGA results (Table 4). The particles shown as bright white spots (spectra 1, 2, 3, and 5) consisted mostly of K and Si with some amount of Ca, showing the presence of silicates in the cyclone ash. Chlorine was also observed in the cyclone ash, probably present as chlorides, but in lower amounts (spectra 2−5 in Figure 4). Similar to cyclone ash samples, the dust particles in the product gas were found to be dominated by inorganic elements with high contents of K and Si and some Ca and Cl (spectra 1−5 in Figure 5), showing the presence of silicates and chlorides. SEM images of dust samples collected after the high-capacity filter (Figure 6) showed only small amounts of inorganic elements, in agreement with the TGA results (Table 4). The bed material samples were found to be dominated by Si with some amount of K and Ca (spectra 1−3 in Figure 7), while Cl and S were found only in trace amounts.

4.3. Release and Retention of Inorganic Elements in the LTCFB System. On the basis of TGA of the collected samples, an overall mass balance on the ash in the LTCFB system could be conducted. The amount of ash put into the system through the fuel feed was estimated from the proximate analysis, shown in Table 1. Table 5 shows that, of the ash in the fed straw, about 45−80% was retained in cyclone ash and 8−10% was released as dust in the exit gas during the plant runs at the two LTCFB facilities. The fraction of ash left unaccounted (10−50%) includes the ash that is accumulated within the gasifier. The large amount of ash in the cyclone bottom confirms that the cyclones play an important role in controlling the retention of the inorganic elements in the LTCFB system.

The release of specific inorganic elements was investigated from the elemental analysis of the samples from tests at the two gasifiers. The compositions of the inorganic fractions of cyclone ash and dust samples collected at selected plant runs are shown in Table 2. The remaining fractions of the cyclone ash and dust included char (as evident from the TGAs) and traces of other inorganic elements present in small amounts. The cyclone ash was found to be dominated by Si, K, and Ca. The dust particles in the product gas had a similar composition, although with lower fractions of Si, K, and Ca. The amount of Cl in the cyclone ash and dust particles was about 1−1.5%, while S was

DOI: 10.1021/acs.energyfuels.5b02464
Energy Fuels 2016, 30, 1050−1061

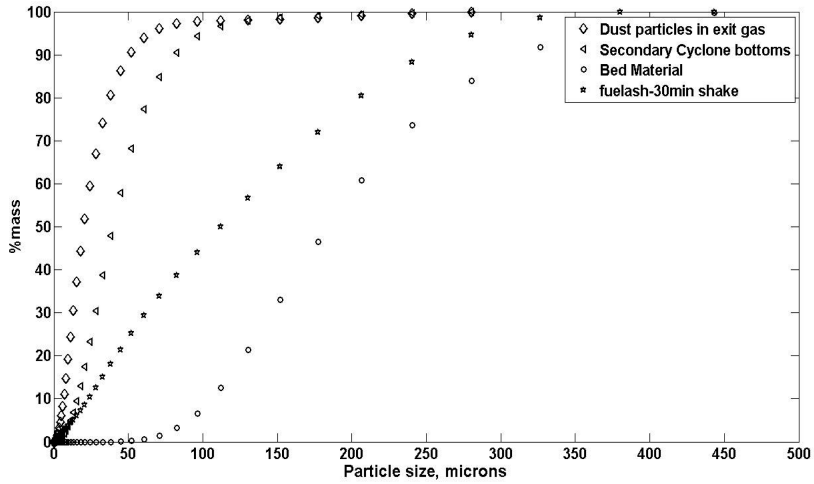

Figure 3. PSD of the secondary cyclone ash, dust particles in exit gas, and bed material samples collected during experiments at the 6 MW gasifier (Kalundborg). Also shown is the fuel ash PSD, obtained from laboratory experiments.

Table 4. TGA Results for Secondary Cyclone Ash, Product Gas Dust, and Bed Material from Runs in the 100 kW Gasifier (Risø)[a]

	cyclone ash				dust in product gas				bed material			
	moisture (%)	volatiles (%)	char (%)	total inorganic content (%)	moisture (%)	volatiles (%)	char (%)	total inorganic content (%)	moisture (%)	volatiles (%)	char (%)	total inorganic content (%)
Risø run 1a	5.2	6	45.4	43.4 (4.2%)	5.7	6.2	35.1	53 (4.1%)	0.01	0.03	0	99.96 (0%)
Risø run 2					1.4	27.2	65.7	5.7 (3%)				

[a]Runs 1a and 2 are without and with a high-capacity filter, respectively. The numbers in parentheses are the percentage of volatiles in the total inorganic content.

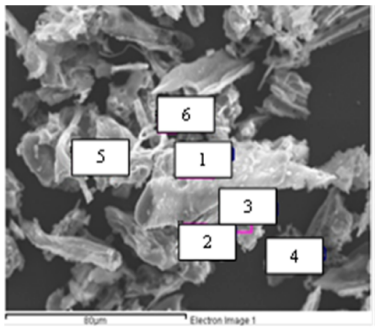

Spectrum	O	Si	P	S	Cl	K	Ca
	mol%	mol%	mol%	mol%	mol%	mol%	mol%
1	54.4	20.0	4.5	0.3	3.4	14.1	3.3
2	38.7	40.7	2.5	0.3	2.4	12.2	3.1
3	31.5	40.5	3.1	1.3	2.8	13.4	7.4
4	15.7	9.6	4.3	4.0	11.6	48.6	6.3
5	50.7	21.8	3.6	2.1	3.1	13.3	5.5
6	38.1	23.5	3.2	5.0	5.5	17.4	7.4

Figure 4. SEM image of cyclone ash samples collected from the 100 kW gasifier (Risø run 1a).

found to be present in low amounts (0.15−0.3%). This shows that cyclone ash and dust particles are dominated by silicates.

Table 6 shows the fractions of K, Ca, Cl, Si, and S in the fuel that were retained in the secondary cyclone ash or released with the dust in the product gas. The table also shows the mass fractions of the elements left unaccounted in the mass balance. These fractions include mass accumulated in the bed material or released as gas-phase species with the product gas. Si was found to be removed in substantial amounts with the cyclone ash (in the range of 50−95%). For the 6 MW gasifier, the Si balance closed well, while for the 100 kW unit, more than 40% Si was left unaccounted. Si was found in high concentrations in the bed material (93.8%; Table 2) and low amounts in the fuel (1.0−1.6%), which makes a closure of the mass balance difficult. For Ca, 30−50% was retained in the secondary cyclone ash, with only a minor fraction found in the product gas dust. The fraction of Ca from the fuel that was left unaccounted (40−60%) was conceivably accumulated in the bed material.

A total of 50−60% of K in the fuel was retained in the secondary cyclone ash, while about 30−40% was left unaccounted. Only a minor fraction of K was found in the product gas dust. S was removed by the cyclone only in low amounts, in the range of 8−20%. About 20−50% of the chlorine from the fuel was retained in the cyclone ash, possibly

DOI: 10.1021/acs.energyfuels.5b02464
Energy Fuels 2016, 30, 1050−1061

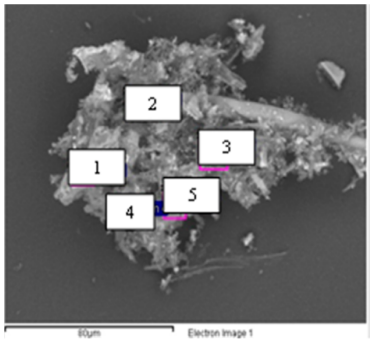

Spectrum	O	Si	P	S	Cl	K	Ca
	mol%	mol%	mol%	mol%	mol%	mol%	mol%
1	46.4	27.3	3.9	0.6	4.1	11.0	6.7
2	47.2	35.5	2.0	0.4	2.4	9.7	2.9
3	47.0	20.8	3.5	0.4	6.5	16.0	5.8
4	50.3	21.3	3.2	1.2	4.3	13.7	6.0
5	47.4	15.6	5.1	0.5	3.7	14.0	13.6

Figure 5. SEM images of dust particles in the exit gas, collected from the 100 kW gasifier (Risø run 1a).

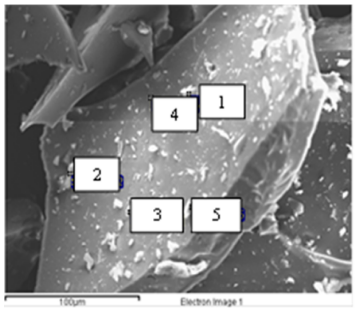

Spectrum	O	Si	P	S	Cl	K	Ca
	mol%	mol%	mol%	mol%	mol%	mol%	mol%
1	92.1	0.9	1.9	5.3	0	0.6	0
2	98.4	4.4	2.5	0	0	0	0
3	82.8	8.8	0.6	3.7	1.2	3.4	0
4	78.8	0	0	6.2	7.5	4.1	8.0
5	87.2	2.6	2.6	1.9	2.5	2.3	0.9

Figure 6. SEM images of dust particles in the exit gas, collected from the 100 kW gasifier with a high-capacity filter (Risø run 2).

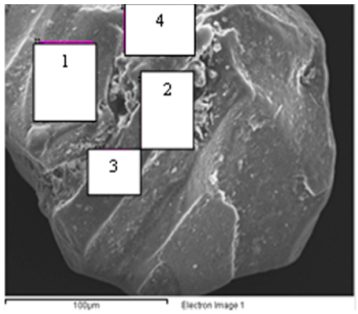

Spectrum	O	Si	P	S	Cl	K	Ca
	mol%	mol%	mol%	mol%	mol%	mol%	mol%
1	50.9	36.6	2.2	0	0.4	6.5	3.5
2	38.0	40.4	4.6	0	0.5	10.3	6.6
3	48.3	41.2	1.9	0	0.1	5.3	3.2
4	45.4	36.6	2.5	0.3	-	11.1	4.1

Figure 7. SEM images of bed material samples collected from the 100 kW gasifier (Risø run 1a).

Table 5. Fraction of Ash in the Fuel Released with the Dust in the Product Gas and Retained within the Cyclone Ash for Tests Conducted in the 100 kW Gasifier at Risø and the 6 MW Gasifier at Kalundborg, Both without a High-Capacity Filter

	ash fraction in product gas (%)	ash fraction in cyclone ash (%)	fraction left unaccounted (%)
Risø run 1a	11	46	43
Kalundborg	8	83	9

as potassium and calcium chlorides in the cyclone ash. The data of Table 6 correspond to large molar ratios of K/Cl in the secondary cyclone ash (5−7) and in the exit gas dust particles (3−4), indicating that K was present in substantial amounts in other forms than KCl. The considerable fractions of Cl and S left unaccounted in the mass balance (60−70%) are attributed to gas-phase release chlorides (CH_3Cl and HCl) and reduced sulfur species (H_2S and OCS). The content of inorganic elements in the dust was low compared to cyclone ash, with levels of K, Ca, Si, and Cl of about 10%, probably present as silicates and chlorides, and S in amounts of 3−4%.

Samples of secondary cyclone ash and bed material were analyzed by chemical fractionation for their water-soluble fractions. As seen from Table 7, 91% Cl and 69% K in the secondary cyclone ash were water-soluble, implying the presence of K as KCl and probably some KOH and K_2CO_3. About 80% Si and 98% Ca were found in the water-insoluble fraction, along with 30% K that probably appeared as silicates. In the bed material samples, all of the major inorganic species (K, Ca, and Si) were predominantly found in the water-

DOI: 10.1021/acs.energyfuels.5b02464
Energy Fuels 2016, 30, 1050−1061

Table 6. Mass Fractions of the Inorganic Elements in the Fuel Retained in Secondary Cyclone Ash and Released with Dust in Product Gas for the 100 kW Gasifier at Risø and the 6 MW Gasifier in Kalundborg, Both without a High-Capacity Filter

		secondary cyclone ash (wt %)	dust (wt %)	unaccounted (wt %)
Risø run 1a	K	49	13	38
	Si	47	9	44
	Ca	33	11	56
	Cl	22	10	68
	S	8	3	89
Kalundborg	K	62	7	31
	Si	95	8	−3
	Ca	52	9	39
	Cl	50	10	40
	S	21	4	75

Table 7. Inorganic Mass Fractions and Water-Soluble Fractions of Major Inorganic Elements in the Secondary Cyclone Ash and the Bed Material

	secondary cyclone ash		bed material	
	mass fraction (wt %)	water-soluble fraction (wt %)	mass fraction (wt %)	water-soluble fraction (wt %)
K	7.5	69.0	2.3	8.7
Si	14.8	18.0	40.1	0.4
Ca	2.7	1.9	1.0	1.6
Cl	1.3	91.0	0.1	16.3

insoluble fraction, showing that potassium mainly appears as water-insoluble silicates.

The tar in the exit gas collected during the plant run in the 100 kW gasifier was analyzed for the inorganic elemental composition, as shown in Table 2. The tar contained very low amounts (<0.004%) of the inorganic elements, corresponding to less than 0.002% of the respective elements in the fuel. These results indicate low probabilities of release of the major inorganic elements with tar in the gasifier. The concentration of methyl chloride in the product gas from the 100 kW gasifier was measured to investigate the presence of Cl in gaseous form.[11] The exit gas contained 90−100 ppm of methyl chlorides, corresponding to about 15% Cl present in the fuel. As mentioned above, most gaseous Cl is presumably released as HCl.

4.4. Behavior of Ash-Forming Elements in LTCFB Gasifiers. It is desirable to understand the mechanism of transformation of the major ash-forming species K, Si, and Cl in the LTCFB system because the ash speciation influences bed sintering and release of inorganic species with the product gas. It is important for the use of product gas in boilers that a minimum amount of inorganic species is present in the product gas.

Thermal equilibrium calculations were made for K, Cl, and Si under reducing conditions, using the FACTSage software with the FACTSage 5.0 compound database. The input data used for calculations are provided in Table SM2 of the Supporting Information. Figure 8 shows the predicted distribution of K species. The calculations did not account for the interaction of ash-forming elements with char. Potassium is predicted to exist mainly as KCl and K silicates in the solid state below 650 °C. Above this temperature, KCl starts to vaporize. Potassium is found as K silicates in the solid state until temperatures around 800 °C, while liquid K silicates are formed above 700 °C.

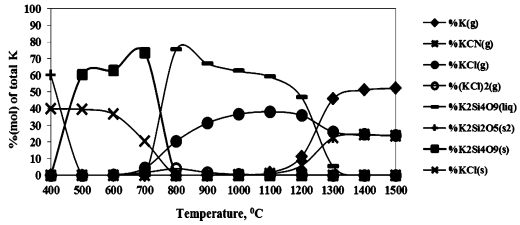

Figure 8. Thermal equilibrium distribution of K under pyrolysis conditions.

The stable species of Cl under reducing conditions according to the equilibrium calculations are shown in Figure 9. It is

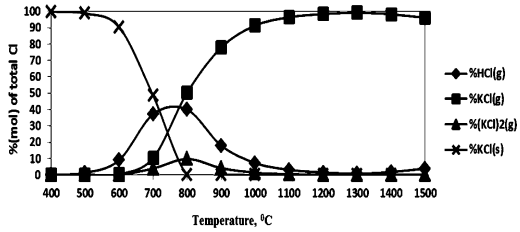

Figure 9. Thermal equilibrium distribution of Cl under pyrolysis conditions.

predicted that Cl mainly exists as KCl in the solid state below 500 °C. Above this temperature, part of the Cl is released as HCl. However, experimental work[9] has shown the release of Cl under reducing conditions at temperatures as low as 200−400 °C in the form of methyl chloride. At temperatures above 650 °C, Cl starts to be present in gaseous form also as KCl and $(KCl)_2$. The equilibrium calculations indicate that Si mainly exists as K silicates in the solid state below 750−800 °C; above this temperature range, liquid K silicates dominate. The predictions rule out the formation of SiO_2 during pyrolysis conditions.

On the basis of the present study and results from the literature, it is possible to evaluate the mechanisms of transformation of K, Cl, and Si in the LTCFB gasifier. The major forms in which K and Si could exist in the gasifier are K salts (KCl, K_2SO_4 K_2CO_3, and KOH), organically bound K, and K silicates. At the temperature in the pyrolysis chamber (650 °C), these K species are mostly in the solid state. Gaseous KCl from the char reactor will condense and form aerosols. K silicates could be formed in the pyrolysis reactor as a result of the reaction of silica present in the fuel and in the bed material with organically bound K and K salts; a reaction that is controlled by kinetic and mass-transfer limitations.[3−5] In the char reactor, KCl(s) will partly vaporize as a result of the higher temperature (730 °C), facilitating the reaction with silica to form silicates. Chlorine will be released from the biomass as methyl chloride at low temperatures,[9] as confirmed by the present measurements, or as HCl, which could be recaptured by either K salts, such as K_2CO_3, or K in the char matrix.[3,4]

The particles leaving the pyrolysis chamber are mostly separated in the primary cyclone and recirculated to the char reactor. A fraction of the remaining particle load in the gas is then retained in the secondary cyclone, while the rest is

DOI: 10.1021/acs.energyfuels.5b02464
Energy Fuels 2016, 30, 1050−1061

released as dust in the product gas from the gasifier. This indicates that the release of particles from the system is controlled largely by the particle size and the cut size of the primary and secondary cyclones. To establish a simple tool to predict the particle release, a model for the particle retention in the cyclones was developed.

4.5. Modeling the Retention of Inorganic Elements in the LTCFB System. The present section describes the development of a model for ash particle retention in the LTCFB system. Figure 1 shows the LTCFB system with the streams, named as ASHi (i = 1−7), that contain the inorganic elements. Char, ash, and bed material enter the char reactor from the primary cyclone (ASH4) and undergo transformation by combustion and gasification within the char reactor, inducing changes in the particle size and composition. The ash from the char reactor (ASH2) is recirculated to the pyrolysis chamber, where it mixes with the fuel (ASH1) to form the ASH3 stream. The efficiency and cut size of the primary cyclone determines the particle size of ash entering the secondary cyclone (ASH5) and that entering the char reactor (ASH4). Similarly, the cut size and efficiency of the secondary cyclone determine the size distribution of the ash retained in the cyclone bottom (ASH6) and that released from the reactor system with the exit gas (ASH7). A simple model for the primary and secondary cyclones is sufficient to predict the partitioning of ash between ASH4, ASH6, and ASH7 and, thereby, provide an estimate of the fate of the inorganic elements in the LTCFB system.

4.5.1. Cyclone Model. The dimensions of the primary and secondary cyclones of the 100 kW and 6 MW LTCFB gasifiers, respectively, are shown in Table SM3 of the Supporting Information. Figure 10 shows the configuration of the cyclones.

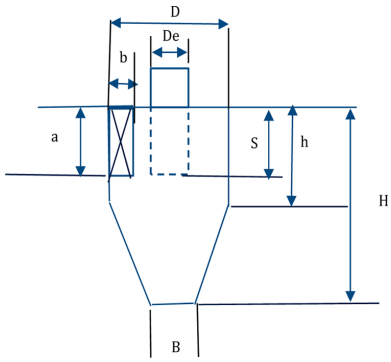

Figure 10. Cyclone configuration.

The cyclone model was adopted from Lapple.[12] The cyclone efficiencies were estimated from eq 1

$$\eta_j = \frac{1}{1 + (d_{pc}/d_{pj})^2} \tag{1}$$

where d_{pj} is the characteristic diameter of the jth particle size range, η_j is the collection efficiency of particles of size d_{pj}, and d_{pc} is the diameter of particles collected with 50% efficiency

$$d_{pc} = \left[\frac{9\mu b}{2\pi N_e v_i(\rho_p - \rho_g)}\right]^{0.5} \tag{2}$$

where μ is the viscosity of the gas, b is the inlet width of the cyclone (Figure 10), v_i is the inlet velocity of the gas, ρ_p is the density of the particles, ρ_g is the density of the gas, and N_e is the number of revolutions made by the dust-laden gas inside the body and the cone. The inlet velocity of the gas v_i can be calculated from eq 3

$$v_i = \left[\frac{Q}{(3600)ab}\right] \tag{3}$$

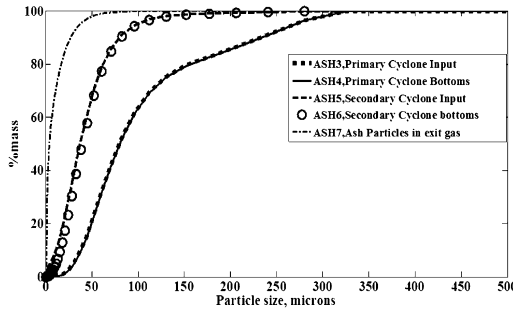

Figure 11. Predicted (ASH3, ASH4, ASH5, and ASH7) and measured (ASH6) PSDs of selected ASH streams for the 6 MW gasifier (Kalundborg).

where Q is the volumetric flow rate of the input feed and a is the inlet height of the cyclone (Figure 11). N_e can be estimated from eq 4

$$N_e = \frac{1}{a}\left[h + \frac{H - h}{2}\right] \tag{4}$$

where H is the total height of the cone. The overall collection efficiency η of the cyclone is a weighted average of the collection efficiencies for the various size ranges

$$\eta = \frac{\sum_{j=1}^{n} \eta_j m_j}{m_{total}} \tag{5}$$

where m_j is the mass flow of particles in the jth size range (of diameter d_{pj}), m_{total} is the total mass flow of particles, and n is the number of size intervals.

4.5.2. Model Predictions for the Retention and Release of Ash. Model calculations were performed on the secondary cyclone with the following assumptions: (i) The ash particle size did not change during the process. (ii) The organic content of the particles did not affect the PSD or the mass fraction of the secondary cyclone bottoms. Thus, the mass flow rates of inorganic ash particles of size d_{pj} collected in the secondary cyclone bottoms (stream ASH6 in Figure 1), $m_{jbottomsec}$, could be estimated from eq 6

$$m_{jbottomsec} = x_{d_{pj}} M_{total} C_{ash} \tag{6}$$

where $x_{d_{pj}}$ is the mass fraction of the secondary cyclone bottoms of particle size d_{pj}, M_{total} is the total mass flow rate of secondary cyclone bottoms collected during the plant runs, and C_{ash} is the concentration of inorganic ash in the secondary cyclone bottoms. (iii) No accumulation of mass took place within the cyclone.

DOI: 10.1021/acs.energyfuels.5b02464
Energy Fuels 2016, 30, 1050−1061

The input to the model included the particle sizes (d_{pj}) and the mass of ash particles of the corresponding particle sizes ($m_{jbottomsec}$) of the secondary cyclone bottoms (stream ASH6), which was obtained from measurements made on the 100 kW and 6 MW gasifiers. The calculations were performed by retracing the system backward from ASH6 to ASH1.

The efficiency of the secondary cyclone (η_{jsec}) for the various particle sizes was calculated using eq 1. The mass flow rates of the ash particles of size d_{pj} entering the cyclone ($m_{jinputsec}$ of ASH5) and leaving the cyclone ($m_{jexitsec}$ of ASH7) were estimated from eqs 7 and 8

$$m_{jinputsec} = m_{jbottomsec}/\eta_{jsec} \quad (7)$$

$$m_{jexitsec} = m_{jinputsec} - m_{jbottomsec} \quad (8)$$

The model calculations were then conducted for the primary cyclone. The assumptions used for the primary cyclone model calculations were similar to those used on the secondary cyclone. Thus, the mass of the ash particles of size d_{pj} entering the primary cyclone ($m_{jinputprim}$ of ASH3) and that collected in the primary cyclone bottoms ($m_{jbottomprim}$ of ASH4) were estimated from eqs 9 and 10

$$m_{jinputprim} = m_{jexitprim}/(1 - \eta_{jprim}) \quad (9)$$

$$m_{jbottomprim} = m_{jinputprim} - m_{jexitprim} \quad (10)$$

The efficiency of the primary cyclone for the corresponding particle sizes (η_{jprim}) was estimated using eq 1. The total mass flow rate of an ash stream in all of the above calculations was obtained by eq 11

$$m = \sum_{j=1}^{n} m_j \quad (11)$$

where m_j is the mass flow rate of a particle of size d_{pj} (of jth size interval) and n is the number of particle size intervals.

On the basis of measured data on ASH6, the total mass of ash streams in the various sections of the gasifier could be calculated. The calculations were performed for both the 100 kW and 6 MW gasifiers. The results were compared to the measurements from the corresponding plant runs (Table 8).

Table 8. Fraction of Ash in Fuel in Plant Runs at the 100 kW (Risø) and 6 MW (Kalundborg) Gasifiers Released with the Exit Gas and That Unaccounted in the Mass Balance Obtained from Model Calculations (with ASH6 as Input and Tracing Backwards) and from Mass Balance Results Based on Measured Data from Corresponding Plant Runs

	predicted release of ash with product gas (%)	release of ash with product gas from mass balance (%)	predicted fraction of ash in fuel left unaccounted (%)	fraction of ash in fuel left unaccounted in mass balance (%)
Kalundborg	7	8	10	9
Risø run 1a	2	11	51	43

For the 6 MW gasifier, the predicted fraction of fuel ash entrained with the exit gas (7%) is close to the measured value from the plant run (8.3%). For the 100 kW gasifier, the estimated percentage of ash entrained (2%) is considerably lower than that obtained from the measured data (10%). In this case, the model overpredicts the performance of the cyclones. The predicted fractions of ash in fuel left unaccounted by the mass balance, i.e., mainly condensed ash species accumulated within the gasifier, of 11 and 56%, respectively, are close to the measured values from the 100 kW and 6 MW plant runs (10 and 48%).

The predicted PSDs for various ash streams for the 100 kW and 6 MW gasifiers are shown in Figures 11 and 12. The measured PSD of ASH6 is used as input to the model, while the PSDs of other ash streams are calculated. The secondary cyclone bottoms (ASH6) have particles predominantly in the range of 30−90 μm, while particles in the exit gas (ASH7) are predicted to be in the range of 1−30 μm. The primary cyclone input stream (ASH3) and primary cyclone bottoms (ASH4) contain particles in the larger size range, 80−200 μm. This agrees with the principle of the LTCFB gasifier, wherein the larger ash particles are retained and recirculated within the system by the primary cyclone, while the smaller ash particles are captured by the secondary cyclone.

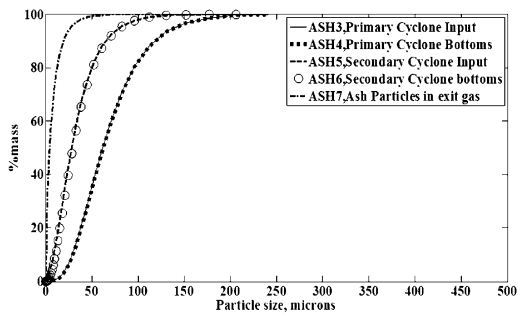

Figure 12. Predicted (lines) and measured (symbols) PSDs for selected ASH streams for the 100 kW gasifier (Risø run 1).

The PSD of the dust particles in the exit gas (ASH7) obtained from the model calculations was compared to that obtained from measurements in the 100 kW and 6 MW gasifiers, as shown in Figures 13 and 14. It can be seen that the predicted PSD of the dust is smaller than the measured results, again showing a better performance of the cyclones according to the model than the measured results.

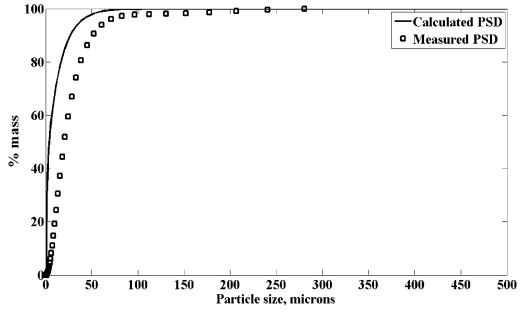

Figure 13. Predicted and measured PSDs of the dust particles in the product gas from the 6 MW gasifier (Kalundborg).

An alternative set of calculations was made, proceeding forward from ASH1 (the fuel input) to ASH6 and ASH7. To conduct these calculations, an estimate of the PSD of the ash species from the wheat straw in the LTCFB system is required. This was obtained by combusting the fuel in a laboratory-scale fixed bed reactor/oven. The temperature was kept below 500

DOI: 10.1021/acs.energyfuels.5b02464
Energy Fuels 2016, 30, 1050−1061

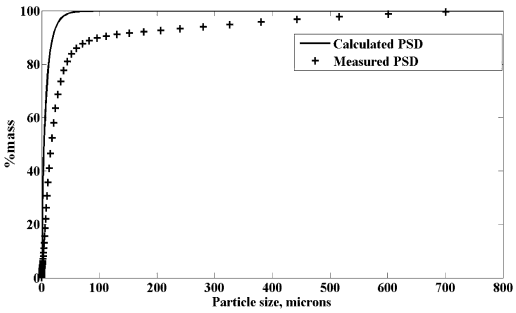

Figure 14. Predicted and measured PSDs for the dust particles in the product gas from the 100 kW gasifier (Risø run 1).

°C to limit release of ash species into the gaseous form. The ash samples were then put in glass bottles and shaken vigorously for 10−30 min. The measured PSD of the ash depended only slightly upon the length of the time interval of shaking (Figure SM3 of the Supporting Information). A PSD assumed to be representative of the ash in the gasifier is shown in Figure 3.

The mass and PSD for the input ash stream to the primary cyclone (ASH3) were calculated by adding values for the ASH1 stream to those of ASH3 (from the previous calculation). The ASH3 stream is dominated by bed material; bed material flows of 4460 kg/h for the 6 MW LTCFB gasifier and 29 kg/h for the 100 kW LTCFB gasifier were used. The mass flows and PSDs for the ash streams ASH4, ASH5, and ASH6 were then obtained from the primary and secondary cyclone model equations. In Table 9, the results of the calculations are compared to the measured data. The predicted fractions of ash retained in the secondary cyclone bottoms (85%) and entrained with the exit gas (9%) are close to the values obtained by measurements in the 6 MW gasifier (82 and 8%, respectively). For the 100 kW gasifier, the predicted fraction of ash released with the product gas (3%) was again lower than that measured (10%). The fractions of ash in fuel left unaccounted in the calculations (6 and 67%) are close to the measured values (10 and 48%) for both gasifiers. In conclusion, the simple model provides a satisfactory prediction of the fraction of ash that is released with the exit gas during LTCFB operation.

4.5.3. Model Predictions for the Distribution of Inorganic Elemental Species. The next step in the modeling was to estimate the distribution of the major inorganic elements (K, Cl, Si, Ca, and S) within the ash particles. The following additional assumptions were made: (i) The distribution of the inorganic elemental species (K, Cl, Si, Ca, and S) was the same for each particle of a particular ash stream. (ii) The concentrations of K, Si, and Ca in all ash streams were the same as those for the ash in the input fuel stream ASH1, obtained from the fuel analysis. (iii) A total of 64% Cl and 60% S in the fuel were released as gas from the pyrolysis chamber of the gasifier, in agreement with experiments on pyrolysis of straw.[7] Thus

$$m_{j\mathrm{Cl}} = (1 - 0.64)m_{j\mathrm{Clfuel}} \quad (12)$$

$$m_{j\mathrm{S}} = (1 - 0.6)m_{j\mathrm{Sfuel}} \quad (13)$$

where $m_{j\mathrm{Cl}}$ and $m_{j\mathrm{S}}$ are mass flow rates of Cl and S in the specific ash streams ASHj (j = 3−7) and $m_{j\mathrm{Clfuel}}$ and $m_{j\mathrm{Sfuel}}$ are the mass flow rates of Cl and S in ash in the fuel stream (ASH1). The mass flow rates m_{ji} of the inorganic species i in a particle of size d_{pj} in the ash streams were obtained from eq 14

$$m_{ji} = m_j C_{ji} \quad (14)$$

where m_j is the mass flow rate of the ash particle of size d_{pj} in the ash stream and C_{ji} is the percentage mass of the inorganic species i in the ash particle of size d_{pj} in the ash stream. The values of C_{ji} used for the model studies are shown in Table 10.

Table 10. Concentrations of K, Si, Ca, Cl, and S (with Reduced Cl and S) in the Ash Streams of the LTCFB System Used for Model Calculations (on the Basis of the Fuel Ultimate Analysis Shown in Table 2)

	K	Si	Ca	Cl	S
6 MW gasifier (Kalundborg) (wt %)	18	24	8	1.4	1
100 kW gasifier (Risø run 1a) (wt %)	13	29	7	1	1

As shown in Table 11, the calculated fractions of condensed ash elements (with ASH6 as input and tracing backward)

Table 11. Fractions of the Elements in the Fuel Released with the Exit Gas and Retained in the Cyclone Ash, Estimated from Model Calculations (with ASH6 as Input and Tracing Backwards) and from the Mass Balance Analysis on the Measured Data from Tests in the 100 kW (Risø) and 6 MW (Kalundborg) Gasifiers

plant		secondary cyclone bottoms (wt %)		dust in exit gas (wt %)	
		predicted	measured	predicted	measured
Kalundborg	K	83	62	7.3	7
	Si	83	95	7.3	8
	Ca	83	52	7.3	9
	Cl	30	50	2.6	10
	S	33	21	2.9	4
		predicted	measured	predicted	measured
Risø run 1a	K	46	49	2.6	13
	Si	46	47	2.6	9
	Ca	46	33	2.6	11
	Cl	17	22	1.0	10
	S	19	8	1.0	3

Table 9. Fractions of Ash in Fuel in Plant Runs at 100 kW (Risø) and 6 MW (Kalundborg) Gasifiers Released with the Exit Gas, Retained in Secondary Cyclone Bottoms, and Left Unaccounted in the Mass Balance Obtained from Model Calculations (with ASH1 as Input and Tracing Forward) and from Mass Balance Results on Experimental Data from Corresponding Plant Runs

	predicted release of ash with product gas (%)	release of ash with product gas from mass balance (%)	predicted fraction of ash retained in secondary cyclone bottoms (%)	fraction of ash retained in secondary cyclone bottoms from mass balance (%)	predicted fraction of ash in fuel left unaccounted (%)	fraction of ash in fuel left unaccounted in mass balance (%)
Kalundborg	9	8	85	83	6	9
Risø run 1a	3	11	30	46	67	43

DOI: 10.1021/acs.energyfuels.5b02464
Energy Fuels 2016, 30, 1050−1061

entrained with the exit gas and retained in cyclone bottoms were mostly in satisfactory agreement with the measured values obtained from the 6 MW and 100 kW gasifiers. The underprediction in the fraction of entrained ash elements in the product gas dust is related to the overprediction by the model of the cyclone performance, as discussed above. However, these predictions rely on the assumption that the elemental composition of the ash particles is independent of the particle size and should be interpreted cautiously.

5. CONCLUSION

The release and retention of inorganic elements within a LTCFB gasifier has been investigated. The ash release with the product gas was quantified through particle measurements on a 100 kW and a 6 MW gasifier, respectively. In addition, secondary cyclone ash bottoms and bed material samples from the gasifiers were collected and analyzed with respect to their inorganic elemental composition. It was seen that, of the total ash that enters the gasifier with the fuel, 40−50% was retained in the secondary cyclone bottoms, while a lower amount (8−10%) was released as dust in the product gas. SEM and TGA of cyclone ash and dust particles showed the samples to be dominated by inorganic ash-forming elements (45−50%) and char (35−40%). Mass balance calculations showed that a dominant fraction of alkali and alkaline earth metals was retained in the ash along with Si. A large fraction of Cl and S (60−70%) left unaccounted in the mass balance was attributed to unmeasured gas-phase concentrations of Cl (CH_3Cl or HCl) and S (OCS or H_2S) in the product gas. Methyl chlorides in levels of 90−100 ppm were measured in the product gas from the 100 kW gasifier. The concentration of K and other inorganic elements in tar was found to be negligible.

In the solid state, K is present in the LTCFB gasifier mainly as K salts (KCl and K_2CO_3), organically bound K (K bound to ion-exchange sites of the char matrix and intercalated K), and K silicates. K silicates could be formed in the pyrolysis reactor as a result of reaction of silica present in the fuel and in the bed material with organically bound K and K salts (in gaseous form). A cyclone model was developed to study the role of the cyclones for ash release and retention in the LTCFB system. Modeling predictions for the fraction of ash retained in the cyclone bottoms and entrained with the exit gas agreed favorably with measured values for the 100 kW and 6 MW gasifiers. This confirms that release of ash particles from the LTCFB system is controlled mainly by the cyclone design.

■ ASSOCIATED CONTENT

Supporting Information

The Supporting Information is available free of charge on the ACS Publications website at DOI: 10.1021/acs.energyfuels.5b02464.

Molar ratios of the inorganic elemental species in the secondary cyclone ash and dust in exit gas collected during plant runs in 100 kW and 6 MW LTCFB gasifiers (Table SM1), molar composition of the inorganic elements used as input for equilibrium calculations (λ = 0.8) (Table SM2), dimensions of the cyclones in the 100 kW and 6 MW LTCFB gasifiers (Table SM3), TGA curve for cyclone ash samples (Figure SM1), concentration of methyl chloride in the exit gas analyzed at various sampling times in the 100 kW gasifier (Risø run 2) (Figure SM2), and PSD of ash produced by burning straw at 500 °C, with the sample size distributions measured by a Malvern Mastersizer instrument (Figure SM3) (PDF)

Input data, data from the plant, calculations, and formulas (XLSX)

■ AUTHOR INFORMATION

Corresponding Author

*Telephone: +4545252840. E-mail: pgl@kt.dtu.dk.

Notes

The authors declare no competing financial interest.

■ ACKNOWLEDGMENTS

The authors thankfully acknowledge the financial support provided by DONG Energy and Energinet.dk.

■ NOMENCLATURE

a = inlet height of the cyclone (m)
b = inlet width of the cyclone (m)
C_{jCl} = mass fraction of Cl in the particle of size d_{pj}
C_{jS} = mass fraction of S in the particle of size d_{pj}
d_{pj} = characteristic diameter of the particle in the jth size range (m)
d_{pc} = cut diameter of the cyclone (m)
H = total height of the cyclone (m)
h = height of the cylindrical section of the cyclone (m)
m_j = mass flow rate of the ash particle of size d_{pj} (kg/h)
m_{ji} = mass flow rate of species i in the particle of size d_{pj} (kg/h)
$m_{jinputfuel}$ = mass flow rate of ash particle size d_{pj} in the input fuel (kg/h)
$m_{jinputsec}$ = mass flow rate of ash particle size d_{pj} in the input stream to the secondary cyclone (kg/h)
$m_{jbottomsec}$ = mass flow rate of ash particle size d_{pj} in the secondary cyclone bottoms (kg/h)
$m_{jinputprim}$ = mass flow rate of ash particle size d_{pj} in the input stream to the primary cyclone (kg/h)
$m_{jbottomprim}$ = mass flow rate of ash particle size d_{pj} in the primary cyclone bottoms (kg/h)
$m_{jexitsec}$ = mass flow rate of ash particle size d_{pj} in the exit stream from the secondary cyclone (kg/h)
$m_{jexitprim}$ = mass flow rate of ash particle size d_{pj} in the exit stream from the primary cyclone (kg/h)
$m_{jrecirculated}$ = mass flow rate of ash particle size d_{pj} recirculated to the pyrolysis cyclone (kg/h)
N_e = number of revolutions made by dust-laden gas inside the body and the cone of the cyclone
Q = volumetric flow rate of gas input to the cyclone (m^3/s)
ν_i = inlet velocity of gas in the cyclone (m/s)
ρ_g = density of gas (kg/m^3)
ρ_p = density of the particle (kg/m^3)
η_j = efficiency of the cyclone for particle size d_{pj}
η_{jprim} = efficiency of the primary cyclone for particle size d_{pj}
η_{jsec} = efficiency of the secondary cyclone for particle size d_{pj}
μ = viscosity of gas (kg/ms)

■ REFERENCES

(1) Stoholm, P.; Nielsen, R. G.; Sarbæk, L.; Tobiasen, L.; Fcok, W. M.; Richardt, K.; Sander, B.; Wolff, L.; Henriksen, U. The Low Temperature CFB Gasifier—Further Test Results and Possible Applications. *Proceedings of the 12th European Biomass Conference*; Amsterdam, Netherlands, June 17−21, 2002; pp 706−709.

DOI: 10.1021/acs.energyfuels.5b02464
Energy Fuels 2016, 30, 1050−1061

(2) Stoholm, P.; Ahrenfeldt, J.; Henriksen, U.; Gomez, A.; Krogh, J.; Nielsen, R. G.; Sander, B. The Low Temperature CFB Gasifier—500 kW Test on Biogas Fiber Residue. *Proceedings of the 16th European Biomass Conference and Exhibition*; Valencia, Spain, June 2−6, 2008.
(3) Van Lith, S. C.; Jensen, P. A.; Frandsen, F. J.; Glarborg, P. *Energy Fuels* **2008**, *22*, 1598−1609.
(4) Knudsen, J. N.; Jensen, P. A.; Dam-Johansen, K. *Energy Fuels* **2004**, *18*, 1385−1399.
(5) Jensen, P. A.; Frandsen, F.; Dam-Johansen, K.; Sander, B. *Energy Fuels* **2000**, *14*, 1280−1285.
(6) Baxter, L. L. *Task 2. Pollutant Emission and Deposit Formation during Combustion of Biomass Fuels*, Quarterly Report to National Renewable Energy Laboratory; Sandia National Laboratories: Livermore, CA, 1994.
(7) Johansen, J. M.; Jakobsen, J. G.; Frandsen, F. J.; Glarborg, P. *Energy Fuels* **2011**, *25*, 4961−4971.
(8) Baxter, L. L.; Miles, T. R.; Miles, T. R., Jr.; Jenkins, B. M.; Milne, T.; Dayton, D.; Bryers, R. W.; Oden, L. L. *Fuel Process. Technol.* **1998**, *54*, 47−78.
(9) Saleh, S. B.; Flensborg, J. P.; Shoulaifar, T. K.; Sárossy, Z.; Hansen, B. B.; Egsgaard, H.; DeMartini, N.; Jensen, P. A.; Glarborg, P.; Dam-Johansen, K. *Energy Fuels* **2014**, *28*, 3738−3746.
(10) Qin, K.; Lin, W.; Fæster, S.; Jensen, P. A.; Wu, H.; Jensen, A. D. *Energy Fuels* **2013**, *27*, 262−270.
(11) Egsgaard, H.; Ahrenfeldt, J.; Henriksen, U. B. On the Significance of Methyl Chloride in Gasification Processes. *Proceedings of the 18th European Biomass Conference and Exhibition*; Lyon, France, May 3−7, 2010.
(12) Lapple, C. E. *Chem. Eng.* **1951**, *58*, 144−151.

DOI: 10.1021/acs.energyfuels.5b02464
Energy Fuels 2016, 30, 1050−1061

Supplementary material:

Table SM1 Molar ratios of the inorganic elemental species in the secondary cyclone ash and dust in exit gas collected during plant runs in 100 Kw and 6 MW LTCFB gasifiers.

Molar ratio	**100 kW**		**6 MW**	
	Secondary cyclone ash	**Dust in exit gas**	**Secondary cyclone ash**	**Dust in exit Gas**
K/Cl	7	4.0	5.2	3.2

Table SM2 Dimensions of the cyclones in the 100 kW and 6 MW LTCFB gasifiers.

Dimensions	**Primary cyclone (mm)**		**Secondary cyclone (mm)**	
	100 kW	**6MW**	**100 kW**	**6MW**
D	139	800	114	700
A	65.5	400	53	350
B	25	160	20	140
De	16.5	400	12	350
S	70.3	400	54.5	350
H	201.5	1200	164	1050
H	461.5	3200	431	2800
B	70	300	43	263

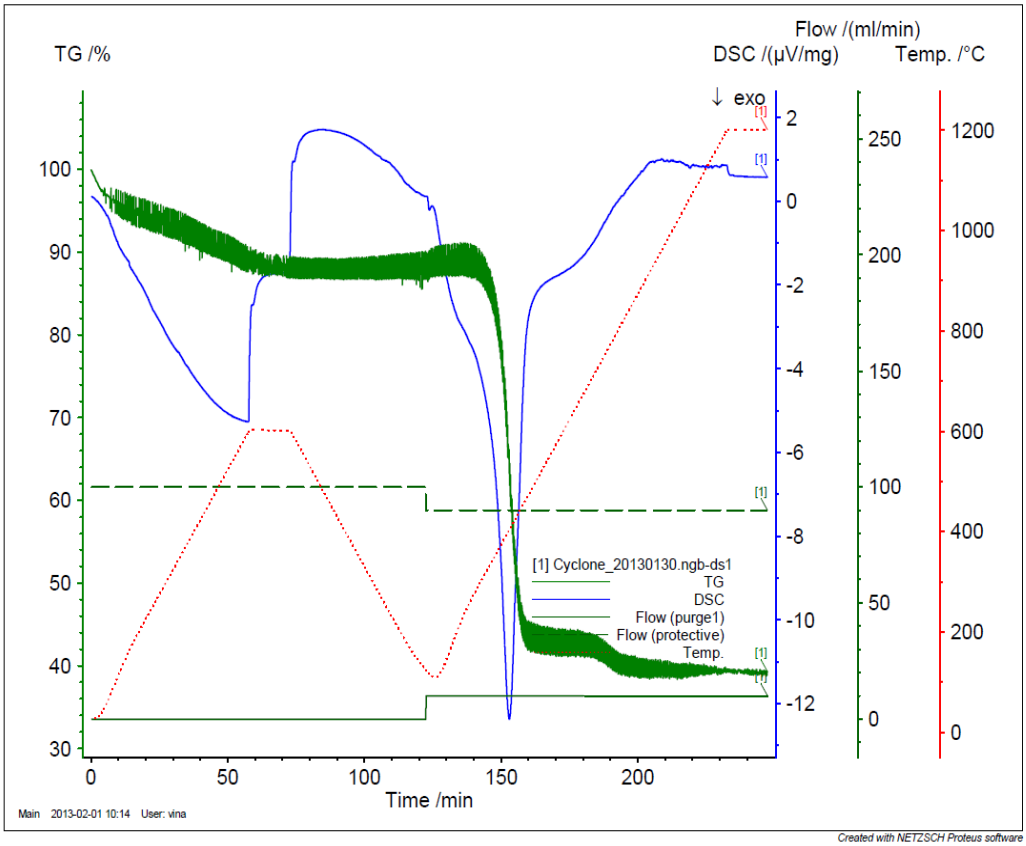

Figure SM1. TGA curve for cyclone ash samples.

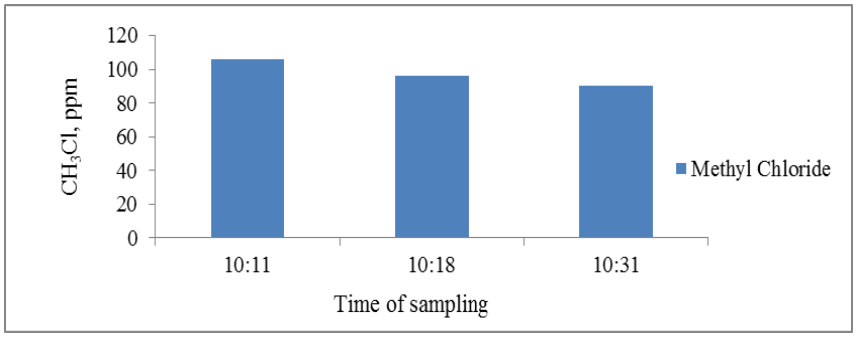

Figure SM2 Concentration of methyl chloride in the exit gas analyzed at various sampling times in 100 kW gasifier (Risø run 2) [11].

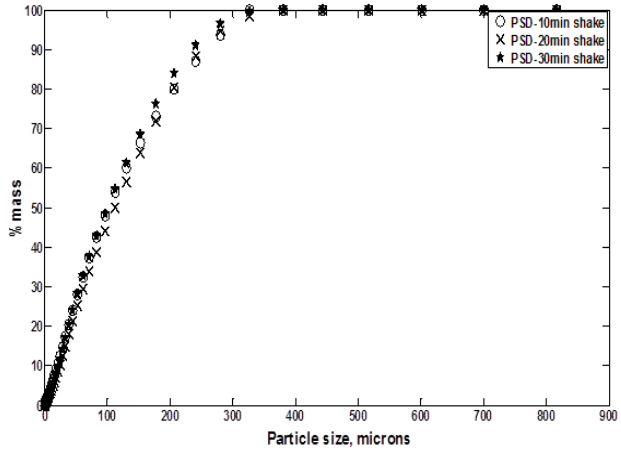

Figure SM3 Particle size distribution of ash produced by burning straw at 500ºC. The sample size distributions were measured by a Malvern Mastersizer instrument.

A.2. Paper 2: Defluidization in Fluidized Bed Gasifiers Using High-Alkali Content Fuels

Authors: Vikas Narayan, Peter Arendt Jensen, Ulrik Birk Henriksen, Peter Glarborg, Rasmus Glar Nielsen.

(The paper is submitted to Biomass and Bioenergy journal)

Biomass and Bioenergy 91 (2016) 160–174

Contents lists available at ScienceDirect

Biomass and Bioenergy

journal homepage: http://www.elsevier.com/locate/biombioe

Research paper

Defluidization in fluidized bed gasifiers using high-alkali content fuels

Vikas Narayan [a], Peter Arendt Jensen [a, *], Ulrik Birk Henriksen [a], Peter Glarborg [a], Weigang Lin [a], Rasmus Glar Nielsen [b]

[a] Department of Chemical Engineering, Technical University of Denmark, Building 229, DK-2800, Lyngby, Denmark
[b] Dong Energy, Nesa Alle1, Gentofte, DK -2820, Denmark

ARTICLE INFO

Article history:
Received 16 July 2015
Received in revised form
25 March 2016
Accepted 8 May 2016

Keywords:
De-fluidization
Alkali
Agglomerate
Biomass
Gasification

ABSTRACT

A major concern in thermal conversion of biomass encountered in fluidized beds is bed agglomeration, which may result in de-fluidization, leading to unscheduled downtime and additional costs. Biomass fuels, especially herbaceous plants, often contain significant amounts of silicon, potassium and calcium, which may form viscous melts that adhere on the surface of the colliding bed particles and bind them to form agglomerates. In this paper, studies were made to understand the behavior of inorganic elements (mainly K, Si and Ca) on agglomeration and de-fluidization of alkali rich bed-material samples under non-oxidizing conditions in a bench-scale fluidized bed reactor set up. The de-fluidization studies involved measurements with sand and pure potassium salts (KCl and K_2CO_3) as well as with bed material samples obtained from a 6 MW Low Temperature Circulating Fluidized Bed (LTCFB) gasifier using straw as a fuel. It was seen that in sand + KCl agglomerates, the sand particles were bound by KCl melts. Only very limited chemical reaction was observed between KCl and the sand particles and no presence of silicate melts in the agglomerates. For sand + K_2CO_3 mixtures and for LTCFB bed material samples, agglomeration could be attributed to viscous silicate melts formed from reaction of inorganic alkaline and alkali earth species with silica from the bed particles. A mathematical model that addresses the de-fluidization behavior of alkali-rich samples was developed based on the experiments performed in the bench-scale fluidized bed reactor as well as on results from literature. The model was then used to predict the de-fluidization behavior of alkali-rich bed material in a large-scale LTCFB gasifier.

1. Introduction

Gasification of herbaceous biomass has a large potential for power generation. One of the most common biomass gasification technologies is fluidized bed gasification. Fluidized beds are characterized by high conversion efficiencies and uniform temperatures owing to an efficient mixing. However, use of biomass with high ash and alkali content in fluidized beds may lead to bed agglomeration [1], which again may result in de-fluidization, leading to unscheduled downtime and additional costs.

Biomass, especially herbaceous biomass, often contains significant amounts of silicon, alkali (mainly potassium, but also sodium), and calcium, together with chlorine and sulphur. These elements tend to form viscous melts which adhere on the surface of the colliding bed particles. When the sticky bed particles collide, the viscous material at the point of contact migrates forming a neck, thus binding the particles to form agglomerates. This phenomenon is called viscous flow sintering. The temperature at which the process of sintering initiates to form agglomerates is called the initial sintering temperature, T_s. As the process continues, the agglomerates increase in size and de-fluidization takes place. The particles tend to change to Class C type (according to the Geldart classification [2]) that is difficult to fluidize. This difficulty arises due to inter-particle forces (adhesive forces), which are greater than those the fluid motion can exert on the particles. The phenomenon of agglomeration is believed to occur through two mechanisms [3,4]:

- *Melt-induced agglomeration:* Inorganic salts present in the fuel ash melt and the melts then act as necks to bind the bed particles to form agglomerates. This mechanism does not involve any chemical reaction between the ash species and the bed material.

* Corresponding author.
E-mail address: PAJ@kt.dtu.dk (P.A. Jensen).

http://dx.doi.org/10.1016/j.biombioe.2016.05.009
0961-9534/

Nomenclature

A_1	Constant, dimensionless
b	Neck radius of the coating layer around the two particles in an agglomerate, M
C, C', C_1', C_2', C_2''	Constants, dimensionless
C_D	Drag Force on the particle in the fluidized bed, N
d	Diameter of the particle in the fluidized bed, M
F_{ad}	Adhesive force between particles in the agglomerate, N
F_{br}	Breaking force on agglomerates within the fluidized bed, N
m_{K0}	Mass of K in input feed, kg
$m_{Kentrained}$	Mass of K entrained with exit gas from the fluidized bed, kg
$m_{Kcoating}$	Mass of K in the coating layer around particles within the agglomerate, kg
$m_{icoating}$	Mass of species i (K, Si, Mg, Na and O) in the coating layer around particles within the agglomerate, kg
$m_{Kcycloneash}$	Mass of K in secondary cyclone ash collected in the LTCFB gasifier, kg
m_{Kdust}	Mass of K in the dust particles in the exit gas leaving the LTCFB gasifier, kg
M_K	Molar mass of K, kg kmol^{-1}
M_i	Molar mass of species i (K, Si, Mg, Na and O), kg kmol^{-1}
n_K	Moles of K, mol
n_i	Moles of species i (K, Si, Mg, Na and O), mol
t_{def}	De-fluidization time, s
t	Time, s
T	Temperature within the fluidized bed, ^{o}C
U	Superficial velocity of fluidizing gas, m s^{-1}
U_{mf}	Minimum fluidization velocity, m s^{-1}
w	Mass fraction of species within coating layer
w_{Kcoat}	Mass fraction of K in the coating layer around particles in the agglomerate, dimensionless
w_{K0}	Mass fraction of K in the fuel, dimensionless

Greek Symbols

σ	Tensile stress of agglomerate, N m^{-2}
μ	Viscosity of coating layer, kg m^{-1} s^{-1}
δ	Thickness of coating Layer, m
β	Mass fraction of K in input feed entrained with the exit gas, dimensionless
ρ_{coat}	Density of the coating layer around particles in the agglomerate, kg m^{-3}
ρ_{bed}	Density of the bed particles in the fluidized bed, kg m^{-3}
$\varnothing$	Mass flow rate of feed into the fluidized bed, kg s^{-1}

- *Coating-induced agglomeration:* Viscous melts are formed due to reaction of inorganic species, from the fuel ash, with the bed material. The melts form a coating layer around the bed particles, making them sticky and adhesive. On intermittent collisions, the sticky coated bed particles bind with each other leading to the formation of agglomerates.

Measurements reported in literature on de-fluidization in fluidized bed biomass gasifiers elucidate the role of alkali and alkaline earth species in the agglomerates formed during the process. A number of studies of fluidized bed gasifiers using herbaceous fuels (wheat straw) indicate the formation of necks between coated agglomerated bed particles, rich in alkali and silicon [1,5–12]. The reported measurements show that the temperatures, at which de-fluidization occurs, vary with the fuel feed and with the composition of inorganic species. From these studies it seems that the concentration and chemistry of the inorganic elements strongly influence the formation of agglomerates and subsequent de-fluidization inside the fluidized bed biomass gasifier.

Very recently, Khadilkar et al. [13] reviewed models of agglomerate growths in fluidized bed reactors. Some of the models for bed agglomeration and de-fluidization are summarized in Table 1. Only a few recent models deal with de-fluidization during conversion of biomass. Moseley et al. [14] used a two-particle collision model to estimate the minimum superficial velocity required to avoid de-fluidization of coal ash particles due to agglomeration at temperatures above the initial sintering temperature T_s, obtained from Ref. [15]. The model assumption was that the particles agglomerate when the energy dissipated by the binding (adhesive) force between two particles during recoil exceeded the initial kinetic energy of the colliding particles. The binding force was assumed to be proportional to the contact surface area between the two particles, with the constant of proportionality expressed as a function of temperature using experimental data from Liss et al. [16]. The adhesive force in the model was not related to material properties but a function of temperature alone.

Ennis et al. [17] followed a similar principle to estimate the modified minimum fluidization velocity of the agglomerated granular particles, bound by a viscous liquid binder. They assumed agglomeration to occur if the ratio of collisional kinetic energy of the particles to the viscous dissipation brought about by interstitial binder was below a critical value. This ratio was proposed to be proportional to the difference between the modified minimum fluidization velocity of the particles with the viscous binder and the initial minimum fluidization velocity without the viscous liquid. The proportionality terms were obtained by regression using experimental data from Gluckman et al. [18].

Tardos et al. [19,20] estimated the gas velocity U_s required to break the largest agglomerate in the fluidized bed and thus maintain the bed fluidized at temperatures exceeding the minimum sintering temperature, T_s. The model was developed for two cases, one in which the particles are bound by a viscous liquid (wet agglomerates) and the other where the particles become sticky due to high temperature softening/sintering (sintered agglomerates). The breakage force for both cases was considered to be the shear force generated by the bubble motion on the agglomerate and was expressed as a function of the dimensions of the agglomerate and the excess velocity above minimum fluidization ($U_s - U_{mf}$). The adhesive force for the wet agglomerates was described as a function of the liquid surface tension, wetting angle and amount of liquid (degree of saturation). The adhesive force between particles with sintered surfaces at high temperatures was considered to be a function of the sinter neck yield strength, which in turn was dependent on the viscosity of the granule surface and the time of contact during which the sintering occurred.

Zhong et al. [21] studied the fluidization of iron particles and proposed a model to estimate the total de-fluidization time by comparing the adhesive force and breakage force between the particles. The breakage force was assumed to be proportional to the drag exerted by the fluidizing gas on the particle. Basu et al. [22] modified the Ergun equation for a fluidized bed of coal ash by including an adhesive force in the force balance. Their model was only qualitative and, according to Seville et al. [23], fundamentally flawed as pointed out by Seville et al. [22], as under conditions of

Table 1a
Model studies in literature on bed agglomeration and de-fluidization.

Author	Model equation
Moseley et al. [14]	$U_{mfs} = U_{mf} + C_3\rho_p^{q_1}\rho_f^{q_2}\mu_f^{q_3}(T - T_s)^{q_4}$
Ennis et al. [17]	$St_D^* = 8\rho\alpha\left(\frac{(U_{mfs}-U_{mf0})a}{9\mu}\right)^{1/2} = \left(1+\frac{1}{e}\right)(\ln(h) - \ln(h_a))$
Tardos et al. [19] [20],	$\frac{(U_s-U_{mf})}{U_{mf}} = k_3\left[\frac{(1-\epsilon)}{\epsilon^2}\right]\left(\frac{d_{ag}^{\frac{7}{2}}d_p^{\frac{1}{2}}}{d_B^{\frac{1}{2}}D_p^{\frac{7}{2}}}\right)\left(\frac{\rho_g\,\sigma_s}{\varnothing\,\rho_s\mu_g g^{1/2}}\right)^{1/2}$
Zhong et al. [21]	$F_d = \frac{C\pi b^2 t}{d_p\mu_s}$
Basu et al. [22]	$U_{mfs} = \frac{1}{1650}\frac{d_p^2 g}{\mu_g}\left(\rho_p - \rho_g + \frac{\psi(T,H_b,d_p)}{(1-\epsilon)}\right)\psi(T,H_b,d_p) = K(T-T_s)f_1 d_p f_2(H_b)$ Where, $T_s = f_3(d_p,H_b)$ and $f_3(d_p,H_b)\psi(T,H_b,d_p) = 0$ at $T \le T_s$
Lin et al. [24]	$t_{def} = C\left(\frac{(U-U_{mf})}{(d_p)}\right)^{1/2} exp\frac{(E_a)}{(RT)}$
Lin et al. [25]	$t_{def} = C\left(\frac{1}{(f_N\,\psi)}\right)^{\frac{1}{2}}\left(\frac{M_b}{(f_N\,\psi)}\right)exp\frac{(E_a)}{(RT)}M = 0.67(1-\epsilon_{mf})\rho_p\left(\frac{1}{\varphi_b}-1\right)\left(U-U_{mf}\right)\varphi_b = \{1-0.3\exp[-8(U-U_{mf})\}\exp(-\beta H_b)\beta = 7.2\{(U-U_{mf})\}\exp(-4.1(U-U_{mf}))$

fluidization, the pressure drop across the bed must equal the weight of the particles per unit area independent of the inter-particle forces.

The force balance approach and statistical analysis discussed above have been extended to predict de-fluidization in fluidized bed biomass combustion/gasification systems. Lin et al. [24] proposed a model for de-fluidization in fluidized bed combustors for wheat straw as a function of temperature, fluidization velocity, and particle size. The particles were considered to be bound due to the viscous coating layer of potassium silicates around the particles, forming necks. The adhesive forces were assumed to be proportional to the tensile strength of the coating layer between the particles which in turn was assumed to be proportional to time and inversely proportional to the viscosity of the coating. The breakage force was attributed to the shear force induced by bubbles and was assumed to be proportional to the difference between the operational velocity of the gas and the minimum fluidizing velocity of the gas. The viscosity of the silicate melts was assumed to follow an Arrhenius relationship with temperature. Later, Lin et al. [25] modified the model to represent the breakage force by the average convective solid mass flow per unit bed area, which was a function of the static bed height, the porosity of the bed, the bubble shape and the gas velocity.

Even though the concentration and chemistry of inorganic

Table 1b
Description of symbols used in Table 1a.

a	Particle or granule radius	μm
b	Neck radius of the coating layer around the two particles in an agglomerate	m
d_b	Bubble diameter	m
D_p, d_p	Particle diameter	m
d_{ag}	Diameter of the agglomerate	m
F_d	Adhesive force	N
H_b	Bed Height	m
h	Binder layer thickness covering colliding granules	μm
h_a	Characteristic length scales of surface asperities	μm
M	Mass flow per unit bed area	kg/m^{2}s
St_D^*	De-fluidization Stokes Number	Dimensionless
t	Time taken for the particles to agglomerate	M
t_{def}	De-fluidization time	s
T	Temperature within the fluidized bed	^{0}C
T_s	Initial Sintering Temperature	^{0}C
U	Superficial velocity of fluidizing gas	m/s
U_{mf} , U_{mf0}	Minimum fluidization velocity	m/s
U_{mfs}	Minimum fluidization velocity	m/s
U_s	Limiting velocity to break the largest agglomerate in the bed	m/s
α	Thickness of coating Layer	m
μ_f, μ_g	Viscosity of fluidizing gas	kg/ms
μ_s	Surface viscosity of solid iron	kg/ms
μ	Binder viscosity	kg/ms
e	Coefficient of restitution	Dimensionless
$f_1, f_2, f_3\ \beta, \psi$	Different functions	
σ_s	Yield strength of the neck within the agglomerate	N/m^2
ϵ	Porosity in the fluidized Bed	Dimensionless
$q_1, C, C_3, q_2, q_3, q_4, K, k_3, k$	Constants	Dimensionless
f_N	Mass fraction of Na in bed material	Dimensionless
ρ_p, ρ_s, ρ	Density of the bed particles in the fluidized bed	kg/m^3
ρ_f, ρ_g	Density of the fluidizing gas	kg/m^3
$\varnothing$	Shape Factor	Dimensionless
ψ_N	Mass of Na fed per unit time	kg/s

elements strongly influence the formation of agglomerates and subsequent de-fluidization inside a fluidized bed reactor, none of these models predict explicitly the influence of the inorganic species. This short-coming was addressed recently by Li et al. [3] who attempted to include the influence of the inorganic species on the bed agglomeration by assuming the adhesive force in their model to be proportional to the fraction of liquid coating, estimated from equilibrium calculations. However, their model was based on empirical parameters obtained in a lab-scale reactor, and predictions would be difficult to extrapolate to larger systems [13]. Furthermore, the model could not account for variations in the composition of the inorganic species on the formation of the coating layer.

In the present work we aim to evaluate the impact of inorganic elements, primarily alkali, on agglomeration and de-fluidization of alkali rich bed-material under non-oxidizing conditions in fluidized bed reactors. We choose to focus on potassium, even though in some biomass feedstock also sodium may be present in significant quantities. The study involves experiments on de-fluidization in a bench scale fluidized bed reactor. Measurements are conducted with sand and potassium salts (potassium chloride and potassium carbonate), as well as with bed material samples obtained from a 6 MW Low-Temperature Circulating Fluidized Bed (LTCFB) gasifier at Kalundborg, Denmark (the Pyroneer Gasifier) using straw as a fuel. A mathematical model for the de-fluidization behavior is developed, based on the bench-scale experiments as well as results from literature. The model addresses the effect of the concentration of inorganic (alkali) species on the thickness and viscosity of the coating layer around the particles, as well as the influence of operation conditions, on de-fluidization. The model is then used to study the de-fluidization behavior in a large scale LTCFB gasifier using alkali-rich fuels.

2. The LTCFB gasifier

Herbaceous fuels contain high amounts of alkali which form species of low melting points that condense on pipelines and reactor surfaces, and cause de-fluidization. The LTCFB system works on the principle of gasifying these fuels at temperatures below those of conventional gasification systems (800–1000 °C) [26]. In this way the release to the exit gas of alkali and alkaline earth species is reduced and a relatively large fraction is retained within the system as ash in the bed material. A brief description of the Low Temperature Circulating Fluidized Bed process is given in this section. As shown in Fig. 1, the LTCFB process consists of two reactors. The biomass fuel enters the pyrolysis chamber, where the fuel is pyrolysed at around 650 °C. Sand bed particles and ash recirculated from the char reaction chamber to the pyrolysis chamber provides heat for the pyrolysis reaction [26,27]. Volatiles, residual char, and inert particles from the pyrolysis reactor are blown upwards to the primary cyclone, which separates char and inert particles and returns them to the bubbling bed char reactor. Here, char is mixed with air and steam to undergo gasification at typically 730 °C [26,27]. The produced gas and the fine ash particles exit at the top of the char reactor and enter the pyrolysis chamber, where the gas contributes to a high gas velocity in the upper part of the chamber. Heavier inert particles re-circulate to the pyrolysis chamber from the bottom of the char reactor. The char particles in the upper part of the char reaction chamber thus experience a high retention time in the process, improving the overall conversion efficiency. The heat released due to the mainly exothermic reactions in the char reactor is consumed by the endothermic processes in the pyrolysis chamber.

The temperature of the exit stream from the pyrolysis chamber, about 650 °C, is lower than that of the char reactor. Consequently, most of the alkali species and similar ash components are present in the solid state and can be separated from the gas by the cyclones. Moreover, the relatively low temperatures in the process limit the tendency of de-fluidization in the system. As shown in Fig. 1, the product gas is fed to two cyclones. Using the primary and secondary cyclones in series, a large fraction of fine ash particles with the problematic alkali species is separated from the product gas.

It is of interest to increase the temperatures in the LTCFB gasifier to improve the overall conversion and efficiency (but still keeping the temperature at a level where gas phase alkali release is prevented). However, due to the alkali and silica rich fuels of interest, an increase in temperature increases the risk of de-fluidization. It is therefore important to understand the de-fluidization behavior of the alkali-rich ash from the LTCFB gasifier, as a function of temperature and alkali concentration.

3. Bench-scale de-fluidization measurements

3.1. Experimental setup

De-fluidization measurements were performed in a bench-scale fluidized bed setup as shown in Fig. 2. The reactor was made of a high temperature resistant steel tube with an inner diameter of 68 mm. The total height of the reactor was 1.2 m. A perforated steel plate distributor that contained 371 0.4 mm holes was located at a height of 0.6 m. Below this position was the gas preheat zone and above the reaction/fluidization zone. The feed samples were fed to the reactor from the top before the start of an experiment. The particles inside the reactor were fluidized using nitrogen gas. The exit gas was cleaned for particles in a cyclone, before being released through ventilation. The pressure drop over the bed was monitored by two pressure transducers located at the top and at the bottom of the bed as shown in Fig. 2. The reactor was electrically heated by three independently controlled heating elements. Temperatures were measured through thermocouples inserted just above the distributor plate and in the freeboard.

During an experiment, the temperatures, the pressure drop across the bed, and the corresponding time of measurement were logged and saved in a computer. Once the particles were fluidized, the reactor heating system was switched on and the temperature increased from room temperature at a rate of 5 K min^{-1}. The operating velocity of the fluidizing gas (U) was maintained at twice the minimum fluidization velocity (U_{mf}), which was of the order of 3–4 cm s^{-1}. De-fluidization in the system was observed by a sudden drop in the pressure and the temperature at which it occurred was defined as the de-fluidization temperature. A number of experiments were performed with quartz sand mixed with varying levels of KCl or K_2CO_3. Table 2 lists the particle sizes and concentrations of K for each experiment.

Additional experiments were performed with bed material samples obtained from the Pyroneer Gasifier. These samples were collected after 672 h of plant runs in the Pyroneer gasifier with Danish wheat straw as the fuel. The particle sizes and composition are shown in Table 3.

3.2. Experimental results

De-fluidization in the system was observed by a sudden drop in the pressure, as shown in Fig. 3. The de-fluidization temperatures obtained for sand + KCl and sand + K_2CO_3 mixtures are shown in Table 4. Mixtures of sand + KCl and sand + K_2CO_3 were de-fluidized at about 760 °C and 730 °C, respectively. The de-fluidization temperatures decreased slightly (4–6 °C) with an increase in K concentration.

The agglomerated samples of sand + KCl and sand + K_2CO_3

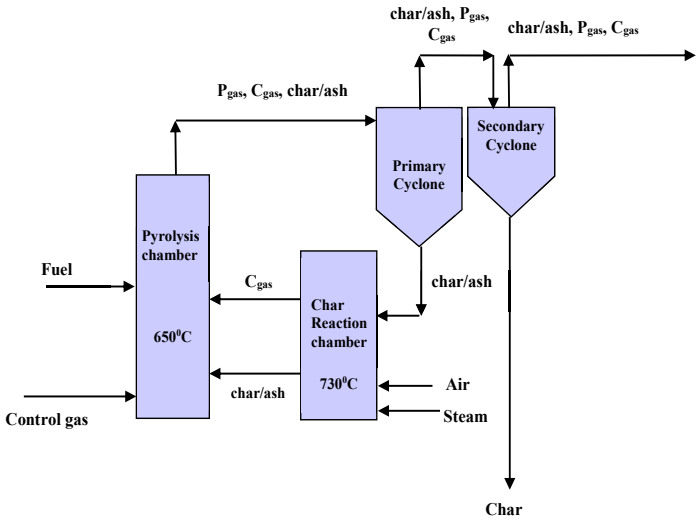

Fig. 1. Schematic diagram of a LT-CFB process, P_{gas}, = Gases produced from pyrolysis chamber (CO, H_2, tar, CO_2, CH_4), C_{gas}, = Gases produced from char reaction chamber (CO_2,CO, H_2).

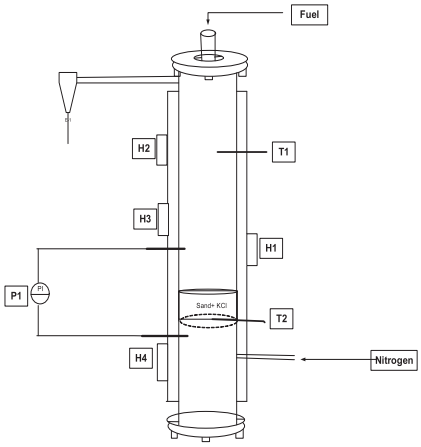

Symbol	Description
T1, T2	Thermocouples
P1	Pressure Indicator
H1,H2,H3,H4	Heating Elements

Fig. 2. Fluidized Bed Set up for De-fluidization studies.

Table 2
Particle sizes and compositions of sand + K mixtures used for de-fluidization measurements.

	% K (by mass)	Particle size (μm)	
Sand + KCl	2, 4.5, 6.5	Sand	200
		KCl	193
Sand + K_2CO_3	1.5, 4.5, 6.5	Sand	200
		K_2CO_3	210

Table 3
Particle sizes and inorganic elemental composition of the bed material samples from the 6 MW Pyroneer Gasifier. The particles included also trace concentrations of other inorganic elements.

	Sample-1	Sample-2
Particle size (μm)	212	193
Composition	% by mass	% by mass
K	4.2	4.8
Si	39.2	37.1
Cl	0.2	0.2
Ca	2.4	3.1
Mg	0.5	0.6

mixtures were analyzed by SEM–EDX to study the mechanism of de-fluidization. Fig. 4 shows the SEM analysis of the de-fluidized samples of sand + KCl mixtures. It can be seen that pure KCl (spectrum 1) binds the sand particles (spectra 2, 3). KCl has reacted with the sand particles only to a very limited degree. The SEM image of sand + K_2CO_3 mixtures shows two distinct phases (Fig. 5). The inner phase (spectrum 6) is rich in Si, which is surrounded by a coating layer (spectra 5, 7, 8) rich in K and Si. The coating layer around the particles could be due to the formation of a eutectic melt of K-silicates, formed from the reaction of K_2CO_3 with silica in sand. These observations indicate that agglomeration in sand + K_2CO_3 mixtures is coating-induced agglomeration.

De-fluidization experiments were performed on bed material

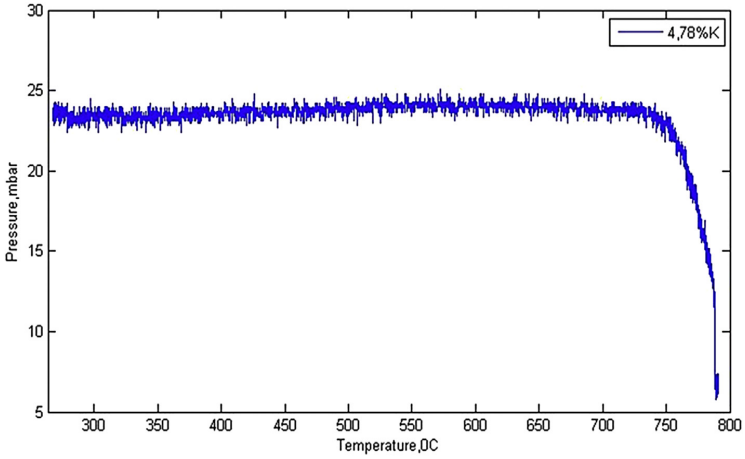

Fig. 3. Pressure measurements showing de-fluidization of 4.78% K_2CO_3 + sand mixtures.

Table 4
De-fluidization temperatures of sand + KCl and sand + K_2CO_3 mixtures.

Sand + KCl		Sand + K_2CO_3	
Potassium content (% by mass)	De-fluidization temperature (°C)	Potassium content (% by mass)	De-fluidization temperature (°C)
2	766	1.5	737
4.5	762	4.5	732
6.5	756	6.5	728

samples with varying alkali content obtained from the Pyroneer Gasifier after 672 h of operation. The results are shown in Table 5. The de-fluidization temperature for bed material samples with 4.2% K was about 785 °C; for 4.8% ash K it was 780 °C. The SEM images of the de-fluidized samples of ash particles are shown in Fig. 6. Similar to the sand + K_2CO_3 mixtures, the ash samples contained two distinct layers; a core (spectrum 2, dominant in Si) is surrounded by a coating layer (spectrum 1) rich in K, Ca, Mg and Si. This shows that the elements K, Ca and Mg have reacted with Si forming a coating layer of eutectic melts of silicates around the bed particles. Thus, as for the sand + K_2CO_3 mixtures, the probable mechanism of agglomeration in this case is also coating-induced agglomeration.

It can be seen that de-fluidization takes place at higher temperatures for ash particles (780 °C) than for sand + K_2CO_3 mixtures (730 °C), although in both cases, the mechanism of agglomeration is the same (coating-induced agglomeration). The presence of Ca and Mg in the ash particles could shift the formation of the eutectic melts to higher temperatures. It can be seen from a ternary diagram of K_2O–CaO–SiO_2 that with increasing concentrations of CaO for a fixed concentration of K_2O, the melting point temperature of the K_2O–CaO–SiO_2 eutectic increases [4]. The influence of the inorganic elemental composition on formation of the eutectic melts at various temperatures can also be analyzed through thermodynamic model studies as explained in the next section.

4. Modeling

4.1. Thermodynamic model study

Similar to Li et al. [3], we conducted thermodynamic equilibrium calculations to understand the melt formation of the ash

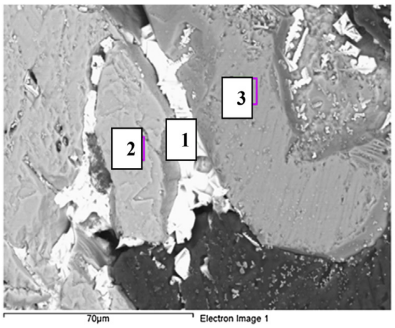

Spectrum	O (mol%)	Si (mol%)	Cl (mol%)	K (mol%)
1	10.4	1.4	40.2	48.1
2	61.0	24.1	0.0	7.5
3	65.6	34.4	0.0	0.0

Fig. 4. SEM image and analysis of the de-fluidized samples of Sand + KCl mixtures.

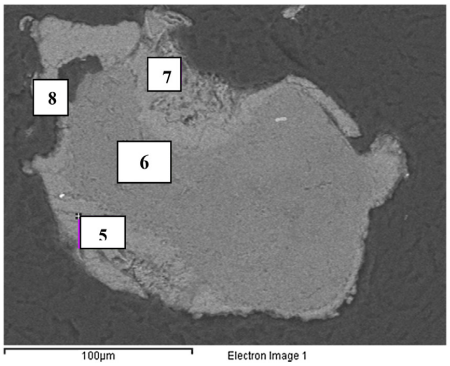

Spectrum	O (mol %)	Si (mol %)	K (mol %)
5	64.7	23.4	11.9
6	66.2	33.1	0.7
7	65.4	20.2	14.4
8	69.3	20.0	10.7

Fig. 5. SEM image and analysis of the de-fluidized samples of Sand + K_2CO_3 mixtures.

Table 5
De-fluidization temperatures of bed material samples from Pyroneer Gasifier.

Sample	% K by mass	Defluidization temperature (°C)
1.	4.2	785
2.	4.8	780

species that constitute the coating layer around the bed material particles. Since potassium has been found to play a key role for low-temperature eutectics [4], the study focused on the predicted fate of potassium.

The thermodynamic studies were made using the FactSage® software, which is based on Gibbs' free energy minimization. The mass fraction and the phases of various K species predicted by the software were studied for a temperature range of 400–1100 °C. The elemental composition of the ash species used for the FactSage calculations is shown in Table 6. The major inorganic species forming the coating layer in sand + K_2CO_3 mixtures are Si and K with a Si/K ratio of 1.87. The bed material samples contained significant fractions of Si and K (Si/K ratio of 3.37), together with Ca, Mg and smaller amounts of Na.

The partitioning of stable forms of K in sand + K_2CO_3 mixtures as a function of temperature obtained from the thermodynamic calculations is shown in Fig. 7. The formation of K_2O (SLAGA), which represents the eutectic molten phase of K-silicates, which eventually form the coating layer around the particles in the fluidized bed, initiates at around 740 °C.

The predicted stable forms of K in the bed material samples obtained from the Pyroneer gasifier at various temperatures are shown in Fig. 8. Similar to sand + K_2CO_3 mixtures, K mainly exists as K-silicates at low temperatures. K starts forming K_2O (SLAGA) at around 760 °C. The initial melt formation of K_2O (SLAGA) occurs at higher temperatures in case of bed material samples as compared to the case of sand + K_2CO_3 mixtures. This is conceivably due to the presence of Ca and Mg in the bed material coatings which were not present in the coatings of sand + K_2CO_3 mixtures.

Fig. 9 shows the stable forms of K without Ca and Mg at various temperatures. Here, the formation of K-silicate melts initiates about 580 °C and it becomes dominant above 740 °C. The observed temperature for melt formation is thus reduced compared to the results with bed material samples containing Ca and Mg (760 °C).

It should be noted that the equilibrium calculations can be used only to provide information on the probable temperature ranges for the formation of K-silicate melts and the influence of inorganic species in shifting the above temperature values. The equilibrium calculation does not take into account mixing or kinetic limitations.

4.2. Dynamic model study: coating-induced agglomeration

A mathematical model was developed to describe the de-fluidization behavior of alkali-rich samples in the bench scale fluidized bed reactor. The mechanism of agglomeration in the model is coating-induced agglomeration where a viscous melt sticks to the fluidized particles and acts as glue that binds the particles together and thus initiates agglomeration. This section describes the model development and the calculations for experiments performed in the bench scale fluidized bed reactor setup.

4.2.1. Adhesive force within the agglomerates

Fig. 10 shows schematically two bed particles with a coating

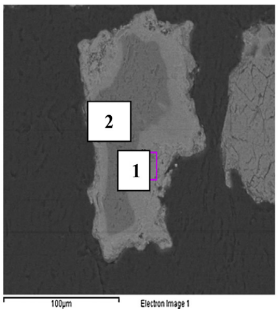

Spectrum	O (mol %)	Mg (mol %)	Si (mol %)	Cl (mol %)	K (mol %)	Ca (mol %)
1	57.7	0.9	28.0	0.2	8.3	3.8
2	64.2	0.0	35.8	0.0	0.0	0.0

Fig. 6. SEM image and analysis of the de-fluidized ash (bed material) samples.

Table 6
Moles of elemental species used as input in the Fact Sage modeling.

	Sand + K_2CO_3 mixtures	Bed material (Pyroneer Gasifier)	Bed material (Pyroneer Gasifier, without Ca and Mg)
Elemental species	Mol	Mol	Mol
Si	0.54	1.03	1.03
K	0.29	0.30	0.30
Ca	0.0	0.14	0.0
Na	0.0	0.02	0.02
Mg	0.0	0.03	0.0
O	1.22	2.4	2.4
N	255	238	238

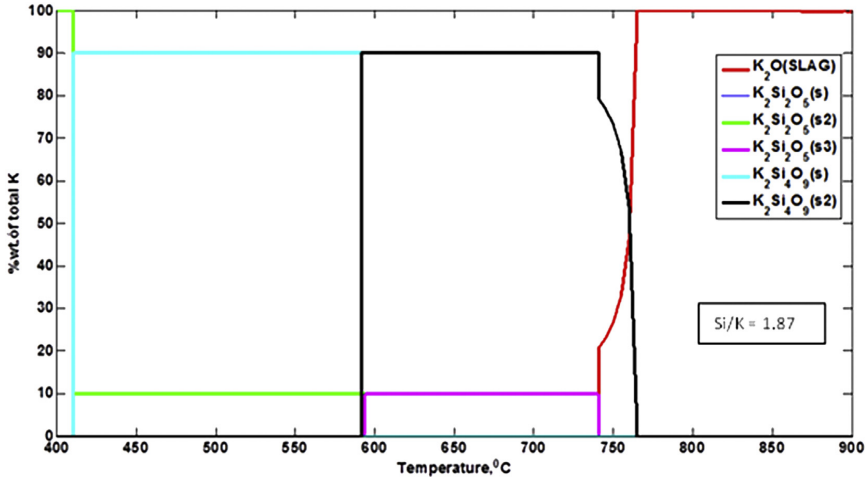

Fig. 7. Mass fractions of stable forms of K in Sand + K_2CO_3 mixtures with increase in temperatures.

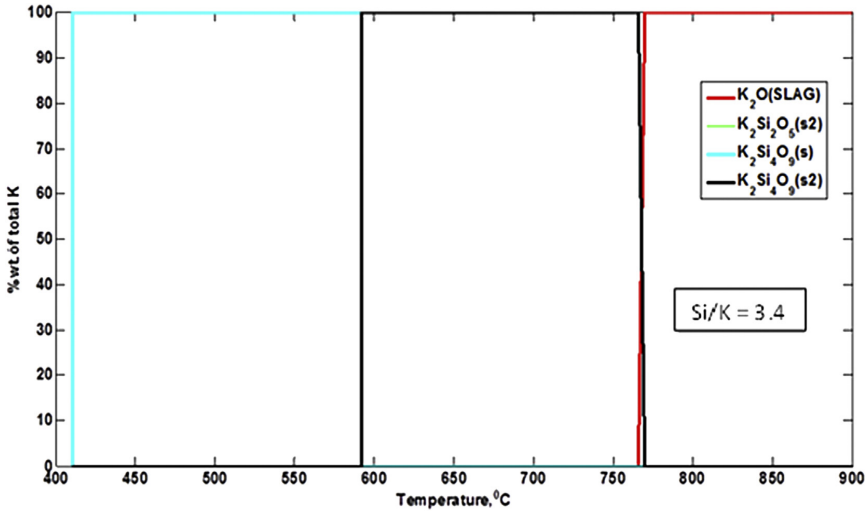

Fig. 8. Mass fractions of various forms of K in ash with increase in temperatures.

layer, as used for the model development. The assumptions for the model are the following:

1. The fluidized bed particles are spheres with uniform size.
2. The particle surfaces are uniformly wetted throughout by a coating layer.
3. The coating layer is composed of K-silicates.
4. The reaction of fuel-K with silica in the bed material is fast and the resistance due to reaction rates is negligible.

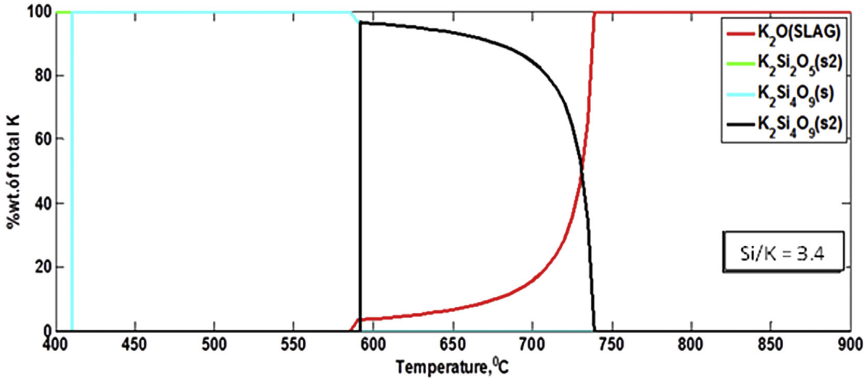

Fig. 9. Mass fractions of various forms of K in ash (without Ca and Mg) as a function of temperatures.

5. All the potassium retained within the fluidized bed reacts with silica in the bed material to form K-melts in the coating layer.
6. The viscous coating layer on each particle binds the two spherical particles initiating agglomeration.
7. The major forces acting on the particle are the adhesive force due to the coating layer and the breaking force on the particle induced by the motion initiated by the fluidizing gas.
8. De-fluidization is considered to occur when the adhesive force exceeds the breaking force.

The assumptions were mostly drawn mostly from previous modeling work [24,25], where they are discussed in more detail. Several of the assumptions are supported by SEM analysis ([24], present work). Assumption 4, introduced in the present work to simplify the model, is believed to be valid for K_2CO_3, but not for other potassium compounds. The reaction of KCl with silica is slow [28,29], but the reaction between potassium carbonate and silica is fast [29,30].

At de-fluidization, the adhesive force (F_{ad}) ≥ the breaking force (F_{br}). The adhesive force between two spherical particles is given by equation (1),

$$F_{ad} = \pi b^2 \sigma \tag{1}$$

where b is the neck radius of the coating and σ is the tensile stress of the agglomerate (N m^{-2}). From Fig. 10, equation (2) can be derived from the geometry,

$$b^2 = d\delta \tag{2}$$

Here, d is the diameter of the particle and δ is the thickness of the coating. The tensile stress of the agglomerate σ is a function of the material of the coating and will strongly depend on the viscosity of the coating layer. Thus,

$$\sigma = f\ (\mu(T,w)\ ) \tag{3}$$

where $\mu(T,w)$, the viscosity of the coating layer, is a function of the temperature (T) and composition of the coating layer (mass fractions w). There have been many correlations suggested in literature [31–35] for predicting viscosity of silicate melts. The Lakatos model [31] for viscosity prediction of silicate melts has been used in this study. The details of the model are given in supplementary material (Appendix A). The Lakatos model was tested with available measurements [36,37] on viscosities of silicate melts for samples having an inorganic elemental composition approximately similar to the samples used in the present study.

As can be seen in Fig. 11, the viscosity values obtained using the Lakatos model agree well with the experimental values reported in literature. However, the uncertainty in the viscosity may be substantial as the Lakatos model is extrapolated to the conditions of the present work (lower temperatures). An error in the viscosity in the model leads to an error of similar magnitude in the predicted de-fluidization time, and more work is desirable to improve the accuracy of the models for viscosity.

Limited information is available in the literature for the relation of tensile stress of the agglomerate with the viscosity of the coating layer. Lin et al. [24] estimated the tensile stress of the agglomerate with viscosity from an empirical equation (4),

$$\sigma = \frac{A^*t}{(\mu(T,X)\ )d} \tag{4}$$

where A is a constant and t is the time. According to this relation the tensile stress increases linearly with time indefinitely. We suggest that the strength of the agglomerate due to chemical reaction and sintering increases with time and then becomes constant, as shown in Fig. 12. We assume that the time taken for the tensile strength of the agglomerate to reach its maximum value (Δt_1) is small as compared to the total time of de-fluidization ($\Delta t_1 + t_2$) as shown in Fig. 12. Since the measurements in the fluidized bed reactor involved stepwise heating of the reactor, it allowed sufficient time for mixing and therefore the time taken due to mixing and kinetic limitations for the coating to reach its maximum tensile strength (Δt_1) was negligible. In cases where the reactor is already preheated and the fuel is fed at a fixed rate, the value of Δt_1 would not be negligible and should be considered. t_2 can be related to the buildup of K in the bed with the slow heating of the bed to the de-fluidization temperatures. We therefore propose a modified empirical correlation for the

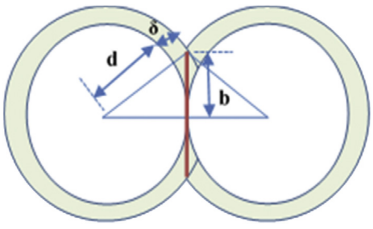

Fig. 10. Two bed particles with viscous coating layer.

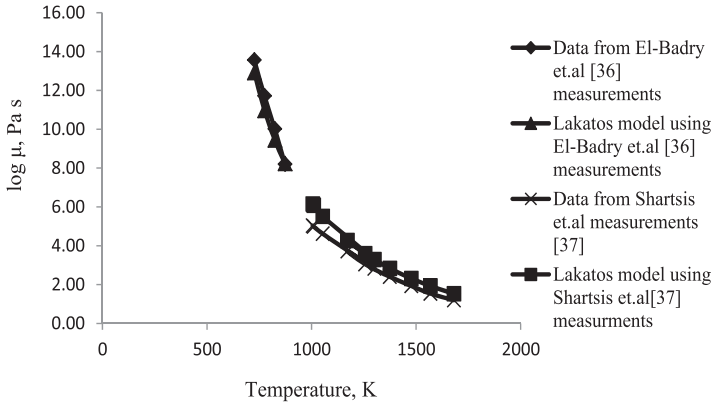

Fig. 11. Comparison of viscosity values obtained from Lakatos model with values obtained from measurements in literature.

tensile strength of the agglomerate being independent of time, as shown in equation (5):

$$\sigma = \frac{A_1}{\{(\mu(T,w))\}^n * d} \tag{5}$$

Here, A_1 and are constants. The basis of the equation (5) is taken from Benson et al. [38], who assumed the tensile strength of the agglomerate to be inversely proportional to viscosity of the coating for coal combustion systems. Working on a different system, we decided to generalize the proportionality relation by adding a parameter n and fit it to our measurements.

To calculate the particle adherence thickness, the thickness of the coating layer needs to be estimated. It is calculated using the following assumptions:

1. The coating layer around each sphere is of uniform thickness δ.
2. The coating layer is composed of a K-silicate slag formed by the reaction of K from the fuel and silica from the bed particles.
3. The reaction of K species with silica is considered to be fast. Thus, a steady state thickness of coating layer is immediately achieved with the available amount of K.
4. All the K retained in the fluidized bed is bound in the coating layer.

With these assumptions, a mass balance of K can be expressed as follows. The mass of K in the input feed (m_{K0}) (during start of the process) – the total mass of K entrained with the exit gas from the fluidized bed ($m_{Kentrained}$) till the time of de-fluidization (t_{def}) = total mass of K retained within the fluidized bed = mass of K in the coating layer ($m_{Kcoating}$):

$$m_{\text{Kcoating}} = m_{K0} - m_{\text{Kentrained}}\left(t_{\text{def}}\right) \tag{6}$$

The mass of K fed to the fluid bed (m_{K0}) can also be expressed as equation (7),

$$m_{K0} = \text{W} * w_{K0} \tag{7}$$

where W is the total mass of the bed particles in the fluid bed and w_{K0} is the mass fraction of K in the fluidized bed at the start of the experiment.

$$m_{\text{Kentrained}}\left(t_{\text{def}}\right) = \beta\left(t_{\text{def}}\right) * m_{K0} = \beta\left(t_{\text{def}}\right) * \text{W} * w_{K0} \tag{8}$$

Here β is the fraction of K in the input feed that is entrained with the exit gas during the process till the time of de-fluidization (t_{def}).

Substituting m_{K0} and $m_{Kentrained}$ from equations (7) and (8) in equation (6) we get equation (9),

$$m_{Kcoating} = \left(1 - \beta\left(t_{def}\right)\right) * W * w_{K0} \tag{9}$$

$m_{Kcoating}$ can also be expressed as shown in equation (10),

$$m_{Kcoating} = n * \left(\pi d^2 \delta\right) * w_{Kcoat} * \rho_{coat} \tag{10}$$

ρ_{coat} is the density of the coating layer. n, the number of bed particles, can be calculated using equation (11),

$$n = \frac{W}{(\pi d^3/6) * \rho_{bed}} \tag{11}$$

Here, ρ_{bed} is density of the bed particles. w_{Kcoat}, the mass fraction of K in the coating layer, can be estimated as per equation (12),

$$w_{Kcoat} = \frac{m_{Kcoating}}{\sum m_{icoating}} \tag{12}$$

where $\sum m_{icoating}$ is the total mass of elements i (K, Si, Ca, Mg, Na and O) in the coating layer, given by equation (13),

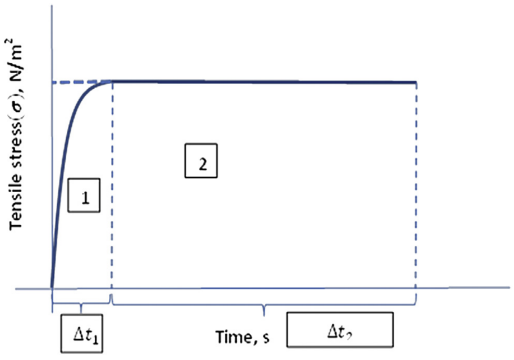

Fig. 12. Profile of Tensile strength vs time during sintering.

$$\sum m_{icoating} = \sum \frac{m_{\mathrm{Kcoating}}}{M_K} * \frac{n_i}{n_K} * M_i \tag{13}$$

M_K is the molecular mass of K, n_i/n_K is the molar ratio of element i with respect to K in the coating layer, and M_i is the molecular mass of i. The molar ratio of species i with K in the coating layer used in the model calculations for the sand + K_2CO_3 mixtures and the bed material samples is listed in Table 7.

The thickness of the coating layer can thus be obtained from equations (9)–(13) and is given by equation (14)

$$\delta = C^* \frac{w_{K0}{}^* d^* \left(1 - \beta\left(t_{def}\right)\right)}{\{w_{Kcoat}\}}, \tag{14}$$

where $C = \frac{\rho_{bed}}{6^*\rho_{coat}}$. By using equations (1), (2), (5) and (14) the adhesive forces acting within the agglomerate F_{ad} can be estimated as shown in equation (15),

$$F_{ad} = C^{'} * \frac{w_{K0}{}^* d^* \left(1 - \beta\left(t_{def}\right)\right)}{\{w_{Kcoat}\}} * \frac{1}{\{(\mu(T,X))\}^n} \tag{15}$$

Here, $C^{'} = A_1{}^*\pi^*C$. Equation (15) shows that the adherence force is related to the concentration of the potassium in the bed, the viscosity of the coating layer, and the two empirical constants, $C^{'}$ and n.

4.2.2. Breaking force on agglomerates

The breaking force on the agglomerates is exerted by the gas flow on the particles. It has been suggested [23] that the breaking force is exerted by the gas bubbles and thus proportional to the excess fluidization velocity of the gas as shown in equation (16).

$$F_{br} = C_1^{'} * \left(U - U_{mf}\right) \tag{16}$$

Here, U is velocity of the fluidization gas, U_{mf} is the minimum fluidization velocity, and $C_1^{'}$ is a constant. It has also been suggested [39] that the breaking force for the agglomerates can be related to the drag force exerted by the fluidization gas on the particles. The breaking force can then be calculated using equation (17).

$$\begin{aligned} F_{\mathrm{br}} &= C^{''} * C_D * \left(\frac{\pi}{8}\right) * d^2 * \rho_g * \left(U - U_{\mathrm{mf}}\right)^2 \\ &= C_2^{'} * C_D * d^2 * \rho_g * \left(U - U_{\mathrm{mf}}\right)^2 \end{aligned} \tag{17}$$

where $C^{''}$ is a constant, ρ_g is the density of the fluidization gas (nitrogen), and $C_2^{'}$ is a constant which is equal to $C^{''}*\left(\frac{\pi}{8}\right)$. C_D, the drag coefficient, is estimated by equation (18),

$$C_D = \frac{24}{Re}\left(1 + 0,173{}^* Re^{0.657}\right) + \frac{0,413}{1 + 16300{}^* Re^{-1.09}} \tag{18}$$

The Reynolds number Re is calculated using the particle diameter and the gas velocity.

As mentioned earlier, at de-fluidization the adhesive force (F_{ad}) ≥ breaking force (F_{br}). The term d in equation (17) is the diameter of a particle in the fluidized bed and not of the agglomerate. All the particles are considered to be spherical with uniform diameter d. These assumptions thus give room for improvement in the equation for drag force on agglomerate in fluidized bed in future studies. We presently go ahead with both equations (16) and (17) in this work.

By combining equations (15) and (16), and (15) and (17), respectively, we get the expressions for the behavior of the particles at de-fluidization as a function of temperature and composition as shown in equations (19) and (20).

$$\frac{w_{K0}{}^* \mathrm{d} * \left(1 - \beta\left(t_{\mathrm{def}}\right)\right)}{\{w_{\mathrm{Kcoat}}\}} * \frac{1}{\{(\mu(T,w))\}^n} = C_1{}^{'} * \left(U - U_{\mathrm{mf}}\right) \tag{19}$$

$$\begin{aligned} &\frac{w_{K0} * \left(1 - \beta\left(t_{\mathrm{def}}\right)\right)}{\{w_{\mathrm{Kcoat}}\}} * \frac{1}{\{(\mu(T,w))\}^n} \\ &= C_2^{''} * C_D * \rho_g * \left(U - U_{\mathrm{mf}}\right)^2 {}^* \mathrm{d} \end{aligned} \tag{20}$$

Here $C_1^{''}$ is $(C_1^{'}/C^{'})$ and $C_2^{'}$ is $(C_2^{'}/C^{'})$.

Equations (19) and (20) can also be rewritten in terms of the level of critical viscosity where de-fluidization takes place, as seen in equations (21) and (22):

$$\mu(T,w) = m^{'} * \left(\frac{w_{K0}{}^* \mathrm{d} * \left(1 - \beta\left(t_{\mathrm{def}}\right)\right)}{\{w_{\mathrm{Kcoat}}\}} * \frac{1}{\left(U - U_{\mathrm{mf}}\right)}\right)^{1/n^{'}} \tag{21}$$

$$\mu(T,w) = m^{''} * \left(\frac{w^* \left(1 - \beta\left(t_{def}\right)\right)}{\{w_{Kcoat}\}} * \frac{1}{\left(C_D{}^* \rho_g * \left(U - U_{mf}\right)^2 {}^* d\right)}\right)^{1/n^{''}} \tag{22}$$

Here, $m^{'}$ is $(1/C_1^{''})^{1/n^{'}}$ and $m^{''}$ is $(1/C_2^{''})^{1/n^{''}}$. The effect of temperature and composition of the bed material on de-fluidization can thus be studied from equations (21) and (22). The unknown constant parameters in the model, m and n, were estimated by a regression fit discussed later in section 4.2.4. The values of the measuring data used for fitting are shown in Table 8.

4.2.3. Comparison of model performance against literature data

The model development was based on the present experiments, as well as the measurements made by Lin et al. [24] on de-fluidization in biomass combustion in a lab-scale fluidized bed combustor. This reactor was preheated to a required temperature and the straw was fed at a fixed flow rate. . Quartz sand was used as the bed material, while air was used as the fluidizing gas. As in the

Table 7
Molar ratios of the species i in the coating layer in sand + K-carbonate mixtures and the bed material particles, used in model calculations.

Molar ratios in the coating layer	Coating layer in sand + K-carbonate mixtures	Coating layer bed material samples
Si/K	1.87	3.37
Ca/K	Not applicable	0.46
Na/K	Not applicable	0.07
Mg/K	Not applicable	0.1
O/K	6.48	6.95

present work, a sudden drop in the pressure indicated de-fluidization. Experiments were made with different air flow rates, particle sizes and temperatures. Since the system of Lin et al. involved continuous feeding of straw at a fixed temperature, equation (9) should be modified as shown in equation (23),

$$m_{\mathrm{Kcoating}} = \left(1-\beta\left(t_{\mathrm{def}}\right)\right) * \varnothing * t_{\mathrm{def}} * w_{K0} \tag{23}$$

where $\varnothing$ is the mass flow rate of the feed.

Under these conditions, the time taken for the coating to reach its maximum strength (Δt_1) cannot be neglected and should be added to estimate the total de-fluidization time. The de-fluidization time can thus be obtained from equations (21)–(23) as shown in equations (24) and (25).

$$t_{def} = \left(\frac{(\mu(T,w))}{m^{'}}\right)^{n^{'}} * \frac{W*\{w_{Kcoat}\}}{\varnothing * w_{K0} * d * \left(1-\beta\left(t_{def}\right)\right)} * \left(U - U_{mf}\right) + \Delta\, t_1 \tag{24}$$

$$t_{\mathrm{def}} = \left(\frac{(\mu(T,w))}{m^{''}}\right)^{n^{''}} * \frac{\mathrm{W} * \{w_{\mathrm{Kcoat}}\}}{\varnothing * X_{K0} * \left(1-\beta\left(t_{\mathrm{def}}\right)\right)} * \left(C_D * \rho_g * \left(U - U_{\mathrm{mf}}\right)^2 * \mathrm{d}\right) + \Delta\, t_1 \tag{25}$$

The values of the various parameters for the fluidized bed straw combustion experiments used for the model calculations are given in Table 9. We assumed the value of $\Delta t_1 x$ to be 15 min (900 s).

4.2.4. Parameterization of the model using the de-fluidization measurements

The model was parameterized based on the measurements from the de-fluidization experiments on sand + K carbonates and bed material samples, respectively, using equations (21) and (22), and on the measurements made by Lin et al. [24] using equations (24) and (25). The values of the parameters $n^{'}$, $n^{''}$, $m^{'}$ and $m^{''}$ were obtained by a regression fit of all the measured data shown in Figs. 13 and 14.

The goodness of the fit was assessed by using the Normalized Root Mean Square Error (NRMSE, described in Supplemental Material) between the measured and calculated values. The values of the fitted parameters and the comparison of the model predictions (21) and (22) with the measured values of the de-fluidization temperatures in the bench-scale fluidized bed reactor are provided in Fig. 13. The corresponding values of the fitted parameters and goodness of fit of the model equations (24) and (25) with the measured values of the de-fluidization time, t_{def}, by Lin [24] are provided in Fig. 14. The measured and calculated values using the above model equations for the bench scale fluidized bed measurements and the measurements by Lin [23] are provided in Tables 10 and 11, respectively.

As seen from Table 10 and Fig. 13, both model equations (21) and (22) provide satisfactory predictions of de-fluidization temperatures in the bench-scale set up. Equations (24) and (25) also predicted the de-fluidization times of Lin et al. [24] well, as seen from Table 11 and Fig. 14. The values of the de-fluidization time t_{def} from Lin et al. [24] were found to be lower than the values obtained from both the model calculations at higher temperatures (>820 °C). We attribute part of this difference to the model assumption that all K is present in the coating layer. The fraction of K entrained with the exit gas, β, is neglected (Table 9). However, measurements [40–42] indicate that K is partially released to the gas phase above 750 °C. This release is not accounted for in the present model.

Both the models, i.e., the one using relative velocity (equation (21) and (24)) and the one using drag force (equation (22) and (25)) as the breaking force, provide good predictions of the measurements. Based on our results it is not possible to distinguish between them. We have arbitrarily chosen the model that uses relative velocity as the breaking force (equation (21) and (24)) for further studies. Below the influence of the concentration of inorganic species on the predicted de-fluidization is discussed, while calculations for the de-fluidization behavior in large scale LTCFB gasifiers using alkali rich fuels are shown in the Supplemental Material.

4.2.5. Influence of the concentration of inorganic species on de-fluidization

The model was used to study the influence of the inorganic elemental composition on de-fluidization in a fluidized bed system similar to our laboratory set up. The predictions were made on bed material samples (Table 3) using model equation (21). Table 12 shows the variations in de-fluidization temperatures with varying specific input parameters, while the other model input values were kept constant. Also the viscosity of the coating layer that is influenced by the coating layer composition and the temperature is shown in Table 12. Figures showing the influence on the de-fluidization temperatures of changes in various input parameters are provided in the supplementary information (Appendix C). As seen from Table 12, with increasing fuel K concentration, the temperature at which de-fluidization occur decreases. An increase in the fluidizing gas velocity leads to an increase in the de-fluidization temperature due to a higher breakage force on the agglomerates. It can also be seen that, an increase in coating layer Si/K or Ca/K molar ratios results in an increase in viscosity, and thereby an increase in the de-fluidization temperature. An increasing viscosity of the coating layer reduces the adhesive strength of the neck between the particles. An increase in particle diameter decreases the temperature of de-fluidization. Particles

Table 8
Values of the known parameters used for the model calculations made on measurements with Sand + K-carbonate mixtures and the bed material particles in bench scale fluidized bed set up.

Feed	w_{K0} (mass fraction of K in the feed)	w_{Kcoat} (mass fraction of K in the coating layer)	De-fluidization temperature T (°C)	Diameter d (μm)	Reynolds number	Drag coefficient CD	Density of the fluidizing gas (nitrogen), ρ_g (kg m^{-3})	Viscosity of the coating layer, $\mu(T,w)$(Pa), estimated using the Lakatos model (App. A)	% Of K entrained with exit gas, β	Minimum fluidization velocity U_{mf} (m s^{-1})
Sand + K-carbonate	0.045	0.25	732	200	0.0603	408.69	0.340	9.1E+05	0	0.02
0.065	0.25	728	200	0.0608	405.19	0.341	1.03E+06	0	0.02	
Bed material	0.042	0.14	785	212	0.0587	547.75	0.324	9.84E+05	0	0.014
	0.0478	0.14	780	193	0.0448	419.42	0.322	1.18E+06	0	0.02

Table 9
Values of parameters used in model calculations on Lin et al. [24] measurements.

Biomass feed rate, ϕ_{feed} (kg/s)	Air flow rate,ϕ_{air} ($m^3\ s^{-1}$)[a]	Diameter of bed particle (μm)	Temperature (˚C)	Measured de-fluidization time (min)	K Entrained with exit gas,β
$5.5 \times 10^{-}$(-5)	2.33×10^{-4}	275	796	42.1	0.0
			797	45.2	
			822	26.0	
			823	26.4	
	2.92×10^{-4}	388	843	19.3	
			845	19.2	
			866	18.3	
			869	17.7	
	4.08×10^{-4}	460	819	26.0	
			820	26.5	

[a] At standard conditions (273 K and 1 atm).

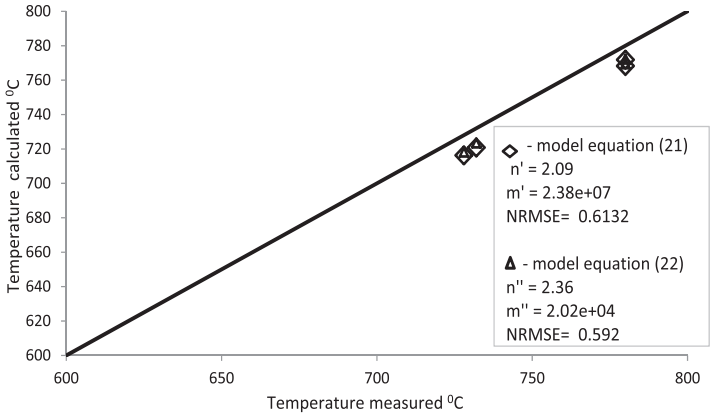

Fig. 13. Comparison of calculated de-fluidization temperatures with experimental data using equation (21) and equation 22.

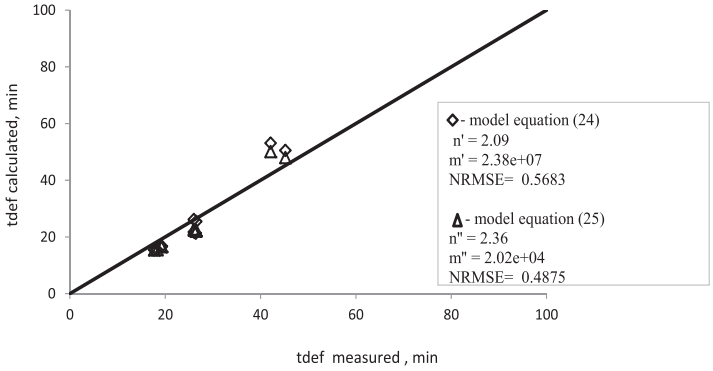

Fig. 14. Comparison of calculated de-fluidization time with experimental data from Lin et al. [24] using equation (24) and equation 25.

Table 10
Validation of the model by comparison of the model results with measurements from the fluidized bed reactor de-fluidization tests on sand + K carbonates and bed material samples.

	Mass fraction of K	T_{def} (°C), experimental values	T_{def} (°C), calculated using equation (21)	T_{def} (°C), calculated using equation (22)
Sand + K-carbonate	0.045	732	723.4	720.8
	0.065	728	718.2	716.3
Bed Material Samples (from Pyroneer Gasifier)	0.042	785	772.2	771.8
	0.0478	780	769.4	768.2

Table 11
Comparison of values of de-fluidization time, t_{def}, obtained from the measurements of Lin et al. [24] and from the present modeling.

Air flow rate (m3 s^{-1})[a]	Particle diameter (μm)	Temp (°C)	Measured defluidization time t_{def} (min) [23]	Defluidization time t_{def} (min) from Model Eq. (24)	Defluidization time t_{def} (min) from Model Eq. (25)
2.33 × 10^-(-4)	275	796	42.1	50.1	53.1
		797	45.2	48.0	50.6
		822	26.0	22.5	21.8
		823	26.4	22.1	21.3
2.92 × 10^-(-4)	388	843	19.3	16.8	16.7
		845	19.2	16.6	16.5
		866	18.3	15.5	15.5
		869	17.7	15.5	15.4
4.08 × 10^-(-4)	460	819	26.0	22.8	26.2
		820	26.5	22.4	25.5

[a] Air flow rates are at standard conditions, 273 K and 1 atm.

Table 12
Variation of de-fluidization temperatures with varying input values.

	INPUT								OUTPUT	
	Input mass fraction of K (w_{K0})	Particle diameter d (μm)	K entrained from system (β)	Molar ratio of the species in coating layer				Operating gas velocity U (m s^{-1})	De-fluidization temperature, (^{0}C)	Viscosity of coating layer (Pas)
				Si/K	Ca/K	Na/K	Mg/K			
Base Case	0.04	212	0	3.37	0.46	0.07	0.11	0.034	770	1.56 E+06
Change in X_{K0}	*0.02*	212	0	3.37	0.46	0.07	0.11	0.034	780	1.10 E+06
	0.06	212	0	3.37	0.46	0.07	0.11	0.034	766	1.86 E+06
Change in d	0.04	*100*	0	3.37	0.46	0.07	0.11	0.034	788	8.6 E+05
	0.04	*250*	0	3.37	0.46	0.07	0.11	0.034	762	2.15 E+06
Change in Si/K	0.04	212	0	*2.5*	0.46	0.07	0.11	0.034	745	1.42E+06
	0.04	212	0	*3.5*	0.46	0.07	0.11	0.034	773	1.58E+06
Change in Ca/K	0.04	212	0	3.37	*0.5*	0.07	0.11	0.034	772	1.57E+06
	0.04	212	0	3.37	*1*	0.07	0.11	0.034	777	1.65E+06
Change in U	0.04	212	0	3.37	0.46	0.07	0.11	*0.05*	780	1.19 E+06
	0.04	212	0	3.37	0.46	0.07	0.11	*0.07*	786	9.54 E+05

Note: The highlighted values in italics in the table represent the input parameters that were changed to study their influence on the de-fluidization temperature, the rest of the parameters being kept constant.

with larger diameters would have a lower specific outer surface area which results in an increase of the thickness of the coating layer. Moreover, the minimum fluidization velocity U_{mf} is larger for larger particles. Thus, at constant U, the ratio of U/U_{mf} decreases with increase in U_{mf} which would result in lower breakage force on the agglomerates. The rate of de-fluidization would thus increase, causing the de-fluidization to occur earlier at lower temperatures.

5. Conclusions

In this study the effect of inorganic species (mainly K, Si and Ca) on agglomeration and de-fluidization of alkali-rich bed material under non-oxidizing conditions has been analyzed. Experiments were conducted in a bench-scale fluidized bed reactor with sand and pure potassium salts (KCl and K_2CO_3), as well as with bed material samples obtained from a 6 MW Low Temperature Circulating Fluidized Bed gasifier. For sand + KCl agglomerates, the sand particles were bound by KCl melts, whereas for sand + K_2CO_3 mixtures and for LTCFB bed material samples, agglomeration occurred due to the coating of bed particles by viscous silicate melts formed from reaction of alkaline and alkali earth species present in the fuel with silica from the bed particles. Possibly, the presence of Ca and Mg in the bed particles acts to the shift of the formation of the eutectic melts to higher temperatures. A mathematical model was developed to predict the de-fluidization temperatures of alkali-rich bed materials. It was validated against experimental results from the present work as well as data from literature. The calculations indicate that both the speciation (chlorides or silicates) and the concentration of K have a significant impact on the agglomeration and de-fluidization characteristics in the fluidized bed system. Contrary to models available in literature, the present model is capable of predicting the effect of these parameters, as well as process parameters, for coating-induced de-fluidization of alkali-rich bed materials.

Acknowledgement

The authors thankfully acknowledge the financial support provided by DONG Energy and Energinet.dk.

Appendix A. Supplementary data

Supplementary data related to this article can be found at http://dx.doi.org/10.1016/j.biombioe.2016.05.009.

References

[1] L.E. Fryda, K.D. Panopoulos, E. Kakaras, Agglomeration in fluidised bed gasification of biomass, Powder Technol. 181 (3) (2008) 307–320.
[2] D. Geldart, Types of gas fluidization, Powder Technol. 7 (5) (1973) 285–292.
[3] S. Li, L. Shang, H. Teng, Q. Lu, A model for agglomeration in bio-fuel fired fluidized bed, J. Therm. Sci. 19 (5) (2010) 451–458.
[4] M. Öhman, A. Nordin, B.J. Skrifvars, R. Backman, M. Hupa, Bed agglomeration characteristics during fluidized bed combustion of biomass fuels, Energy Fuels 14 (1) (2000) 169–178.
[5] S.T. Mac an Bhaird, E. Walsh, P. Hemmingway, A.L. Maglinao, S.C. Capareda, K.P. McDonnell, Analysis of bed agglomeration during gasification of wheat straw in a bubbling fluidised bed gasifier using mullite as bed material, Powder Technol. 254 (2014) 448–459.
[6] A. Ergudenler, A.E. Ghaly, Agglomeration of silica sand in a fluidized bed gasifier operating on wheat straw, Biomass Bioenergy 4 (2) (1993) 135–147.
[7] G. Olofsson, Z. Ye, I. Bjerle, A. Andersson, Bed agglomeration problems in fluidized-bed biomass combustion, Ind. Eng. Chem. Res. 41 (12) (2002) 2888–2894.
[8] M. Zevenhoven-Onderwater, R. Backman, B.J. Skrifvars, M. Hupa, T. Liliendahl, C. Rosén, The ash chemistry in fluidised bed gasification of biomass fuels. Part I: predicting the chemistry of melting ashes and ash-bed material interaction, Fuel 80 (10) (2001) 1489–1502.
[9] M. Zevenhoven-Onderwater, R. Backman, B.J. Skrifvars, M. Hupa, The ash chemistry in fluidised bed gasification of biomass fuels. Part II: ash behaviour prediction versus bench scale agglomeration tests, Fuel 80 (10) (2001) 1503–1512.
[10] B.-M. Steenari, A. Lundberg, H. Pettersson, M. Wilewska-Bien, D. Andersson, Investigation of ash sintering during combustion of agricultural residues and the effect of additives, Energy Fuels 23 (11) (2009) 5655–5662.
[11] B. Olanders, B.-M. Steenari, Characterization of ashes from wood and straw, Biomass Bioenergy 8 (2) (1995) 105–115.
[12] H. Liu, Y. Feng, S. Wu, D. Liu, The role of ash particles in the bed agglomeration during the fluidized bed combustion of rice straw, Bioresour. Technol. 100 (24) (2009) 6505–6513.
[13] A. Khadilkar, P.L. Rozelle, S.V. Pisupati, Models of agglomerate growth in fluidized bed reactors: critical review, status and applications, Powder Technol. 264 (2014) 216–228.
[14] J.L. Moseley, T.J. Obrien, A model for agglomeration in a fluidized-bed, Chem. Eng. Sci. 48 (17) (1993) 3043–3050.
[15] J.H. Siegell, High-temperature defluidization, Powder Technol. 38 (1) (1984) 13–22.
[16] B. Liss, T.R. Blake, A.M. Squires, R. Bryson, Incipient defluidization of sinterable solids, in: I.V. Fluidization, D. Kunii, R. Toei (Eds.), Engineering Foundation, 1983, pp. 249–256.
[17] B.J. Ennis, A microlevel-based characterization of granulation phenomena, Powder Technol. 65 (1–3) (1991) 257–272.
[18] M.J. Gluckman, J. Yerushalmi, A.M. Squires, D.L. Keairns (Eds.), Hemisphere, vol. II, Fluidization Technology, New York, 1975, p. 395.
[19] G. Tardos, D. Mazzone, R. Pfeffer, Destabilization of fluidized beds due to agglomeration part I: theoretical model, Can. J. Chem. Eng. 63 (3) (1985) 379–383.
[20] G. Tardos, R. Pfeffer, Destabilization of fluidized beds due to agglomeration part II: experimental verification, Can. J. Chem. Eng. 63 (3) (1985) 384–389.
[21] Y. Zhong, Z. Wang, Z. Guo, Q. Tang, Defluidization behavior of iron powders at elevated temperature: influence of fluidizing gas and particle adhesion, Powder Technol. 230 (2012) 225–231.
[22] P. Basu, A study of agglomeration of coal-ash in fluidized beds, Can. J. Chem. Eng. 60 (6) (1982) 791–795.
[23] J.P.K. Seville, H. Silomon-Pflug, P.C. Knight, Modelling of sintering in high temperature gas fluidisation, Powder Technol. 97 (2) (1998) 160–169.
[24] W. Lin, K. Dam-Johansen, F. Frandsen, Agglomeration in bio-fuel fired fluidized bed combustors, Chem. Eng. J. 96 (1–3) (2003) 171–185.
[25] C.-L. Lin, M.-Y. Wey, C.-Y. Lu, Prediction of defluidization time of alkali composition at various operating conditions during incineration, Powder Technol. 161 (2) (2006) 150–157.
[26] P. Stoholm, H.R.G. Nielsen, L. Sarbæk, L. Tobiasen, W.M. Fcok, K. Richardt, B. Sander, L. Wolff, U. Henriksen, The low temperature CFB gasifier-further test results and possible applications, in: Proceedings of the 12. European Biomass Conference (ISBN) ETA-Florence & WIP-Munich, 2002, pp. 706–709.
[27] P. Stoholm, J. Ahrenfeldt, U. Henriksen, A. Gomez, J. Krogh, R.G. Nielsen, B. Sander, The low temperature CFB Gasifier-500 kW Test on biogas fiber residue, in: 16th European Biomass Conference and Exhibition Valencia Spain, 2008.
[28] Y. Zheng, P.A. Jensen, A.D. Jensen, A kinetic study of gaseous potassium capture by coal minerals in a high temperature fixed-bed reactor, Fuel 87 (15–16) (2008) 3304–3312.
[29] C. Sevonius, P. Yrjas, M. Hupa, Defluidization of a quartz bed – laboratory experiments with potassium salts, Fuel 127 (2014) 161–168.
[30] S. Arvelakis, P.A. Jensen, K. Dam-Johansen, Simultaneous thermal analysis (STA) on ash from high-alkali biomass, Energy Fuels 18 (2004) 1066–1076.
[31] T. Lakatos, Viscosity-temperature relations in glasses composed of silicon dioxide-aluminum oxide-sodium oxide-potassium oxide-lithium oxide-calcium oxide-magnesium oxide-barium oxide-zinc oxide-lead(II) oxide-boron oxide, Glastek. Tidskr. 31 (3) (1976) 51–54.
[32] G. Urbain, Y. Bottinga, P. Richet, Viscosity of liquid silica, silicates and alumino-silicates, Geochim. Cosmochim. Acta 46 (6) (1982) 1061–1072.
[33] Y. Bottinga, D.F. Weill, The viscosity of magmatic silicate liquids; a model calculation, Am. J. Sci. 272 (5) (1972) 438–475.
[34] Y. Bottinga, P. Richet, A. Sipp, Viscosity regimes of homogeneous silicate melts, Am. Min. 80 (3–4) (1995) 305–318.
[35] H.R. Shaw, Viscosities of magmatic silicate liquids; an empirical method of prediction, Am. J. Sci. 272 (9) (1972) 870–893.
[36] K. ElBadry, N.A. Ghoneim, Low temperature viscosity of some aluminosodium silicate glasses, Glas. Ber. 56 (1983) 975–979.
[37] L. Shartsis, S. Spinner, W. Capps, Density, expansivity, and viscosity of molten alkali silicates, J. Am. Ceram. Soc. 35 (6) (1952) 155–160.
[38] S.A. Benson, M.L. Jones, J.N. Harb, Ash formation and deposition, in: L.O. Smoot (Ed.), Fundamentals of Coal Combustion—for Clean and Efficient Use, Elsevier, Amsterdam, 1993.
[39] Y. Zhong, Z. Wang, Z. Guo, Q. Tang, Prediction of defluidization behavior of iron powder in a fluidized bed at elevated temperatures: theoretical model and experimental verification, Powder Technol. 249 (2013) 175–180.
[40] D. Boström, N. Skoglund, A. Grimm, C. Boman, M. Öhman, M. Broström, et al., Ash transformation chemistry during combustion of biomass, Energy Fuels 26 (1) (2012) 85–93.
[41] S.C. van Lith, P.A. Jensen, F.J. Frandsen, P. Glarborg, Release to the gas phase of inorganic elements during wood combustion. Part 2: influence of fuel composition, Energy Fuels 22 (3) (2008) 1598–1609.
[42] J.N. Knudsen, P.A. Jensen, K. Dam-Johansen, Transformation and release to the gas phase of Cl, K, and S during combustion of annual biomass, Energy Fuels 18 (5) (2004) 1385–1399.

Supplementary Material

A. Viscosity of silicate melts (Lakatos equation)

$$log\mu = a + b/(T - c) \quad \text{A.1}$$

Where, μ = viscosity of the coating layer, Pas and T = Temperature inside the reactor, K

The values of a and b can be obtained from equations A.2-A.4.

$$a = 1.5183 * Al_2O_3 - 1.603 * CaO - 5.4936 * MgO + 1.4788 * Na_2O - 0.835 * K_2O - 2.455$$

A.2

$$b = 2253.4 * Al_2O_3 - 3919.3 * CaO + 6285.3 * MgO(+ + MnO) - 6039.7 * Na_2O - 1439.6 * K_2O +$$

5736.4 A.3.

$$c = 294.4 * Al_2O_3 + 544.3 * CaO - 384 * MgO - 25.07 * Na_2O - 321 * K_2O + 471.3 \quad \text{A.4}$$

Where, the symbols Na_2O, K_2O, CaO, MgO and Al_2O_3 represent the molar fraction of each species per mole SiO_2, i.e. Na_2O = mole Na_2O/mole SiO_2.

B. Normalized Root Mean Square Error calculation

The normalized root mean square error between the measured values and the calculated values is estimated by the following equation in Matlab.

$$NRSME = 1 - \frac{\sqrt{\sum(y-\hat{y})^2}}{\sqrt{\sum(y-mean(y))^2}} \quad \text{B.1}$$

Where, y is the measured value and $\hat{y}$ is the value obtained from the model calculations.

NRMSE values vary between -Infinity (bad fit) to 1 (perfect fit).

C. SEM Images of de-fluidized samples.

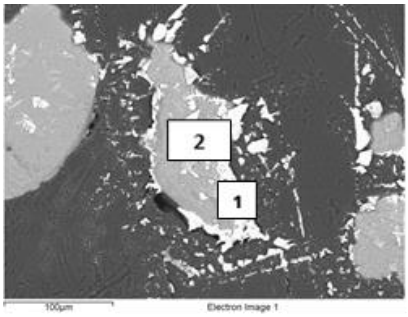

Spectrum	O (mol%)	Si (mol%)	Cl (mol%)	K (mol%)
1	10.2	4	45.5	40.3
2	59.1	32.4	1.8	6.7

Figure C.1. SEM image and analysis of the de-fluidized samples of Sand + KCl mixtures.

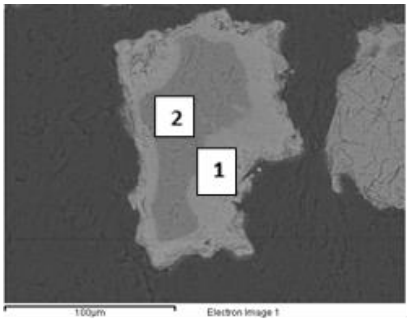

Spectrum	O (mol%)	Si (mol%)	Cl (mol%)	K (mol%)
1	57.7	28	0.2	14.1
2	64.2	35.8	-	-

Figure C.2. SEM image and analysis of the de-fluidized samples of Sand + K_2CO_3 mixtures.

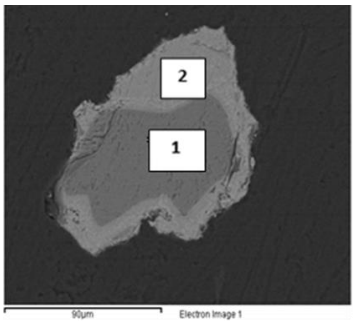

Spectrum	O (mol %)	Mg (mol %)	Si (mol %)	Cl (mol %)	K (mol %)	Ca (mol %)	Na (mol %)
1	65.9		34.1				
2	60.5	1.0	26.4	0.3	8.9	2.3	0.7

Figure C.3. SEM image and analysis of the de-fluidized ash (bed material) samples

D. Influence on de-fluidization temperatures with varying input parameters

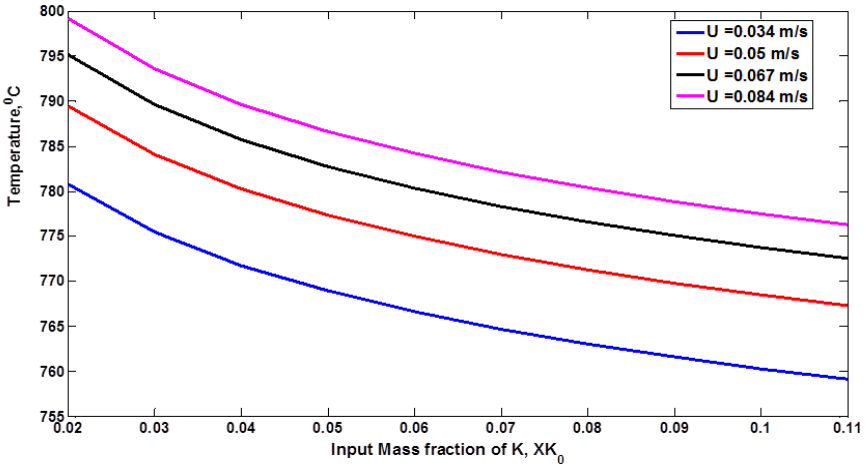

Figure D.1 De-fluidization temperatures with varying input concentration of K at different gas velocities in the fluidized bed. Other parameters are kept constant which include particle diameter, (d) = 212 µm, percentage of potassium entrained from the system (β) = 0, molar ratios of species in coating layer (Si/K = 3.37, Ca/K =0.46, Mg/K =0.11, Na/K =0.07)

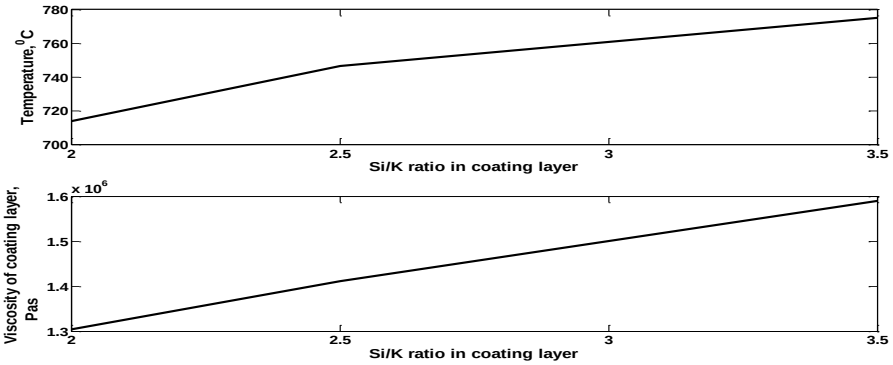

Figure D.2 Variation of De-fluidization temperatures and viscosities of coating layer as a function of varying Si/K ratios. Other parameters are kept constant which include input potassium concentration, (XK_0 = 0.042), particle diameter, (d = 212 μm), molar ratios of other species in coating layer (Ca/K =0.46, Mg/K =0.11, Na/K =0.07), percentage of potassium entrained from the system (β = 0) and Velocity of the fluidizing gas (U = 2*U_{mf})

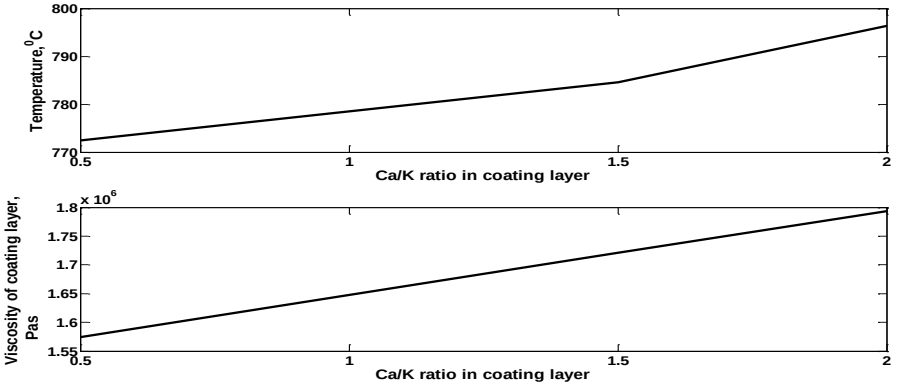

Figure D.3 Variation of De-fluidization temperatures and viscosities of coating layer as a function of varying Ca/K ratios. Other parameters are kept constant which include input potassium concentration, (XK_0 = 0.042), particle diameter, (d = 212 μm), molar ratios of other species in coating layer (Si/K = 3.37, Mg/K =0.11, Na/K =0.07), percentage of potassium entrained from the system (β = 0) and Velocity of the fluidizing gas, (U = 2*U_{mf})

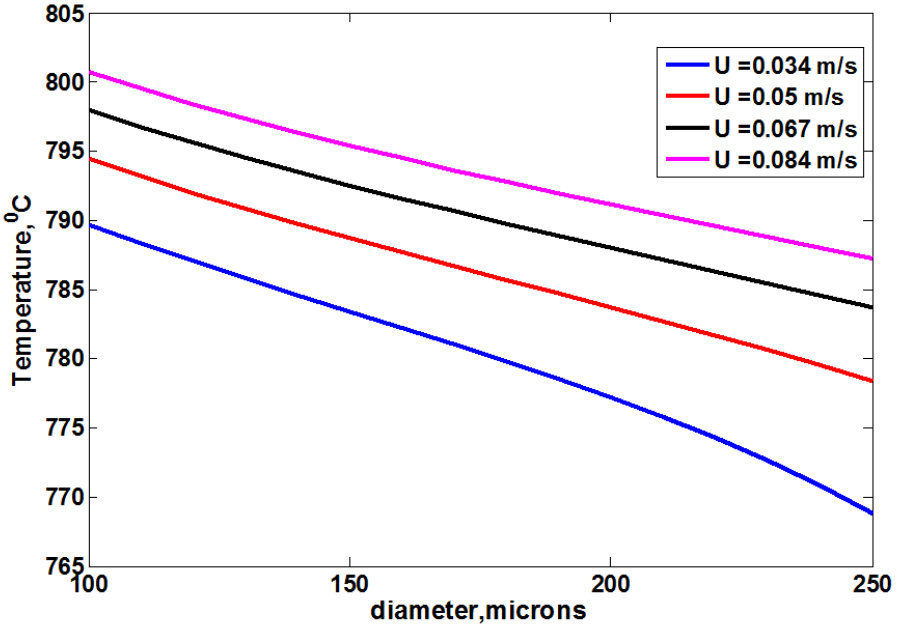

Figure D.4 De-fluidization temperatures with varying average particle diameter at different gas velocities in the fluidized bed. Other parameters are kept constant which include input potassium concentration, (XK_0) = 0.042, percentage of potassium entrained from the system (β) = 0, molar ratios of species in coating layer (Si/K = 3.37, Ca/K =0.46, Mg/K =0.11, Na/K =0.07)

E. Influence on de-fluidization time with varying input parameters.

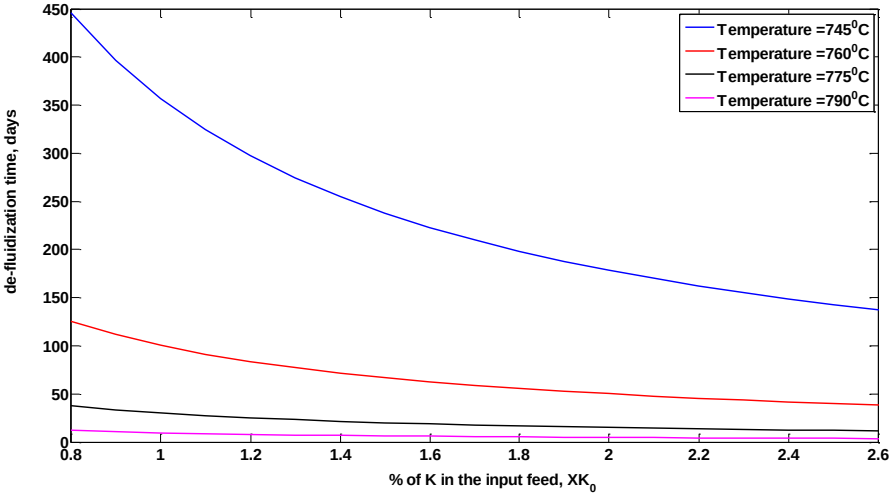

Figure E.1 Variation of de-fluidization time with % mass of K in input feed. Other parameters are kept constant which include particle diameter, (d = 212 μm), molar ratios of species in coating layer (Si/K = 3.37, Ca/K =0.46, Mg/K =0.11, Na/K =0.07) and percentage of potassium entrained from the system (β = 0.55), Velocity of the fluidizing gas, (U = 0.25 m/s)

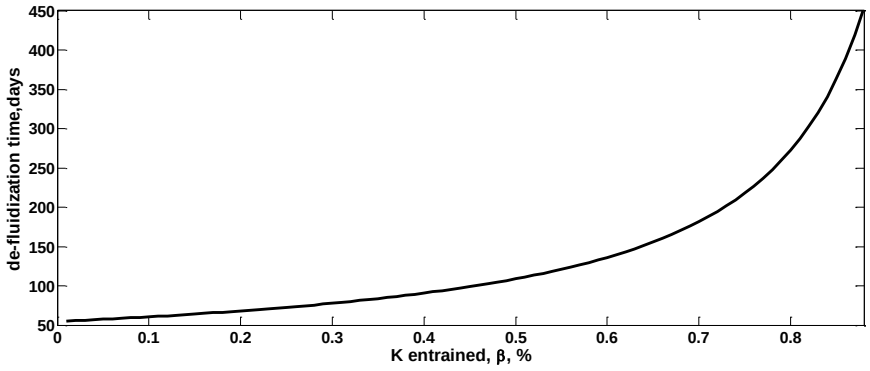

Figure E.2 Variation of de-fluidization time with percentage of K entrained from the gasifier, β. Other parameters are kept constant which include input potassium concentration, (XK_0) = 0.0083, particle diameter, (d) = 212m, Temperature (T = 760°C), molar ratios of species in coating layer (Si/K = 3.37, Ca/K =0.46, Mg/K =0.11, Na/K =0.07) and Velocity of the fluidizing gas, (U = 0.25 m/s)

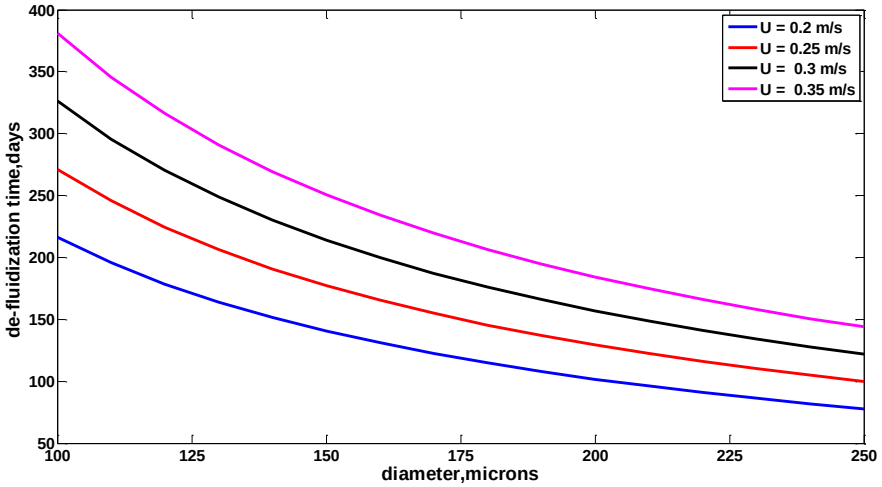

Figure E.3 Variation of de-fluidization time with bed particle diameter. Other parameters are kept constant which input potassium concentration, (XK_0 = 0.0083), Temperature (T = 760°C), molar ratios of species in coating layer (Si/K = 3.37, Ca/K = 0.46, Mg/K =0.11, Na/K =0.07), percentage of potassium entrained from the system (β = 0.55)

F. Model Predictions on de-fluidization in LTCFB system

The model study was extended to study the de-fluidization behavior of alkali rich ash in the LTCFB gasification system. The values of the various parameters used in the study were obtained from available data and measurements made during plant runs in the 6 MW LTCFB gasifier at Kalundborg (Pyroneer) and a 100 kW LTCFB gasifier at DTU. The assumptions for the model studies in the LTCB system were similar to those applied to model the conditions of Lin et al. [24] discussed above. The model equation (24) was used to study the influence of the concentration of fuel alkali species and bed temperature on the time of de-fluidization in a LTCFB system. The values of the various parameters used in the model study are listed in Table E1.

Table F1 Values of input parameters used in model studies for de-fluidization in LTCFB gasifiers.

Mass flow rate of feed, φ (kgs^{-1})	0.358
Diameter of particles inside the char reactor, d (μm)	212
Total weight of bed material inside the LT-CFB reactor, W (kg)	10000
Fraction of K entrained from the char reactor, β	0.55
Velocity of the fluidizing gas, U (ms^{-1})	0.25

It is of interest to increase the temperatures in the LTCFB gasifier to improve the overall conversion and efficiency (but still keeping the temperature at a level where gas phase alkali release is prevented). However, due to the alkali and silica rich fuels of interest, an increase in temperature increases the risk of de-fluidization. It is therefore important to understand the de-fluidization behavior of the alkali-rich ash from the LTCFB gasifier, as a function of temperatures and alkali concentration. Therefore, the model study was made at increased temperatures (745-775°C).

Table E2 shows the predicted variation in de-fluidization time in the LTCFB system with varying input parameters. At a given bed temperature, the de-fluidization time decreases with increase in concentration of K in the feed. With a constant input feed of K, as the bed temperature increases, the de-fluidization time decreases. The de-fluidization time decreases from 445 days to 38 when the bed temperature is increased from 745 °C to 775 °C.

Table F2 Variation of de-fluidization time with varying input values.

	INPUT									OUTPUT
	Input mass fraction of K (w_{K0})	Particle diameter d, (μm)	K entrained from system (β)	Molar ratio of species in coating layer				Operating gas velocity U (m s^{-1})	Temperature (^{0}C)	De-fluidization time (days)
				Si/K	Ca/K	Na/K	Mg/K			
Base Case	0.008	212	0.55	3.37	0.46	0.07	0.11	0.25	760	125
Change in w_{K0}	*0.009*	212	0.55	3.37	0.46	0.07	0.11	0.25	760	111
	0.01	212	0.55	3.37	0.46	0.07	0.11	0.25	760	100
Change in temperature	0.008	212	0.55	3.37	0.46	0.07	0.11	0.25	*745*	446
	0.008	212	0.55	3.37	0.46	0.07	0.11	0.25	*775*	38
Change in d	0.008	*100*	0.55	3.37	0.46	0.07	0.11	0.25	760	271
	0.008	*250*	0.55	3.37	0.46	0.07	0.11	0.25	760	99
Change in β	0.008	212	*0.25*	3.37	0.46	0.07	0.11	0.25	760	72
	0.008	212	*0.7*	3.37	0.46	0.07	0.11	0.25	760	180
Change in U	0.008	212	0.55	3.37	0.46	0.07	0.11	*0.2*	760	90
	0.008	212	0.55	3.37	0.46	0.07	0.11	*0.3*	760	134

Note: The highlighted values in italics in the table represent the input parameters that were changed to study their influence on the de-fluidization time, the rest of the parameters being kept constant.

It should be noted that in this analysis, the fraction of K entrained from the LTCFB system ($\beta = 0.55$) includes only K entrained with solid ash particles (in ash collected in the secondary cyclone bottoms and in dust particles entrained with the exit gas). It is known, however, that K is also released in gaseous form as chlorides and hydroxides at temperatures greater than 750 °C [40-42]. Increasing temperatures within the LTCFB gasifier would therefore also result in increase in the fraction of K entrained (β), thereby partially increasing the de-fluidization time. As seen from Table 15, the de-fluidization time increases from 72 days to 180 days for an increase in β from 0.25 to 0.7.

Similar to predictions for the bench scale set up, at constant gas velocity, an increase in particle diameter decreases the temperature of de-fluidization. The de-fluidization time decreases from 271 days to 99 days with an increase in bed particle diameter from 100 to 250 microns.

Department of Chemical and Biochemical Engineering
Technical University of Denmark
Søltofts Plads, Building 229
2800 Kgs. Lyngby
Denmark

Phone: +45 45 25 28 00
Web: www.kt.dtu.dk/